Holography andquantum information

Espíndola Romero , R.

Publication date
2022
Document Version
Final published version

Holography and Quantum Information

Holography and Quantum Information

Ricardo Espindola Romero

Ricardo Espindola Romero

Holography and quantum information

This work has been accomplished at the Institute for Theoretical Physics (ITFA) of the University of Amsterdam (UvA) and is funded by the ERC Consolidator Grant QUANTIVIOL.

Cover: This cover has been designed using images from Freepik.com

Holography and quantum information

Academisch Proefschrift

ter verkrijging van de graad van doctor

aan de Universiteit van Amsterdam

op gezag van de Rector Magnificus

prof. dr. ir. P.P.C.C. Verbeek

ten overstaan van een door het College voor Promoties

ingestelde commissie,

in het openbaar te verdedigen in de Agnietenkapel

op dinsdag 18 oktober 2022, te 12:00 uur

door

Ricardo Espíndola Romero

geboren te Distrito Federal

Promotiecommissie

Promotores

prof. dr. J. de Boer	Universiteit van Amsterdam
dr. B. W. Freivogel	Universiteit van Amsterdam

Overige leden

prof. dr. E.P. Verlinde	Universiteit van Amsterdam
dr A. Castro Anich	Universiteit van Amsterdam
dr. J. Armas	Universiteit van Amsterdam
dr. D.M. Hofman	Universiteit van Amsterdam
dr. T.M. Anous	Universiteit van Amsterdam
dr. E. Cáceres	University of Texas Austin

Faculteit der Natuurwetenschappen, Wiskunde en Informatica

Publications

This thesis is based on the following publications:

[1] S. Bintanja, R. Espíndola, B. Freivogel, and D. Nikolakopoulou
"How to make traversable wormholes: eternal AdS_4 wormholes from coupled CFT's," JHEP **10** (2021), 173. arXiv: 2102.06628 [hep-th].
Presented in Chapter **2**.

[2] J. de Boer, R. Espíndola, B. Najian, D. Patramanis, J. van der Heijden, and C. Zukowski, "*Virasoro Entanglement Berry Phases*", JHEP **03** (2022), 179. arXiv: 2111.05345 [hep-th].
Presented in Chapter **3**.

[3] R. Espíndola, B. Najian, and D. Nikolakopoulou, "*Islands in FRW Cosmologies,*" arXiv: 2203.04433 [hep-th].
Presented in Chapter **4**.

Other publications by the author:

[4] R. Espíndola, A. Güijosa, and J. F. Pedraza, "*Entanglement Wedge Reconstruction and Entanglement of Purification*", Eur. Phys. J. C **78** no.8, 646 (2018). arXiv: 1804.05855 [hep-th].

[5] R. Espíndola, A. Güijosa, A. Landetta, and J. F. Pedraza, "What's the point? Hole-ography in Poincaré AdS", Eur. Phys. J. C **78** (2018) no.1, 75. arXiv: 1708.02958 [hep-th].

[6] R. Espíndola and J. Antonio García, "Cusp Anomalous dimension and rotating open strings in AdS/CFT", JHEP **1803** (2018) 116. arXiv:1607.05305 [hep-th].

Contribution of the author to the publications

The following publications are the result of close collaborations with my coauthors. Most of the ideas are the result of group discussions and the calculations were worked out by more than one author.

[1] S. Bintanja, R. Espíndola, B. Freivogel, and D. Nikolakopoulou *"How to make traversable wormholes: eternal AdS_4 wormholes from coupled CFT's,"* JHEP **10** (2021), 173. arXiv: 2102.06628 [hep-th].

The author contributed to all conceptual discussions, and in writing the entire paper. In particular, the author was responsible for sections 2.1, 2.2 and 3.1. The author also wrote the first draft of sections 3.3 and 4.1.

[2] J. de Boer, R. Espíndola, B. Najian, D. Patramanis, J. van der Heijden, and C. Zukowski, "*Virasoro Entanglement Berry Phases*", JHEP **03** (2022), 179. arXiv: 2111.05345 [hep-th].

The author contributed to all conceptual discussions and many of the computations. In particular, the author wrote the first draft of sections 2.2.1 and 3.1. In section 3, the author found the relation between the complex plane coordinate and the radial coordinate in the hyperbolic black hole through the Casini-Huerta-Myers map, which helped to interpret the non-standard vector fields as plane waves in the hyperbolic black hole geometry. In section 3.3, the author was responsible for the consistency check.

[3] R. Espíndola, B. Najian, and D. Nikolakopoulou, "*Islands in FRW Cosmologies*," arXiv: 2203.04433 [hep-th].

The author contributed to all conceptual discussions, and in writing the entire paper. In section 4, the author found the candidate island in the case of a closed universe.

A mis padres con cariño

Contents

1 Introduction **1**
1.1 Black holes . . . 2
1.1.1 Hawking radiation . . . 3
1.2 Holographic Principle . . . 5
1.3 AdS/CFT correspondence . . . 6
1.3.1 Entanglement entropy . . . 9
1.3.2 Black holes in AdS . . . 11
1.3.3 Traversable wormholes . . . 13
1.3.4 Modular Berry phases . . . 13
1.4 Information Paradox . . . 17
1.4.1 Entanglement islands . . . 18
1.5 Outline . . . 20

2 Eternal AdS_4 Wormholes from Coupled CFT's **23**
2.1 Introduction and Results . . . 23
2.2 Massless fermions in AdS_4 . . . 26
2.2.1 Dynamics . . . 26
2.2.2 Boundary conditions . . . 28
2.2.3 Modified boundary conditions . . . 30
2.2.4 Propagators and stress tensor . . . 31
2.3 Wormhole geometry . . . 34
2.3.1 Two regimes . . . 34
2.3.2 Matching . . . 36
2.3.3 Non-linear solution . . . 39
2.4 Thermodynamics . . . 42
2.4.1 Hamiltonian ground state . . . 42
2.4.2 Stability . . . 45
2.5 Discussion . . . 48

A Appendices **51**

B Stress tensor **53**

C Matching **57**

D Correlators in $\langle H_{\mathbf{int}} \rangle$ **59**

3 Virasoro Entanglement Berry Phases **61**
3.1 Introduction . . . 61
3.2 Geometric Berry phases . . . 64
3.2.1 States . . . 64
3.2.2 Density matrices . . . 66
3.3 State-changing parallel transport . . . 70
3.3.1 Example . . . 77
3.3.2 Lie algebra . . . 78
3.3.3 Central extension . . . 80
3.4 Coadjoint orbit interpretation . . . 83
3.5 Bulk phase space interpretation . . . 85
3.5.1 The conical singularity geometry . . . 85
3.5.2 Symplectic form . . . 89
3.5.3 Contour prescription . . . 91
3.6 Discussion . . . 93

A Kinematic space example **97**

B General formulation **103**

C Non-diagonalization for Virasoro **107**

4 Islands in FRW Cosmologies **117**
4.1 Introduction . . . 117
4.2 General framework . . . 120
4.3 Flat slicing . . . 122
4.3.1 Zero cosmological constant . . . 123
4.3.2 Positive cosmological constant . . . 124
4.3.3 Negative cosmological constant . . . 124
4.4 Positive curvature . . . 126
4.4.1 Zero cosmological constant . . . 126
4.4.2 Positive cosmological constant . . . 129
4.4.3 Negative cosmological constant . . . 132
4.5 Negative curvature . . . 134
4.5.1 Zero or positive cosmological constant . . . 134

4.5.2 Negative cosmological constant 135
4.6 Discussion 138

A Islands conditions **141**

5 Future directions **145**
5.1 Traversable wormholes 145
5.2 Modular Berry phase 146
5.3 Islands in FRW Cosmologies 147
5.4 Final thoughts 148

Summary **151**

Samenvatting **155**

Acknowledgements **159**

1 Introduction

Our current understanding of the microscopic world lies within the mathematical framework of quantum field theory (QFT). Basic building blocks called quantum fields permeate the spacetime and mediate the fundamental interactions of nature. Particles appear just as a consequence of their fluctuations. Together with a few basic principles: locality, symmetries, and renormalization group flow, the QFT framework sets the stage to model interactions at different energy scales and allows us to study different phenomena within each particular theory.

The Standard Model of Particle Physics represents a great success in the QFT approach. Three of the four fundamental forces of nature can be described, with very good precision, using the Standard Model. Despite its favorable outcomes in a lot of experiments, many open questions remain to be answered. For example, how to incorporate gravity at the quantum level, *i.e.,* at lengths of order the Planck length $l_P \approx 10^{-33}$cm, is yet to be understood.

One of the most exciting questions of theoretical physics is: *what is the theory of quantum gravity?* First attempts tried to quantize gravity starting from the Einstein-Hilbert action. However, one runs into problems very quickly since gravity is a non-renormalizable interaction. It is not well defined at arbitrarily high energies. This implies that General Relativity is just an effective field theory, and it needs to be replaced by something else at ultraviolet (UV) scales.

String theory has stood out as the main candidate for a theory of quantum gravity. It comprises a very ambitious program of unification. Regardless of whether or not string theory is *the* theory of quantum gravity, it provides us with a consistent and very rich theoretical framework to study Einstein gravity and quantum mechanics on the same footing.

Going back to the original discussion, we need new radical ideas of spacetime at quantum scales. This makes the theory of quantum gravity a complicated and challenging conceptual problem. It is needed though if we are interested in the

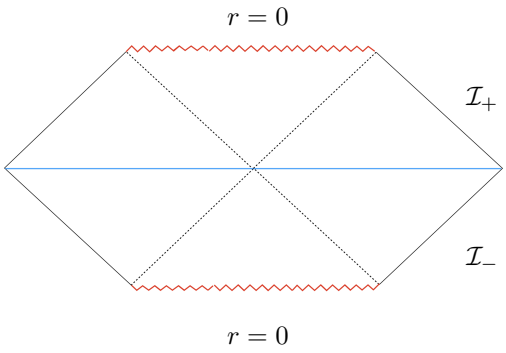

Figure 1.1: Penrose diagram for the Schwarzschild black hole. The horizons are denoted by dashed lines. There is a sphere $\mathcal{S}^2$ at each point, which shrinks at the singularities (red). The spacelike region (blue) connects two asymptotically flat regions.

physics behind the big bang, and at the center of a black hole.

1.1 Black holes

Black holes are fascinating objects of nature whose geometry is so drastically disturbed that light cannot escape from their interior. Surprisingly, the rich classical dynamics of uncharged black holes is governed by the vacuum Einstein equation

$$R_{\mu\nu} = 0 \ . \tag{1.1.1}$$

This elegant equation encodes very complicated phenomena, for example, the collision of two black holes, their merging, and gravitational radiation. The Schwarzschild geometry is a solution to Einstein's equations with spherical symmetry in the vacuum, whose metric is given by

$$ds^2 = -\left(1 - \frac{r_s}{r}\right) dt^2 + \left(1 - \frac{r_s}{r}\right)^{-1} dr^2 + r^2 d\Omega_2^2 \ , \tag{1.1.2}$$

where $r_s := 2GM$ is the Schwarzschild radius. The apparent singularities at $r = r_s$ are just an artifact of the chosen coordinates. The Penrose diagram in the $r - t$ plane can be seen in Fig. 1.1. Each point of the diagram represents a $\mathcal{S}^2$ sphere. Null lines are at 45 degrees. The $r = 0$ locations are curvature singularities. The future and past event horizons are located at $r = r_s$. There is a second asymptotically flat region to the left of the diagram. The spacelike slice passing through the origin contains an Einstein-Rosen bridge connecting the two regions.

The Schwarzschild solution (1.1.2) is an ideal configuration, pretty much like the simple pendulum in classical mechanics. Black holes in nature are formed by the collapse of gravitating matter. Black hole formation can be a complicated problem

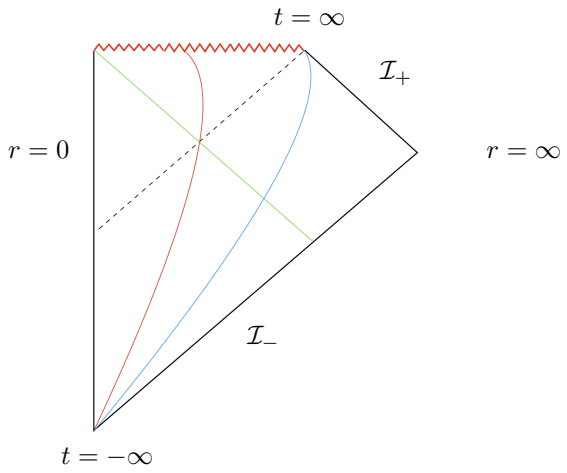

Figure 1.2: Penrose diagram for an evaporating black hole as a result of spherical collapse of a shell of photos (green). The timelike red curve describes an infalling observer while the blue describes an asymptotic observer. The event horizon is denoted by the dashed line.

that involves various elements of physics. However, we can study many properties of the general case using a simplified model. Imagine for example a collapsing shell of photons with total energy M. Starting with flat Minkowski space, the null ray of infalling particles coming from $\mathcal{I}_-$ divides the spacetime in two. By Birkoff's theorem, the region outside the photons shell is described by Schwarzschild geometry. Therefore, the Penrose diagram consists of flat Minkowski and Schwarzschild spacetimes stitched together at the location of the shell of photons (after a conformal transformation to match the radial coordinates across the boundaries).

In Figure 1.2, we depict two observer trajectories: asymptotic observer (blue) and infalling observer (red). The asymptotic observer collects information that arrives at any instant from his past light cone. Any particle falling through the horizon is seen as approaching the horizon asymptotically; in this way, the horizon represents the end of time. On the other hand, the infalling observer never sees the asymptotic observer cross the event horizon, instead, he sees the asymptotic observer slowing down as it approaches the horizon.

1.1.1 Hawking radiation

Before Hawking's derivation, it was believed that static black holes were completely inert, and they could only absorb and never emit particles. Adding quantum effects to the physics of black hole evolution would change this common belief. Hawking carried out the hard task of calculating the spontaneous emission of particles

during the collapse and formation of a black hole reaching a surprising conclusion: black holes are not completely black (see [4] for a historical review).

The setup consists of a black hole formed from the spherical collapse of a pure initial state $|\psi\rangle$. At late times, we consider a massless scalar field propagating in this background. It is convenient to introduce the coordinates

$$u = t - r_* = -2r_s \ln(-U/r_s) \ , \quad v = t + r_* = 2r_s \ln(V/r_s) \ , \tag{1.1.3}$$

where $r_* = r + r_s \ln(r - r_s)$ is the tortoise coordinate. The Kruskal coordinates (U, V) are smooth across the horizon so they are adequate for the infalling observer. The null coordinates (u, v) can be used for the asymptotic observer. Due to spherical symmetry, the scalar field propagation reduces to an effective $1 + 1$ dimensional problem, which can be canonically quantized. The Klein-Gordon equation is simply

$$\partial_u \partial_v \phi = \partial_U \partial_V \phi = 0 \ . \tag{1.1.4}$$

The infalling observer can expand the right-moving part of ϕ in modes of τ-frequency ν as

$$\phi(U) = \int_0^\infty \frac{d\nu}{2\pi\sqrt{2\nu}} \left(a_\nu e^{-i\nu U} + a_\nu^\dagger e^{i\nu U} \right) \ , \tag{1.1.5}$$

while the asymptotic one in terms of modes of t-frequency ω with a similar form as (1.1.5). Importantly, both expansions are not the same. This is just a consequence of the very non-linear relation between the time coordinates of both observers along an out-going null ray $d\tau = e^{-t/r_s} dt$.

Hawking, in his famous work [5], showed that the spectrum of particles that the asymptotic observer would detect is thermal

$$\langle \psi | \, b_\omega^\dagger b_{\omega'} \, | \psi \rangle = |T_\omega|^2 \frac{2\pi\delta(\omega - \omega')}{e^{\omega/T_H} - 1} \ , \tag{1.1.6}$$

where T_ω is the transmission amplitude, b_ω are the modes of the quantum fields with t-frequency ω, and $T_H = 1/4\pi r_s$ is the Hawking temperature. This result has a profound implication: black holes can emit radiation and evaporate. We can use the first law of thermodynamics to compute the black hole entropy

$$dS = \frac{dM}{T_H} = -\frac{dT_H}{8\pi G T_H^3} \to S_{BH} = \frac{\pi r_s^2}{G} = \frac{A_{\text{hzn}}}{4G} \ , \tag{1.1.7}$$

where A_{hzn} is the horizon area. Importantly, (1.1.7) is a 'coarse-grained' entropy, in the sense that it arises because we cannot keep track of all the variables of the problem. The proportionality between entropy and area was first proposed by Bekenstein [6] combining thermodynamics and thought experiments of matter

falling into a black hole. Moreover, he introduced the concept of "generalized entropy" as the sum of black hole entropy and matter entropy

$$S_{gen} = \frac{A_{\text{hzn}}}{4G} + S_{\text{out}} \ , \tag{1.1.8}$$

which satisfies the generalized second law

$$dS_{\text{gen}} \geq 0 \ . \tag{1.1.9}$$

Following the statistical interpretation of the entropy $S_{BH} = \log n$, with n the number of microscopic degrees of freedom of the system. The Bekenstein-Hawking formula (1.1.7) suggests that the microstates are localized on the event horizon. This counterintuitive property of black holes paved the way toward what we now know as the holographic principle, as we review in the next section.

1.2 Holographic Principle

The holographic principle answers the question: *what is the number of degrees of freedom of a fundamental system?* The number of degrees of freedom of a quantum system N is defined as the logarithm of the dimension of the Hilbert state

$$N := \ln \mathcal{N} = \ln \dim \mathcal{H} \ . \tag{1.2.1}$$

For example, a system with two spins would have $\mathcal{N} = 2^2$ states. By 'fundamental', we mean an abstract description of a quantum mechanical system, in a particular region of spacetime, down to its most basic constituents. Imagine for example that we take a local quantum field theory on a classical background spacetime satisfying Einstein's equations as a fundamental system. The number of degrees of freedom would be infinite in this case since there is one degree of freedom at each point of spacetime. However, we can get a finite estimate by introducing a cutoff of Planck length size. So we introduce a grid of width l_P with one oscillator per Planck volume. The total number of oscillators is V and each has n discreet number of states. Thus, the number of degrees of freedom is given by

$$N \sim V \ln n \gtrsim V \ . \tag{1.2.2}$$

Therefore, the number of degrees of freedom in local QFT then grows with the volume. Let us restrict to a finite spherical region with a surface area A. This imposes an infrared (IR) cut-off forbidding long wavelengths in the counting. Most of the states will come from very high-energy modes. However, a spherical surface cannot contain more mass than a black hole of the same area. We know that the entropy of a black hole is given by the Bekenstein-Hawking formula (1.1.7) and the number of states is then

$$N = \frac{A}{4} \ , \tag{1.2.3}$$

in Planck units. Therefore, we see that when we include the physics of black holes, the QFT overcounts the number of degrees of freedom. In fact, long before the quantum fields can be excited to very high energies, a black hole would form. If this black hole is contained in a spherical region of area A its entropy is given by (1.1.7). There is no quantum field theory that can do this, and a new theory should provide the UV completion.

The key element to argue that the total number of degrees of freedom of a fundamental system is in fact less than the field theory prediction is unitarity. Suppose that a region was described by a Hilbert space of dimension e^V, and suppose the region is converted to a black hole. According to the Bekenstein-Hawking entropy formula (1.1.7), the region is now described by a smaller Hilbert space of dimension $e^{A/4}$. The number of states then decreased, and it would not be possible to recover the initial state from the final one. Unitarity would be violated. Therefore, the Hilbert space must have had dimension $e^{A/4}$ to begin with.

Together unitarity and black hole physics led 't Hooft and Susskind to propose a more radical, "holographic" interpretation of the Bekenstein-Hawking formula. The Holographic principle [7, 8] (see [9] for a review):

"A region with boundary of area A is fully described by no more than $A/4$ degrees of freedom, or about 1 bit of information per Planck area. A fundamental theory, unlike local field theory, should incorporate this counterintuitive result."

Black holes have very intriguing features that make them the perfect theoretical lab to study quantum gravity. They are great theoretical tools to study features of quantum gravity. Perhaps, in the long-term, they will lead us to understand the quantum mechanical nature of spacetime.

As we review below, the AdS/CFT or holographic correspondence is the most explicit realization of the holographic principle.

1.3 AdS/CFT correspondence

The AdS/CFT correspondence can be understood as a *geometric implementation of the renormalization group* (see [10–12] for a review). Let us consider a local QFT_d at some energy scale μ. The idea is to promote the energy scale together with the other field theory coordinates, x^μ, to a new set of variables: (μ^{-1}, x^μ) where x^μ preserves its meaning but the energy scale becomes a spatial coordinate. It is convenient to denote it with the radial coordinate $z := \mu^{-1}$. The set $x^m := (x^\mu, z)$ coordinatizes a higher-dimensional spacetime. Of course, this statement would only be meaningful if x^m transforms appropriately under whatever the symmetries

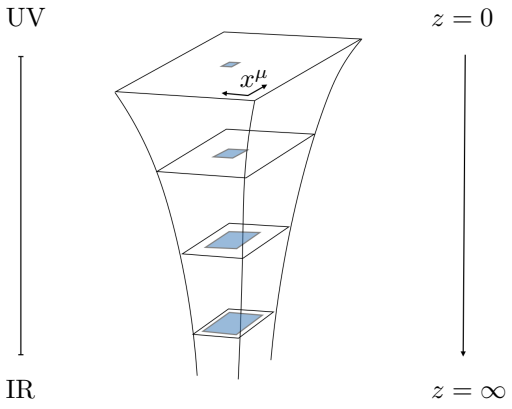

Figure 1.3: Higher dimensional spacetime that geometrizes the energy scale μ. Each slice at constant z_c defines a quantum field theory with coordinates x^μ. In blue, we exemplify how a small square of characteristic length $\mu_c = \ell_c^{-1}$ grows as we probe low energies.

of the theory are.

Every value of the energy scale defines a slice $z = \mu^{-1}$ in the $d+1$ spacetime. The set of all slices receives the name of bulk. We can visualize this higher dimensional space as an infinite pile of cards where at each value of its height there is a copy of the spacetime with coordinates x^μ. At the top ($z \to 0$) lies the UV of the theory while at the bottom ($z \to 0$) is the IR information. In other words, a localized excitation is located at the UV, at the so-called 'boundary' of the bulk. As this excitation is pushed into the bulk interior, it gets spread in the QFT over a bigger and bigger area.

The AdS/CFT correspondence states that there is a physical theory defined in the $d+1$ dimensional spacetime that captures the same information as the original QFT in d dimensions. In other words, the two theories are *dual* to each other.

Implicit in the duality statement is that physics is to some extent local along the radial direction. Local QFT operators $\mathcal{O}(x)$ would have a holographic bulk dual $\phi(x, z)$. Since the coordinates x^μ are common to both descriptions, both operators should transform in the same way under Lorentz transformations. An important operator that is present in all local QFT's is the stress-energy tensor $T_{\mu\nu}(x)$, its dual in the geometric description must be a spin two field $g_{mn}(x, z)$. It turns out that this field is nothing but the metric itself. The metric is a dynamical object that satisfies Einstein's equations, therefore the original QFT is dual to a theory where spacetime itself is dynamical, *i.e., a theory of quantum gravity.*

The AdS/CFT correspondence is the most explicit manifestation to date of the holographic principle. The term holographic is used in analogy to a two-dimensional hologram that captures three-dimensional information. Similarly, in the AdS/CFT duality the physics of the boundary theory is captured through an emergent higher-dimensional spacetime.

We can be more precise with the holographic statement. Consider a conformal field theory (CFT) defined in Minkowski space. The CFT vacuum $|0\rangle$, is not only Poincaré invariant but also invariant under reescalings $x^\mu \to \lambda x^\mu$ ($\lambda \in \mathbb{R}$). The energy scale gets also transformed as $\mu \to \mu/\lambda$. In the geometric picture, this implies the invariance under the joint transformation $x^m \to \lambda x^m$. The unique metric that respects these symmetries is the anti-de Sitter (AdS) spacetime.

$$ds^2 = \frac{\ell^2}{z^2}\left(-dt^2 + dx^2 + dz^2\right) \ , \tag{1.3.1}$$

where ℓ is the curvature radius. The metric (1.3.1) is a solution to Einstein's equations with a negative cosmological constant. Therefore, AdS spacetime is the 'geometrization' of a CFT in the vacuum state. The radial coordinate range is $z \in [0, \infty)$. The AdS boundary at $z = 0$ is located at an infinite proper distance. However, null geodesics reach the boundary at a finite time. Thus, the boundary can affect the physics in the bulk interior, and in defining any theory on this spacetime it will be important to specify boundary conditions at $z = 0$.

Not only the CFT vacuum can be geometrized, but also excited states on top of the vacuum. In the field theory, this can be realized by acting with operators $|\psi_\mathcal{O}\rangle := \mathcal{O}(x)\,|0\rangle$ on the original state. On the gravity side, the AdS geometry can be excited using the dual bulk operators $\phi(x, z)$. At high enough energies, the excited state $|\psi\rangle$ will look like the vacuum $|0\rangle$. This implies that whatever the new dual geometry is, close to the boundary it would look like AdS. Therefore, the class of geometries that would be dual to excited states $|\psi_\mathcal{O}\rangle$ are asymptotically AdS spacetimes with the correct matter content.

More generally, AdS/CFT relates quantum field theories on a rigid d-dimensional spacetime with string theory in certain curved backgrounds in $d + 1$ dimensions. The holographic duality was first discovered in the context of string theory. Maldacena conjectured that type IIB string theory on $\mathrm{AdS}_5 \times \mathcal{S}^5$ is dual to $\mathcal{N} = 4$ super Yang-Mills with gauge group $SU(N)$ in four spacetime dimensions. The relation between the parameters on both sides is

$$g^2_{\mathrm{YM}} = 4\pi g_s \ , \quad \lambda = \ell^4/l_s^4 \ , \tag{1.3.2}$$

where the 't Hooft coupling is defined as $\lambda := g^2_{\mathrm{YM}} N$, g_s and g_{YM} the gauge and string theory coupling constants respectively. The duality is valid for all values of

these parameters. However, we do not know how to quantize strings for all values of g_s. In order to have semi-classical control we need ℓ large in string units, which translates to $\lambda \gg 1$. On the other hand, to suppress quantum corrections, we need g_s small. Therefore, classical gravity is valid in the regime $N \gg \lambda \gg 1$. This shows another interesting feature of AdS/CFT, it is a *strong/weak coupling duality*: when the gauge theory is strongly-coupled (and hence perturbative techniques fail), we can study it using string theory in a semi-classical background.

A crucial entry in the holographic dictionary is the equivalence between partition functions that governed interactions on both sides

$$Z_{CFT}[J_I] = Z_{ST}[\phi_I \to \phi_I^{(0)}] \quad \text{for} \quad J_I(x) = \phi_I^{(0)}(x) \ , \tag{1.3.3}$$

where Z_{ST} is the string partition function with the appropriate boundary condition $\phi_I^{(0)}$ at the AdS boundary, which is identified with the source $J_I(x)$ of the dual operator $\mathcal{O}(x)$ with conformal dimension Δ. In fact, the dynamics of a massive bulk field $\phi(x,z)$ has two independent solutions, which behave like $z^{d-\Delta}$ and z^{Δ}, where

$$\Delta = \frac{d}{2} \pm \sqrt{\frac{d^2}{4} + \ell^2 m^2} \tag{1.3.4}$$

The non-normalizable mode defines the boundary value

$$\phi_I^{(0)}(x) := \lim_{z\to 0} z^{\Delta - d}\phi_I(x,z) \ , \tag{1.3.5}$$

while the normalizable mode corresponds to a different state in the field theory.

Since its discovery, the AdS/CFT correspondence has passed many precision tests and the zoo of examples is very rich. It has become the most powerful tool to study quantum gravity. This theoretical framework leads to profound consequences and insights for both sides. In one direction, holographic techniques give us a novel geometric approach to studying strongly-coupled phenomena in field theory. Going in the opposite direction, the boundary state of the quantum fields can be used to probe aspects of quantum gravity in the bulk. One of the most exciting challenges in holography is to understand the emergence of dynamic spacetime out of degrees of freedom living on a lower dimensional rigid background.

The holographic dictionary is still under construction and a very active area of research. In what follows, we introduce some examples that are relevant for this thesis.

1.3.1 Entanglement entropy

Entanglement represents a very counterintuitive feature of quantum mechanics. A simple example of an entangled state is a two-qubit system in the Hilbert space

$\mathcal{H} = \mathcal{H}_{\text{qubit}} \otimes \mathcal{H}_{\text{qubit}}$

$$|\psi\rangle = \frac{1}{\sqrt{2}} \left(|\uparrow\downarrow\rangle + |\downarrow\uparrow\rangle \right) \ . \tag{1.3.6}$$

More generally, if the state of the system is $|\psi\rangle$ and A a spatial region that divides the system in two parts, we can define the reduced density matrix on A but tracing out over the complement $\bar{A}$, $\rho := |\psi\rangle \langle\psi|$. The entanglement entropy is defined as the von Neumann entropy (or fine-grained entropy) $S_A := -\operatorname{Tr}(\rho_A \log \rho_A)$. It is a measure of the amount of correlation between A and $\bar{A}$. For example, for the state (1.3.6) the entropy of the qubit is $S_{\text{qubit}} = \log 2$.

A very deep connection between geometry and quantum information was pointed out in the context of holography by the Ryu-Takayanagi (RT) prescription [13], and its covariant generalization (the HRRT prescription) [14]. Consider a quantum field theory defined in the spacetime $\mathcal{B}$ on a particular excited state $|\psi\rangle$ whose gravity dual is denoted by M_ψ. We take a subregion on a particular Cauchy slice $\Sigma \subset \mathcal{B}$. This region can be either connected or a union of disconnected regions. The entanglement entropy of $A \subset \Sigma$ is given by the area of the minimal surface X_A of codimension two

$$S_A = \frac{\text{Area}(X_A)}{4G_N} \ . \tag{1.3.7}$$

The surface X_A satisfies various properties: 1) the boundaries of the surface X_A and region A coincide. 2) X_A is homologous to A, *i.e.,* the union $X_A \cup A$ form the boundary of some d-dimensional spacelike surface in M_ψ. 3) the surface X_A extremizes the area functional. If there are various saddles, we choose the surface with minimal area. The RT proposal (1.3.7) has been derived using the Euclidean path integral by applying the replica trick in bulk [15, 16].

In the case of a black hole in the bulk, this formula reproduces the Bekenstein-Hawking entropy formula (1.1.7). In this case, the surface X_A is nothing but the event horizon. In this way, the RT formula generalizes the Bekenstein-Hawking entropy formula for arbitrary subregions.

The RT formula captures the leading order result of the entropy in semiclassical gravity. Quantum corrections can be incorporated by adding the effect of the bulk fields living on the spacetime geometry [17]. The RT formula (1.3.7) gets then an extra contribution given by the generalized entropy [18]

$$S_{\text{gen}}(X) = \frac{\text{Area}(X)}{4G_N} + S_{\text{mat}}(X) \ , \tag{1.3.8}$$

where $S_{\text{mat}}(X)$ is a von Neumann entropy of bulk quantum fields on one side of X. When relevant, the quantum corrections would move the location of the original RT surface to the so-called: quantum extremal surface (QES) $\mathcal{X}$. The quantity

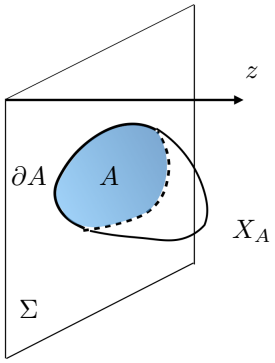

Figure 1.4: Ryu-Takayanagi surface, X_A, homologous to the region A.

(1.3.8) might look ambiguous, as its two constituents depend on regularization schemes. However, the generalized entropy is finite under RG flow [19].

Another equivalent formula is given by the maxi-min prescription [20]

$$S = \max_{\Sigma} \ \min_{X} \left(\frac{\text{Area}(X)}{4G_N} + S_{\text{mat}}(X) \right) \ , \tag{1.3.9}$$

where first we choose a particular Cauchy slice $\Sigma \subset \mathcal{B}$ and minimize the generalized entropy. Then we maximize among all possible choices of Cauchy slices.

When quantum corrections are small, the RT surface coincides with the QES location. However, when a large amount of bulk entanglement is comparable to the Bekenstein-Hawking entropy the location of the QES will move. One example of such a physical situation occurs in evaporating black holes. After some time, the entanglement produced by the Hawking pairs of radiation become important in comparison with the Bekenstein-Hawking entropy of the original black hole [21,22]. This phenomenon was crucial to deriving the so-called island formula [23] that we will review below.

1.3.2 Black holes in AdS

The Schwarzschild AdS geometry describes a spherical black hole in global AdS coordinates given by

$$ds^2 = -f(r)dt^2 + \frac{dr^2}{f(r)} + r^2 d\Omega_{d-1}^2 \ , \quad f(r) = 1 + \frac{r^2}{\ell^2} - \frac{\mu}{r^{d-2}} \ , \tag{1.3.10}$$

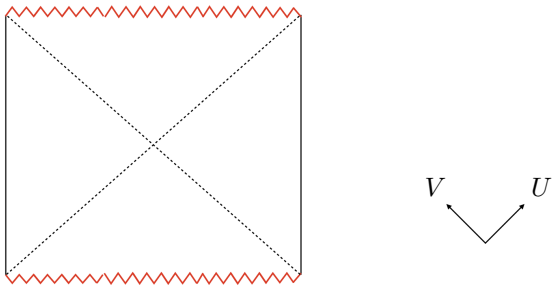

Figure 1.5: Penrose diagram for the extended BTZ black hole. The two vertical lines represent the AdS boundaries.

where μ is proportional to the mass. The solution has a regular horizon for any $\mu > 0$. The black hole mas has the form

$$M = \frac{(d-1)\Omega_{d-1}\mu}{16\pi G} \ . \tag{1.3.11}$$

Let us focus on the AdS_3 case for simplicity. Introducing Kruskal coordinates

$$U = -e^{\frac{r_* - t}{2}} \ , \quad V = e^{\frac{r_* + t}{2}} \ , \tag{1.3.12}$$

the metric becomes

$$ds^2 = \frac{-4\ell^2 dU dV + r_h^2 (1 - UV)^2 d\phi^2}{(1 + UV)^2} \ , \tag{1.3.13}$$

where r_h is the horizon radius, ℓ is the AdS radius and ϕ should be periodically identified as $\phi \sim \phi + 2\pi$. The two horizons are located at $U = 0$ and $V = 0$, the boundaries at $UV = -1$, and at $UV = 1$ the two singularities (see Figure 1.5).

On the other hand, let us take two identical CFT_2 with temperature β in a particular entangled state

$$|TFD\rangle := \frac{1}{\sqrt{Z}} \sum_n e^{-\beta E_n/2} \, |n\rangle_L \otimes |n\rangle_R \ , \tag{1.3.14}$$

the thermofield double state where $|n\rangle_{L,R}$ are energy eigenstates of the left and right CFT's with energy E_n.

Maldacena made the following proposal [24]: "two copies of the CFT in the particular pure (entangled) state (1.3.14) is approximately described by gravity on

the extended AdS Schwarzschild spacetime (1.3.13)." Entanglement is the key ingredient that allows the dual bulk geometry to be connected by an Einstein-Rosen bridge [25].

1.3.3 Traversable wormholes

Notice the following interesting property of the extended geometry (1.3.13). It contains a marginally traversable wormhole, as signals sent early enough from the right boundary almost make it to the second asymptotic boundary. How can we make the wormhole traversable?

Recently, it was shown by Gao-Jafferis-Wall (GJW) that traversable wormholes can be constructed in the context of holography [26]. The idea is to include in the action a non-local coupling between the two causally disconnected boundaries. Turning on a relevant double trace deformation of the form

$$\delta S = \int dt d\phi \; h(t,\phi)\mathcal{O}_R(t,\phi)\mathcal{O}_L(-t,\phi) \; , \tag{1.3.15}$$

where $\mathcal{O}_{R,L}$ are local operators in the Right and Left asymptotic boundary, resulting in a stress tensor that violates the average null energy condition (ANEC)

$$\int d\lambda \; T_{\mu\nu}k^\mu k^\nu \geq 0 \; , \tag{1.3.16}$$

where k^μ is the tangent vector to a null congruence of geodesics parametrized by λ. The violation of condition (1.3.16) is needed for the null rays to defocus allowing for a wormhole to 'open up' (see Figure 1.6). These wormholes are so-called 'long' wormholes, since they do not lead to causality violations in the ambient space.

The backreacted geometry can be computed in perturbation theory and will include a shifted horizon that allows signals to travel from one side to the other, *i.e.,* a traversable wormhole has been formed as a consequence of (1.3.15). A physical quantity that can be computed is the wormhole opening

$$\Delta V = 4\pi G_N \int dU \langle T_{UU} \rangle \; . \tag{1.3.17}$$

Traversable wormholes are the subject of Chapter 2, where we construct a static traversable wormhole in AdS_4 implementing the GJW protocol.

1.3.4 Modular Berry phases

Another interesting quantity in the holographic dictionary is the concept of modular Berry phase. As we will review below, it makes manifest the connection between entanglement and the connectivity of spacetime.

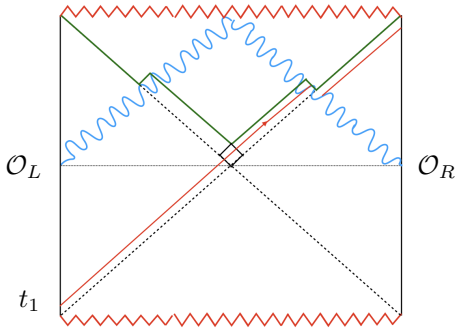

Figure 1.6: Penrose diagram of the traversable wormhole as result of the non-local deformation (1.3.15). In blue the negative energy shocks. In green we depict the backracted horizon. A signal (red) is sent at time t_1 through the wormhole from the left boundary to the right.

In quantum mechanics, the Berry phase of a system, $|\psi\rangle$, is the holonomy developed when it undergoes cyclic evolution. If the Hamiltonian of the system $H(\lambda)$ varies adiabatically and $|\psi\rangle$ is an eigenstate during the whole evolution, then as a result of a parallel transport along a closed loop, the state vector can 'rotate' with respect to its original direction. Therefore, it accumulates a holonomy [27]

$$\gamma_{\text{Berry}} = -i \oint d\lambda \langle \psi(\lambda) | \dot{\psi}(\lambda) \rangle \ . \tag{1.3.18}$$

Let us now consider a quantum field theory in the state state $\rho = WW^\dagger$. We can define a transport problem by slowly transforming the matrix $\rho(\lambda)$. Operators Q_i that commute with $\rho(\lambda)$ are called *modular zero modes*. The unitary flow generated by zero modes defines a symmetry within subregion A under which operators $\mathcal{O}$ restricted to A transform as

$$\mathcal{O} \to U_Q^\dagger(s_i)\ \mathcal{O}\ U_Q(s_i) \ , \quad \forall\ \mathcal{O} \in \mathcal{A}_A, \tag{1.3.19}$$

where U_Q is the unitary associated with Q_i. This represents a gauge symmetry in the choice of zero-mode frame[1]. The main idea in [28, 29] is that entanglement allows for a notion of connection that renders the relative zero-mode frames physical after parallel transport. The parallel transport problem [30] can be defined by requiring for all λ that $V(\lambda)$ has no zero modes and the density matrix changes as

$$d\lambda\, [V(\lambda), \rho(\lambda)] = \rho(\lambda + d\lambda) - \rho(\lambda) + \text{zero modes of } \rho(\lambda) \ . \tag{1.3.20}$$

[1]Similar to the freedom in the choice of Lorentz frame in General Relativity.

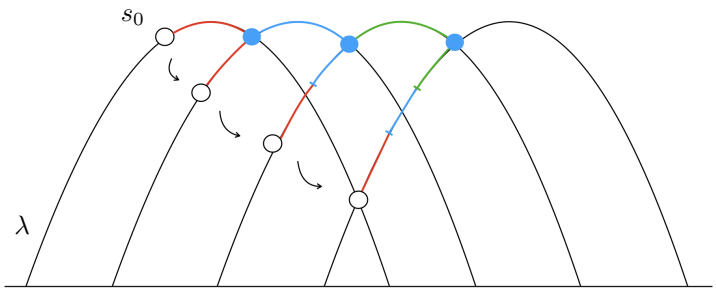

Figure 1.7: Modular transport in AdS_3.

These conditions imply that a projector onto zero modes exists: $P_0[V(\lambda)] = 0$. The operator $V(\lambda)$ will then generate the parallel transport acting like

$$W(t+dt) = (1 + V(\lambda(t))dt)W(t) \ , W(0) = W_{\text{initial}} \ . \tag{1.3.21}$$

Taking a closed loop, the Berry operator relates initial and final W's

$$W_{\text{final}} := \Gamma_{\text{Berry}} W_{\text{initial}} = P \ e^{\oint d\lambda V(\lambda)} W_{\text{initial}} \ . \tag{1.3.22}$$

We then see that the game in town is to find the 'golden' $V(\lambda)$ that has no zero modes and generates the berry transport (1.3.22). The parallel transport equations can also be recast in terms of the family of modular Hamiltonians $H_{\text{mod}} := -\log \rho$ as

$$d\lambda \, [V(\lambda), H_{\text{mod}}(\lambda)] = H(\lambda + d\lambda) - H_{\text{mod}}(\lambda) + \text{zero modes of } H_{\text{mod}}(\lambda) \ . \tag{1.3.23}$$

We can give a simple holographic interpretation of the parallel transport problem in the case of AdS_3. Let us take a particular Cauchy slice at some time $t = t_0$. λ, in this case, parametrizes a family of intervals in the CFT_2. Consider the family of bulk geodesics $\lambda(\sigma)$ such that for a closed loop they intersect for all values of σ. By subregion duality, the modular zero modes are symmetries of the associated entanglement wedge $W(A)$. Between neighboring geodesics λ and $\lambda + \delta\lambda$, they map the entanglement wedge $W(\lambda)$ into $W(\lambda + d\lambda)$. Let us focus on the intersection point between two neighbouring geodesics. The condition (1.3.23) would imply that this point is mapped to a different point on the new entanglement wedge. This new point can also be reached by a diffeomorphism of $W(\lambda + \delta\lambda)$, *i.e.,* by the action of a zero-mode of $W(A)$. This possibility is forbidden by the

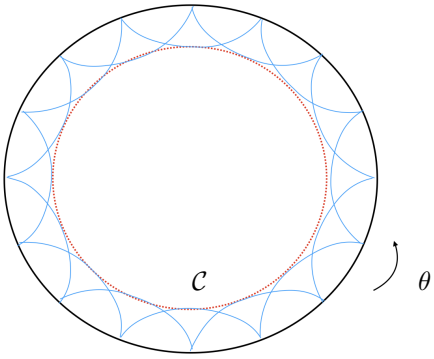

Figure 1.8: Modular transport in AdS_3.

requirement that $V(\lambda)$ does not contain zero-modes. Therefore, the transport equations (1.3.23) imply that the intersection point is kept fixed (see Figure 1.7). The generator of the modular transport would then act as a rotation about the intersection point $V \sim \partial_\theta$.

When transporting along a closed loop this implies a condition of 'rolling without slipping' on the common envelope curve (see Figure 1.8). Let us see what happens to a particular point $s = s_0$ on λ. At the end of the transport, such a point displaces an amount equal to the length of the bulk curve $\mathcal{C}$. The Berry transport then coincides with another interesting quantity called differential entropy [31] derived using the same family of CFT_2 intervals or, equivalently, the set of tangent geodesics to the curve $\mathcal{C}$

$$L[\mathcal{C}] = \frac{1}{2}\int_0^{2\pi} d\theta \frac{\partial S(\alpha)}{\partial \alpha} \ , \tag{1.3.24}$$

where $\alpha(\theta)$ parametrizes the family of tangent geodesics to $\mathcal{C}$. In this way, differential entropy is a particular example of a modular Berry phase. More generally, the bulk modular Berry connection, Γ_{Berry}, relates different modular frames associated with neighboring entanglement wedges in an arbitrary CFT state. It was shown in [32], how the Berry curvature computes the bulk Riemann curvature close to the RT surfaces.

In Chapter 3, we study modular transport as a result of a change in the global CFT state. In the bulk, we relate the Berry curvature to the symplectic form for a Euclidean conical singularity geometry obtained from the backreaction of a cosmic brane.

1.4 Information Paradox

It is a basic principle of quantum mechanics that pure states always evolve into pure states in unitary systems. Hawking, in his famous work [33], posited a puzzle for the unitary evolution of an evaporating black hole (see [34] for a review).

In Section 1.1.1, we reviewed in some detail Hawking's conclusion that a black hole radiates. The reason for the thermal aspect of the final state is due to the short-range entanglement between Hawking pairs. Intuitively, the original vacuum state contains Hawking pairs that are being created and annihilated. The black hole horizon causally separates the interior ingoing Hawking modes from the outgoing quanta, *i.e.,* those modes that escape to asymptotic infinity. The two particles are entangled forming a pure state. However, the asymptotic observer only has access to the outgoing radiation looking like a thermal state at Hawking temperature $T_H = 1/4\pi r_s$.

Suppose that we start outside of the black hole with a pure state consisting of a large number of N EPR pairs. Some of these particles fall into the black hole while others escape to infinity. We then have a large amount of entanglement

$$S_{\text{out}} = N \log 2 \ . \tag{1.4.1}$$

Let the black hole completely evaporate. The amount of entanglement cannot decrease due to causality. We end up with a bunch of Hawking quanta in a highly mixed state with total entropy (1.4.1). The information associated with the entropy increases when a black hole evaporates as well as the information falling into the black hole is then lost forever. This is the so-called 'information paradox.'

One might argue that something very dramatic happens to the state of the system when the black hole has Planckian size. However, the information problem happens way before the black hole has completely evaporated. We run into trouble as soon as the entropy of radiation is bigger than the thermodynamic entropy of the black hole. Simply because the number of states in the radiation would be bigger than what the black hole has room for. In fact, for ordinary quantum systems, the maximum fine-grained entropy at a given energy is the thermodynamic entropy (a coarse-grained entropy). A black hole should not be the exception.

To restore unitarity in the evaporating process, the entropy of radiation should follow the so-called Page curve [35]. At early times, the radiation entropy increases due to the Hawking effect, while the Bekenstein-Hawking entropy decreases as the horizon shrinks. Then at a particular time t_P, called the Page time, the decreasing black hole entropy equals the radiation entropy. If the final state of the Hawking radiation is to be pure, as unitarity would demand, then the entropy must drop

to zero when the black hole completely evaporates. Roughly around the midpoint of the life of the black hole, then the Page curve follows the Bekenstein-Hawking entropy curve down to zero.

The AdS/CFT correspondence supports the idea that information is not lost. We can see this through a simple thought experiment. Imagine that we inject high-energy particles with total energy less than the transition to a stable black hole in AdS. They will form a dynamical black hole that will then decay. This whole process has a holographic dual, which by unitarity of the boundary CFT implies that information must be preserved at the end of evaporation. A more refined version of the paradox was formulated by Maldacena in the case of an eternal black hole in [24].

Even if we restrict to holographic theories, boundary unitarity does not answer various questions: how is the information preserved? how to recover the Page curve in semiclassical gravity? What part of the black hole interior is encoded outside and where? It was not until recent years that the island formula shed light on resolving various aspects of the information paradox.

1.4.1 Entanglement islands

The Hawking information paradox has been a puzzle for many years. Since Hawking's derivation only relies on gravity as an effective field theory, it is very difficult to pin down what goes 'wrong' in the derivation. In recent years, a gravitational formula for the fine-grained entropy of Hawking radiation (the *Island formula*) was derived using gravitational path integral methods [23, 36]. Hawking's computation is corrected by non-perturbative gravitational effects: *Euclidean replica wormholes*. These new saddles were shown to be dominant after the Page time, and reproduce the Page curve for evaporating black holes.

Let us state the island formula and apply it to the case of an evaporating black hole. The Island formula for the fine-grained entropy is given by

$$S(\mathbf{R}) = \min_{I}\Big\{\operatorname*{ext}_{I}\Big[\frac{\text{Area}(\partial I)}{4G_N} + S_{\text{mat}}(R\cup I)\Big]\Big\}\,, \tag{1.4.2}$$

where $\text{Area}(\partial I)$ is the area of the boundary of the island I (the QES), R the region that collects radiation (commonly defined in the region where gravity is not important), and $S_{\text{mat}}(R\cup I)$ is the entropy of the quantum fields on the union of the regions R and I (*i.e.,* the exterior of the QES). The formula instructs us to extremize and minimize over all possible islands.

Consider a black hole formed from the spherical collapse of a pure state $|\psi\rangle$. Imagine slicing the black hole geometry with so-called 'nice slices', *i.e.,* Cauchy

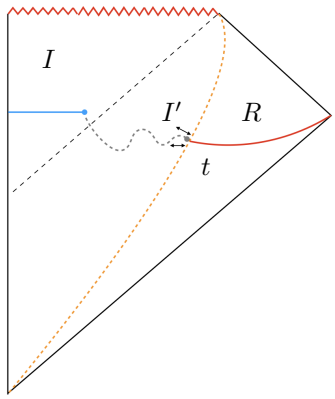

Figure 1.9: Penrose diagram for an evaporating black hole. The cutoff surface is shown in orange. The region R (red) is defined in the asymptotically flat region on the Cauchy slice at time t. The candidate surface $\partial I'$ (gray) is deformed until find the surface ∂I (blue) that extremizes (1.4.2).

slices that stay away from the singularity in all regions. At each particular slice, we can define the regions involved in (1.4.2). Region R can be defined by introducing a cutoff surface far away from the black hole. Starting from the cutoff surface, we introduce a candidate island region I'. The idea is then to move the location of $\partial I'$, even across the black hole interior, until we achieve the extremization of (1.4.2) at ∂I (see Figure 1.9). At very early times, the configuration that dominates is the empty set $I = \emptyset$, giving an entropy contribution that starts at zero and grows monotonically. Shortly after the black hole forms, a non-empty island I emerges in the black hole's interior. Roughly around half of the life of the black hole, the non-empty island I dominates. At late times, the island is very close to the black hole horizon. Its area is given approximately by the horizon area while the matter entropy is almost zero since we are including almost all the modes in I that purify the Hawking partners in R, *i.e.,* $S_{\text{mat}}(I \cup R) \approx 0$. The fine-grained entropy then decreases as the black hole completely evaporates. In this way, the island formula correctly reproduces the Page curve.

After the Page time, most of the black hole interior is contained in the island. The state of the black hole interior is then encoded in the radiation region R where gravity is unimportant. This conclusion can be derived formally within the framework of quantum error correction. A simple way to see this is to consider a Bell state with one qubit in the region R and its entangled partner in the region I. Clearly, this pair does not contribute to $S_{\text{mat}}(I \cup R)$, nor $S(\mathcal{R})$, because together the pair is a pure state. Since entanglement between R and I does not contribute

Figure 1.10: Before the Page time at very early time $t_1 \ll t_P$, the empty island $I = \emptyset$ dominates. After the Page time $t_2 > t_P$, a non-empty island ∂I emerges. Most of the black hole interior is encoded in the entanglement of radiation shown in blue. The entanglement wedge associated with the black hole degrees of freedom is depicted in green.

to the entropy, it must be the case that I is secretly encoded in R. This is similar to a holographic duality but in the same number of spacetime dimensions.

It is important to emphasize that the left hand side of (1.4.2) is the full entropy of radiation while the right hand side is defined in the semiclassical description. It is surprising that the island formula computes the entropy of the exact state of the quantum system only using gravity as an effective field theory.

One of the main obstructions to find islands in more general backgrounds is the computation of the bulk entropy in (1.4.2). In higher-dimensions, for example, this represents a serious challenge. This problem was overcome in [37] by introducing three simple necessary conditions for the existence of islands in any given spacetime and quantum state. In the last Chapter 4, we discuss the possible existence of islands in the cosmological context by applying this criteria.

1.5 Outline

This thesis is devoted to studying three aspects of holographic entanglement entropy introduced above.

In Chapter 2, we discuss the topic of traversable wormholes. Entanglement is a key feature of the teleportation protocol [38] that allows sending information from one asymptotic boundary to the other. We present the paper [1], were we use the Gao-Jafferis-Wall protocol [26] to construct a four-dimensional asymptotically anti-de Sitter (AdS) *eternal* traversable wormhole. From the boundary point of view, we identify a family of Hamiltonians consisting of two copies of a conformal field theory (CFT) coupled with simple local interactions whose ground state is dual to

the traversable wormhole solution. As the ground state of a simple Hamiltonian, it may be possible to make these wormholes in the lab or on a quantum computer.

Modular Berry phases are the topic of Chapter 3, which is based on the paper [2]. In the context of AdS_3/CFT_2, we studied the parallel transport of modular Hamiltonians governed by a global state change. This *state-changing* transport contrasts to the original *shape-changing* situation considered in [32], where the state is held fixed while the interval location is varied. We found that the Berry curvature for a fixed interval and changing state computes the symplectic form for a Euclidean conical singularity geometry obtained from the backreaction of a *cosmic brane*.

Finally, Chapter 4 discusses the subject of entanglement islands [21,22]. Island regions have brought new insights into the resolution of some aspects of the black hole information paradox and give an explicit realization of the ER=EPR proposal [39]. For an evaporating black hole, the entropy of Hawking radiation increases with time causing information loss at the end of evaporation. These novel disconnected regions of spacetime contribute to the entanglement entropy reproducing the Page curve in agreement with unitarity. It is natural to wonder if islands can exist in cosmological spacetimes. In the paper [3], we address whether entanglement islands can exist in Friedmann-Robertson-Walker (FRW) cosmologies supported by thermal radiation, cosmological constant Λ, and non-zero spatial curvature. We use the necessary criteria presented in [37]. Looking at both open and closed universes, we conclude that the key ingredient that allows the existence of islands is the negative cosmological constant. These regions are encoded in non-gravitating regions of ancillary systems.

We conclude this thesis by making some final remarks and directions to pursue in the future.

2 Eternal AdS_4 Wormholes from Coupled CFT's

2.1 Introduction and Results

Wormholes have been a puzzling topic for physicists for a century. Many efforts have been made to build traversable wormholes using different kinds of fields and techniques, most of which require either the insertion of exotic matter [40–46] or higher derivative theories [47–50] which lack UV completions [51].

Recent work has shown how to build traversable wormholes in physically sensible theories. Gao, Jafferis, and Wall (GJW) [52] showed how to make asymptotically AdS black holes traversable for a short time by coupling the boundaries to each other. This approach has been extended in a number of other works since then [38, 53–67]. The first eternal traversable wormhole was constructed by Maldacena and Qi [68] in asymptotically nearly-AdS_2 spacetime. More recently, Maldacena, Milekhin and Popov [69] found a long-lived $4D$ asymptotically flat traversable wormhole solution in the Standard Model (see also [70]).

In this paper, we make use of the ingredients developed by GJW and MMP in order to construct an eternal traversable wormhole in asymptotically AdS_4 spacetime. Our motivation is twofold. First, by constructing wormholes in asymptotically AdS spacetime, we can use AdS/CFT to learn more about them. Second, our wormhole solution can be used to learn more about CFT's. To this end, we identify a family of Hamiltonians consisting of two copies of a CFT coupled by simple, local interactions whose ground state is dual to the traversable wormhole.

This last point is significant for constructing traversable wormholes in a lab or on a quantum computer. Some very interesting ideas on how to do this are described in [71–73]. Given access to a holographic CFT, one simply needs to implement the coupling and allow the system to cool to its ground state, which is dual to a traversable wormhole.

Concretely, the bulk theory we consider is described in Section 2.2 and consists of

Einstein-Maxwell theory with negative cosmological constant, a $U(1)$ gauge field and massless Dirac fermions coupled to the gauge field. A particular solution is the magnetically charged Reissner-Nordström (RN) black hole. Due to the magnetic field, the charged fermions develop Landau levels. The lowest Landau level has exactly zero energy on the sphere, so we can think of them as effectively $2D$ fermionic degrees of freedom once we dimensionally reduce on the sphere.

The classical solution consists of two magnetically charged RN black holes connected through an Einstein-Rosen bridge which is non-traversable. The traversability of the wormhole is achieved by introducing a coupling between the two CFT's (labelled L, R) of the form

$$S_{\text{int}} = i \int d^3x \; h \left(\bar{\Psi}_-^R \Psi_+^L + \bar{\Psi}_+^L \Psi_-^R \right) \; . \tag{2.1.1}$$

Here Ψ^R is the bulk field at the right boundary that is dual to the charged fermions in the right CFT, and Ψ^L is defined analogously. Note that this is a local coupling involving a single, low dimension operator in each CFT; this contrasts with the beautiful construction of Maldacena and Qi [68] in the AdS_2 context, where a large number of operators must be coupled.

In Sections 2.2.3 and 2.2.4, we describe how this interaction has the effect of modifying the boundary conditions and the vacuum state. The stress tensor receives a quantum correction of the form

$$\langle T_{++}(x) \rangle = -\frac{1}{2\pi^3} \frac{q\lambda(h)}{R^2} \; , \tag{2.1.2}$$

where R is the sphere radius, q is the charge of the black hole, and λ is given by (2.2.33). For small coupling h, $\lambda(h) \approx h$, but our analysis remains valid for *finite* h. A priori it is not clear whether a self-consistent solution exists in which the negative null energy supports a traversable wormhole. Since it is only the quantum correction that has a chance of making the wormhole traversable, the quantum effects have a large backreaction on the metric.

Typically, this would constitute an intractable problem: we cannot calculate the quantum state, and hence the stress tensor, until we know the geometry, but on the other hand we cannot solve the Einstein equations to determine the geometry until we know the stress tensor. In this case, we are able to self-consistently solve the system because the stress tensor takes a particularly simple form, depending locally on the metric (up to an overall factor).

In Section 2.3, we discuss properties of both the linearized and non-linear solutions. The wormhole geometry has the following two regimes. The middle of the wormhole is nearly $AdS_2 \times \mathcal{S}^2$. As we move away from the middle of the wormhole, the geometry smoothly interpolates to the near-extremal region of two RN

black holes. Far away, the quantum contribution (2.1.2) becomes negligible and the geometry is that of two magnetically charged RN black holes (see Fig. 2.2).

As a consequence of the boundary perturbation, the mass of the wormhole is slightly *decreased* by a term proportional to the coupling

$$M = M_{\text{ext}} + \Delta M \ , \quad \text{with} \quad \Delta M \sim -\lambda^2(h) \ . \tag{2.1.3}$$

An infalling observer will experience that she is approaching a naked singularity from infinity. All of a sudden, deep in the throat region, the wormhole opens up and she comes out to the other side safely.

In Section 2.4.1, we identify a simple Hamiltonian whose ground state is dual to the wormhole. The procedure is to begin with two identical holographic CFT's, each with a global $U(1)$ symmetry, so that they are dual to Einstein-Maxwell theory at low energies. We then turn on a chemical potential for each CFT separately, and turn on a coupling of the form $\bar{\mathbf{\Psi}}^R \mathbf{\Psi}^L$ where the $\mathbf{\Psi}$ operators are dual to a bulk massless charged fermion.

Concretely, the Hamiltonian we analyze is

$$H = H_L + H_R + \mu(Q_L - Q_R) - \frac{ih}{\ell} \int d\Omega_2 \left(\bar{\mathbf{\Psi}}^R_- \mathbf{\Psi}^L_+ + \bar{\mathbf{\Psi}}^L_+ \mathbf{\Psi}^R_- \right) \ , \tag{2.1.4}$$

This Hamiltonian is similar to the construction of Cottrell et al [74]. The authors showed that the Hamiltonian in their case has the thermofield double state as its ground state. That construction, however, did not have a semiclassical gravity dual.

We show that the ground state of this theory is dual to our eternal traversable wormhole geometry for some range of the coupling h and chemical potential μ. We compare the wormhole to other geometries with the same boundary conditions, which may dominate the ensemble. In particular, we consider two disconnected black holes and empty AdS. We compute the ground state for different values of the parameters h and μ, and find that the wormhole is the ground state for $h > h_c$ and $\mu > \mu_c$, with the critical values given by

$$h_c = \frac{\bar{r}^2}{G_N q} \sqrt{\frac{2\pi}{3\mathcal{C}} \left(1 + \frac{2\bar{r}^2}{\ell^2} \right)} \ \text{ and } \ \mu_c = \sqrt{\pi} m_p \ , \tag{2.1.5}$$

with m_p the Planck mass. Interestingly, as the non-local coupling vanishes, there is a triple point located at $h = 0$, $\mu = \mu_c$ where the three phases meet. For values $h < 0$, the ground state is dominated by either empty AdS or the black hole phase.

The challenge of building a traversable wormhole is to have enough negative energy to allow defocusing of null geodesics, allowing the sphere to contract and

re-expand. Here we have added two ingredients so that the bulk dual remains semiclassical. First, the chemical potential makes the decoupled system closer to being traversable, since the near-horizon geometry for an extremal black hole is $AdS_2 \times S^2$. Because the size of the sphere is constant near the horizon, a small amount of negative energy will allow the sphere to re-expand, and render the wormhole traversable[1]. Second, by using bulk charged fermions in combination with a magnetically charged black hole, as was done in MMP [69], we enhance the negative energy due to the quantum effects. The key point is that a single 4d charged fermion acts like a large number q of 2d light charged fields due to the large degeneracy of lowest Landau levels.

Note: We understand that overlapping results will appear in [75]. We thank S. Banerjee for discussions. Also, [76] appeared very shortly before this work. There, asymptotically AdS_4 wormholes are also constructed, but with rather different ingredients. In addition, the solutions of [76] have different symmetries than our solution: they preserve the full Poincaré invariance in the boundary directions. It would be interesting to understand the relationship between the two constructions better. We thank M. Van Raamsdonk for discussions.

2.2 Massless fermions in AdS_4

We start this section by describing the particular theory of interest, as well as setting up the notation and conventions of spinors in curved space. Afterwards, we describe how the boundary conditions change once we couple the asymptotic boundaries. Finally, we compute the resulting stress tensor.

2.2.1 Dynamics

The theory consists of Einstein-Maxwell gravity with matter described by the action

$$S = \int d^4x\sqrt{g}\left(\frac{1}{16\pi G_N}(R-2\Lambda) - \frac{1}{4g^2}F^2 + i\bar{\Psi}\not{D}\Psi\right) . \tag{2.2.1}$$

In particular, we are considering a single massless Dirac fermion of charge one. In this section, we follow the approach and conventions of [69].

We consider g to be small, so that loop corrections are suppressed. A general class of spherically symmetric solutions with magnetic charge, denoted by the integer q, can be parametrized as follows

$$ds^2 = e^{2\sigma(x,t)}(-dt^2+dx^2) + R^2(x)\ d\Omega_2^2 , \quad A = \frac{q}{2}\cos\theta d\phi . \tag{2.2.2}$$

[1] We thank Daniel Jafferis for suggesting this approach.

Note that in this metric the range of x is compact and fixing this range can be seen as a gauge choice. For now we use $x \in [0, \frac{\pi}{2}]$. To have a well-defined representation of the Clifford algebra at each point of the spacetime we introduce the vierbein

$$e^1 = e^\sigma dt, \quad e^2 = e^\sigma dx, \quad e^3 = R d\theta, \quad e^4 = R \sin\theta d\phi \ . \tag{2.2.3}$$

and by solving

$$de^a + \omega^{ab} \wedge e^b = 0, \qquad \omega^{ab} = -\omega^{ba} \ , \tag{2.2.4}$$

we compute the spin connection components

$$\omega^{12} = \sigma' dt + \dot{\sigma} dx, \ \ \omega^{32} = R' e^{-\sigma} d\theta, \ \ \omega^{42} = R' \sin\theta e^{-\sigma} d\phi, \ \ \omega^{43} = \cos\theta d\phi \ . \tag{2.2.5}$$

Here a prime denotes a derivative with respect to x, while a dot denotes a derivative taken with respect to t. We use the following basis for the gamma matrices in flat space

$$\gamma^1 = i\sigma_x \otimes 1, \quad \gamma^2 = \sigma_y \otimes 1, \quad \gamma^3 = \sigma_z \otimes \sigma_x, \quad \gamma^4 = \sigma_z \otimes \sigma_y \ . \tag{2.2.6}$$

In this basis the Dirac operator has the form

$$\begin{aligned} \not{D} =& e^{-\sigma} \Big[i\sigma_x \Big(\partial_t + \frac{\dot{\sigma}}{2} \Big) + \sigma_y \Big(\partial_x + \frac{\sigma'}{2} + \frac{R'}{R} \Big) \Big] \otimes 1 \\ &+ \frac{\sigma_z}{R} \otimes \Big[\sigma_y \frac{\partial_\phi - iA_\phi}{\sin\theta} + \sigma_x \Big(\partial_\theta + \frac{1}{2} \cot\theta \Big) \Big] \ . \end{aligned} \tag{2.2.7}$$

In the static case, the metric (2.2.2) has two Killing vectors ∂_t and ∂_ϕ. Introducing the following ansatz will allow us to decompose in Fourier modes on the sphere $\mathcal{S}^2$,

$$\Psi = \frac{e^{-\frac{\sigma}{2}}}{R} \sum_m \psi^m(t,x) \otimes \eta^m(\theta,\phi) \ . \tag{2.2.8}$$

Here ψ^m and η^m are bi-spinors. In the rest of the paper we will suppress the indices on ψ. In this ansatz the Dirac equation is given by

$$\begin{aligned} \frac{e^{-\frac{3}{2}\sigma}}{R} \left(i\sigma_x \partial_t + \sigma_y \partial_x \right) \psi \otimes \eta &= -\lambda \ , \\ \frac{e^{-\frac{\sigma}{2}}}{R^2} \sigma_z \psi \otimes \left(\sigma_y \frac{\partial_\phi - iA_\phi}{\sin(\theta)} + \sigma_x \left(\partial_\theta + \frac{1}{2} \cot(\theta) \right) \right) \eta &= \lambda \ . \end{aligned} \tag{2.2.9}$$

Restricting to the lowest Landau level decouples the equations and admits solutions of the form

$$\psi_\pm = \sum_k \alpha_k^\pm \ e^{ik(t \mp x)} \ , \quad \eta_\pm^m = \Big(\sin\frac{\theta}{2} \Big)^{j_\pm \pm m} \Big(\cos\frac{\theta}{2} \Big)^{j_\pm \mp m} e^{im\phi}, \quad j_\pm = \frac{1}{2}(-1 \mp q) \ , \tag{2.2.10}$$

where $\psi_\pm$ are the components of ψ, and we choose $\sigma_z\eta_\pm = \pm\eta_\pm$ as the basis for η. If we take $q > 0$, the solution is

$$\eta_+ = 0, \quad \eta_- = \sum_m \mathcal{C}^j_m \eta^m_-, \quad -j \leq m \leq j \ , \tag{2.2.11}$$

where we define the quantum number $j := j_-$, so that in the lowest Landau level the degeneracy of the two-dimensional fields is q. The normalization constant is given by

$$(\mathcal{C}^j_m)^2 = \frac{1}{2}\frac{\Gamma(2+2j)}{\Gamma(1+j-m)\Gamma(1+j+m)} \ , \tag{2.2.12}$$

so that

$$\int d^2\Omega \ \bar{\eta}^{m_1}\eta^{m_2} = \delta_{m_1 m_2} \ . \tag{2.2.13}$$

2.2.2 Boundary conditions

According to the AdS/CFT dictionary, a bulk Dirac spinor of mass m is dual to a spin 1/2 primary operator $\mathcal{O}$ of conformal dimension

$$\Delta_\pm = \frac{3}{2} \pm \sqrt{m^2\ell^2} \ , \tag{2.2.14}$$

where ℓ is the AdS radius [77,78]. The stability bound requires $m \geq 0$ [79]. When applying the correspondence, we should consider that the first order nature of the Dirac action goes hand in hand with the different dimensionality between the bulk and boundary spinors. The extrapolate dictionary instructs us to identify the two bulk chiral components with the same boundary field. In addition, when solving the Dirichlet boundary value problem, we should impose boundary conditions only on half of the spinor degrees of freedom. Our gamma matrix in the holographic radial direction satisfies $(\gamma^2)^2 = 1$ and $(\gamma^2)^\dagger = \gamma^2$. We can then decompose the bulk fermions onto the eigenspace of γ^2

$$\Psi_\pm := \mathcal{P}_\pm\Psi \ , \quad \mathcal{P}_\pm = \phi 12\left(1 \pm \gamma^2\right) \ , \tag{2.2.15}$$

and similarly for the Dirac conjugate. The orthogonal projection operator satisfies the two conditions $\mathcal{P}^2 = \mathcal{P}$ and $\mathcal{P}^\dagger = \mathcal{P}$. More explicitly

$$\begin{aligned} \Psi_+ &:= \frac{1}{2}\frac{e^{-\frac{\sigma}{2}}}{R}\begin{pmatrix} \psi_+ - i\psi_- \\ i(\psi_+ - i\psi_-)\end{pmatrix} \otimes \begin{pmatrix}\eta_+ \\ \eta_-\end{pmatrix} \ , \\ \Psi_- &:= \frac{1}{2}\frac{e^{-\frac{\sigma}{2}}}{R}\begin{pmatrix} \psi_+ + i\psi_- \\ -i(\psi_+ + i\psi_-)\end{pmatrix} \otimes \begin{pmatrix}\eta_+ \\ \eta_-\end{pmatrix} \ . \end{aligned} \tag{2.2.16}$$

The variation of the Dirac part of the action (2.2.1) with respect to $\Psi_\pm$ after integration by parts becomes

$$\Delta S_D = \text{bulk terms} + i\int_\partial d^3x \ \sqrt{\gamma}\left(\bar{\Psi}_-\delta\Psi_+ - \bar{\Psi}_+\delta\Psi_-\right) \ , \tag{2.2.17}$$

where γ is the determinant of the induced metric at the boundary.The bulk terms are proportional to the equations of motion. In order to have a well-defined boundary value problem, we should include a boundary term of the form

$$S_\partial = i \int_\partial d^3x \sqrt{\gamma} \left(a_1 \bar{\Psi}_- \Psi_+ + a_2 \bar{\Psi}_+ \Psi_- \right) \ . \tag{2.2.18}$$

We can then either fix $\Psi_+ = 0$ or $\Psi_- = 0$ (and thus $\bar{\Psi}_+ = 0$ or $\bar{\Psi}_- = 0$) at the boundary depending on whether we set $(a_1 = -1, a_2 = 0)$ or $(a_1 = 0, a_2 = 1)$ respectively in the total variation of the action $\delta S_D + \delta S_\partial$.

In the massless case, both modes $\Psi_\pm$ are normalizable. We can then identify the asymptotic values

$$\Psi_\pm^0 := \lim_{x \to \frac{\pi}{2}} R(x)^{-\phi 32} \Psi_\pm \ , \tag{2.2.19}$$

with the normalizable part of the dual operator $\mathcal{O}$. After reducing on the $\mathcal{S}^2$ sphere, the effective $2D$ fermions obey reflective boundary conditions in both types of quantizations

$$\psi_+ = e^{i\alpha} \ \psi_- \ , \quad \text{with} \quad \alpha = \begin{cases} \frac{\pi}{2} \ , & \text{standard} \\ \frac{3\pi}{2} \ , & \text{alternate} \end{cases} \ , \tag{2.2.20}$$

which correspond to taking $\Psi_+^0 = 0$ or $\Psi_-^0 = 0$ respectively. Intuitively, they would not allow the charge and energy to leak out at the boundary. In fact, by using the conservation equations it is easy to see that at the boundary

$$\dot{E} = T_{12}\Big|_\partial = 0 \quad \text{and} \quad \dot{Q} = J_2\Big|_\partial = 0 \ , \tag{2.2.21}$$

where J_2 is the x component of the $U(1)$ current

$$J_2 = \psi^\dagger \sigma_z \psi \otimes \eta^\dagger \eta = \left(\psi_-^\dagger \psi_+ - \psi_+^\dagger \psi_- \right) \otimes \eta^\dagger \eta \ , \tag{2.2.22}$$

and T_{12} is the energy flux, which is given by the tx-component of the stress tensor

$$T_{12} = \frac{i}{2R^2} \left(\psi_+^\dagger (\partial_x - \partial_t) \psi_+ + \psi_-^\dagger (\partial_x + \partial_t) \psi_- - (\partial_x - \partial_t) \psi_+^\dagger \psi_+ - (\partial_x + \partial_t) \psi_-^\dagger \psi_- \right) \otimes \eta^\dagger \eta \ . \tag{2.2.23}$$

Now consider two decoupled and identical conformal theories with fermionic degrees of freedom. In principle, each one has its own bulk gravity dual. The boundary action then acquires the form[2]

$$S_\partial = i \int_\partial d^3x \sqrt{\gamma} \left(a_1 \bar{\Psi}_-^R \Psi_+^R + a_2 \bar{\Psi}_+^R \Psi_-^R + b_1 \bar{\Psi}_-^L \Psi_+^L + b_2 \bar{\Psi}_+^L \Psi_-^L \right) \ . \tag{2.2.24}$$

[2]Note that since we consider two copies of the theory we now have $x \in [-\frac{\pi}{2}, \frac{\pi}{2}]$, and we denote the left (right) boundary at $x = \mp \frac{\pi}{2}$ with L (R).

There are various options depending on what type of boundary sources we would like to keep turned-on. The guiding principle we will follow is CPT invariance. CPT-related boundary conditions imply a vanishing T_{++} component consistent with the fact that vacuum AdS_2 cannot support finite energy excitations [80]. For the purpose of this work, we choose the following CPT conjugate boundary conditions

$$\Psi_+^R = 0 \xrightarrow{\text{CPT}} \bar{\Psi}_-^L = 0 \ , \tag{2.2.25}$$

which correspond to the coefficients $a_1 = -1$, $b_2 = 1$, and $a_2 = b_1 = 0$. The vanishing energy can also be understood as due to the conformal anomaly contribution present in the mapping between the energy of a CFT on the strip to AdS_2 [68].

2.2.3 Modified boundary conditions

We are interested in the case where the two bulk geometries are two magnetically charged RN black holes. Intuitively, we can think on them as being connected through an Einstein-Rosen bridge. A priori, however, it is not obvious how to connect both bulk geometries through the horizon. Moreover, in order to render the wormhole traversable, we need to establish a connection between the two asymptotic boundaries. We achieve that by using a non-local coupling of the form[3]

$$S_{\text{int}} = -i \int d^3x \sqrt{\gamma} \left(h_1 \bar{\Psi}_+^R \Psi_-^L + h_2 \bar{\Psi}_-^L \Psi_+^R + h_3 \bar{\Psi}_-^R \Psi_+^L + h_4 \bar{\Psi}_+^L \Psi_-^R \right) \ . \tag{2.2.26}$$

This term will provide us with the negative energy we need and will open up the wormhole. It is important to mention that if instead of fermions, we considered interacting scalar fields, similar to [52], the lowest Landau levels would have positive energy on the $\mathcal{S}^2$ sphere, making the problem of finding a traversable geometry much harder.

We are looking for an eternal traversable wormhole, so we let the coupling constants be turned on for all times. For the purposes of this work, we focus on the case where the coupling constants are real and $h_1 = h_2 = 0$[4]. The boundary conditions turn out to be

$$\Psi_+^R + h\Psi_+^L = 0, \quad \text{and} \quad \Psi_-^L + h\Psi_-^R = 0 \ , \tag{2.2.27}$$

[3] In general, the coupling constants can be complex. However, they must satisfy $h_1 = h_2^*, h_3 = h_4^*$, in order for (2.2.26) to be real.

[4] It would be interesting to understand other combinations of the non-local couplings.

where $h_3 = h_4 = -h$. Notice that the sources at the boundary are vanishing. In terms of the spinor components this implies the following boundary conditions

$$\psi_+^R - i\psi_-^R + h\psi_+^L - ih\psi_-^L = 0 \ , \quad \text{and} \quad \psi_+^L + i\psi_-^L + h\psi_+^R + ih\psi_-^R = 0 \ . \tag{2.2.28}$$

See Fig. 2.1 for an illustrations of the modified boundary conditions.

In order to obtain a solution to the equations of motion (2.2.9) with the boundary conditions (2.2.28), for the lowest Landau level, we use the following ansatz:

$$\psi_+ = \sum_k \frac{\alpha_k}{\sqrt{\pi}} e^{i\omega_k(t-x)} \quad \text{and} \quad \psi_- = \sum_k \frac{\beta_k}{\sqrt{\pi}} e^{i\omega_k(t+x)} \ . \tag{2.2.29}$$

Filling in this ansatz in to the boundary conditions (2.2.28) leads to the following constraint equations[5]

$$\begin{aligned} (i^{3\omega_k} + hi^{\omega_k})\alpha_k + (i^{\omega_k+3} + hi^{3\omega_k+3})\beta_k &= 0 \ , \\ (i^{\omega_k} + hi^{3\omega_k})\alpha_k + (i^{3\omega_k+1} + hi^{\omega_k+1})\beta_k &= 0 \ , \end{aligned} \tag{2.2.30}$$

with solution

$$\omega_k = 2k - \frac{i}{\pi}\log\left(\frac{-2h \pm i|1-h^2|}{1+h^2}\right), \quad \beta_k = (-1)^{k+1}\alpha_k \ , \tag{2.2.31}$$

where $k \in \mathbb{Z}$. The solution can be written in the following form

$$\omega_k = \frac{2k+1}{2} + (-1)^k \frac{2}{\pi}\lambda(h) \ , \tag{2.2.32}$$

where λ is a function of h given by

$$\lambda(h) = \frac{1}{2}\arctan\left(\frac{2h}{|1-h^2|}\right) \ . \tag{2.2.33}$$

2.2.4 Propagators and stress tensor

Using the solution (2.2.32), we write the fermionic fields as[6]

$$\psi_+ = \sum_k \frac{1}{\sqrt{\pi}}\alpha_k e^{i\omega_k(t-x)} \ , \quad \text{and} \quad \psi_- = \sum_k \frac{(-1)^{k+1}}{\sqrt{\pi}}\alpha_k e^{i\omega_k(t+x)} \ . \tag{2.2.34}$$

[5]Note that the equations are invariant under $h \mapsto \frac{1}{h}$ and $\beta_k \mapsto -\beta_k$, so the theory exhibits S-duality.

[6]In the remainder of this work, we will use light-cone coordinates defined by $x_\pm = t \pm x$, whenever they are more convenient.

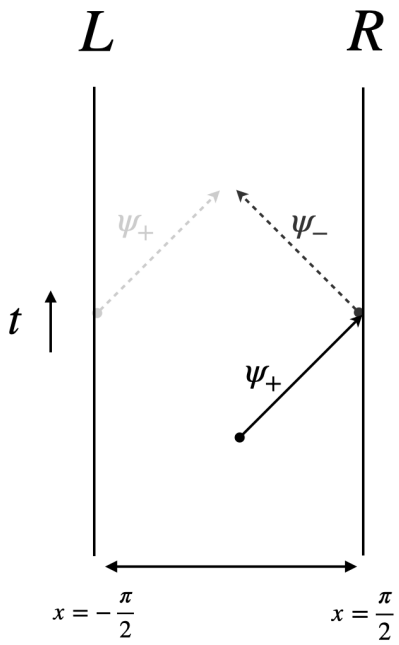

Figure 2.1: A right moving massless fermion, with amplitude $|\psi_+^R| = 1$, traveling on the strip hits the right boundary. The probability of the resulting left mover is equal to $\frac{(h^2-1)^2}{(h^2+1)^2}$, and the right mover emerging from the left boundary has amplitude $\frac{4h^2}{(h^2+1)^2}$.

The modes α_k obey the following anti-commutation relations

$$\{\alpha_k, \alpha_j^\dagger\} = \delta_{k,j} \ , \quad \{\alpha_k, \alpha_j\} = 0 \quad \text{and} \quad \{\alpha_k^\dagger, \alpha_j^\dagger\} = 0 \ , \tag{2.2.35}$$

and the vacuum is defined as

$$\alpha_k \left|0\right\rangle = 0 \quad \forall \ k \in \mathbb{Z}_{<0}, \quad \text{and} \quad \alpha_k^\dagger \left|0\right\rangle = 0 \quad \forall \ k \in \mathbb{Z}_{\geq 0} \ . \tag{2.2.36}$$

Using equations (2.2.34)-(2.2.36) we calculate the propagators. We present one of them here and the rest can be found in the Appendix A

$$\langle \psi_+^\dagger(x_-)\psi_+(x'_-)\rangle = \frac{1}{\pi}\frac{e^{\frac{i}{2}(x'_- - x_-)}}{1-e^{i(x'_- - x_-)}} + \frac{e^{\frac{i}{2}(x'_- - x_-)}}{1+e^{i(x'_- - x_-)}}\frac{2i\lambda(h)}{\pi^2}(x'_- - x_-) + \cdots \ . \tag{2.2.37}$$

We proceed by stating the relevant components of the stress tensor. Since (2.2.2) is spherically symmetric and does not depend on time, the only off-diagonal component of the stress tensor that could be nonzero is T_{12}. However, in Appendix B we show explicitly that T_{12} vanishes for our setup. Therefore, we only need the diagonal components of the stress tensor, which are given by

$$\begin{aligned}
T_{11} &= \frac{i}{2R^2}\left(\psi_+^\dagger\partial_t\psi_+ + \psi_-^\dagger\partial_t\psi_- - \partial_t\psi_+^\dagger\psi_+ - \partial_t\psi_-^\dagger\psi_-\right)\eta^\dagger\eta \ , \\
T_{22} &= -\frac{i}{2R^2}\left(\psi_+^\dagger\partial_x\psi_+ - \psi_-^\dagger\partial_x\psi_- - \partial_x\psi_+^\dagger\psi_+ + \partial_x\psi_-^\dagger\psi_-\right)\eta^\dagger\eta \ , \\
T_{33} &= -\frac{ie^{-2\sigma}}{2}\frac{R'}{R}\psi^\dagger\sigma_z\psi\eta^\dagger\eta \ , \\
T_{44} &= -\frac{i\sin(\theta)}{2}\frac{e^{-2\sigma}}{R}R'\sin(\theta)e^{-\sigma}\psi^\dagger\sigma_z\psi\eta^\dagger\eta \ .
\end{aligned} \tag{2.2.38}$$

In order to compute the quantum contribution to the components of the stress tensor due to the non-local coupling, we apply the point-splitting formula

$$\langle T_{\mu\nu}\rangle = \lim_{x'\to x}\frac{i\eta_{ab}}{2}\left(e^a_{(\mu}\gamma^b\nabla'_{\nu)} - \nabla_{(\mu}e^a_{\nu)}\gamma^b\right)\langle\bar{\Psi}(x)\Psi(x')\rangle \ . \tag{2.2.39}$$

By using the propagators and after subtracting the vacuum contribution, we end up with the following finite result

$$\langle T^h_{\mu\nu}\rangle = -\frac{1}{2\pi^3}\frac{q\lambda(h)}{R^2}\text{diag}\,(1,1,0,0) \ , \tag{2.2.40}$$

where the factor q comes from the fact that in the lowest Landau level the degeneracy of the two-dimensional fields is q. The range for the compact radial coordinate ($\Delta x = \pi$) is present in the prefactor in the above expression. Picking a different gauge would result in a rescaling of the stress tensor. One can easily check that the stress tensor is conserved and traceless due to conformal symmetry. Details of the stress tensor calculation can be found in Appendix B.

2.3 Wormhole geometry

We start this section by describing the two different regimes of the wormhole geometry, after which we analytically solve the (linearized) Einstein equations in both regimes. We continue by showing that the solutions in the two regimes can be consistently patched together through a coordinate transformation in the overlapping region of validity. We end the section by solving the full, nonlinear Einstein equations numerically.

2.3.1 Two regimes

The next task is to solve the semi-classical Einstein equations to find a magnetically charged geometry sourced by (2.2.40)

$$G_{\mu\nu} + \Lambda g_{\mu\nu} = 8\pi G_N \langle T_{\mu\nu} \rangle \ . \tag{2.3.1}$$

As we approach the AdS_4 boundaries located at $r \to \pm\infty$, the electromagnetic contribution of the stress tensor dominates over the Casimir energy. Then, far away from the wormhole throat the solution should look like Reissner-Nordström AdS_4

$$ds^2 = -f(r)d\tau^2 + \frac{dr^2}{f(r)} + r^2 d\Omega_2^2 \ , \tag{2.3.2}$$

with emblackening factor

$$f(r) = 1 - \frac{2G_N M}{r} + \frac{r_e^2}{r^2} + \frac{r^2}{\ell^2}, \quad \text{and} \quad r_e^2 = \frac{\pi q^2 G_N}{g^2} \ . \tag{2.3.3}$$

Here M denotes the mass of the black hole, q is an integer and r_e^2 denotes the magnetic charge of the black hole. Close to extremality, the geometry developes an infinitely long throat. The value of the extremal radius has the form

$$\partial_r f(r)\Big|_{r=\bar{r}} \stackrel{!}{=} 0 \quad \Rightarrow \quad \bar{r}^2 = \frac{\ell^2}{6}\left(-1 + \sqrt{1 + 12\frac{r_e^2}{\ell^2}}\right) \ . \tag{2.3.4}$$

Inverting this relation gives the charge of the black hole in terms of the extremal horizon radius and the AdS length

$$r_e^2 = \bar{r}^2\left(1 + 3\frac{\bar{r}^2}{\ell^2}\right). \tag{2.3.5}$$

In the range of masses that we are interested in, the quartic polynomial $f(r) = 0$ admits complex conjugate roots[7]. We choose to parametrize them by $r_{1,2} = \hat{r}(1 \pm$

[7] As a function of r_e, the disciminant interpolates between $\Delta(r_e = 0) = -16G_N^2 M^2 \ell^8(\ell^2 + 27G_N^2 M^2)$ to infinity. In particular, $\Delta \approx 256\ell^6 r_e^6$ when $r_e \gg \ell$ and $\Delta \approx -16G_N \ell^{10} M^2$ when $r_e \ll \ell$. In both cases, there is at least one pair of complex conjugate roots.

$i\epsilon$) with $\epsilon > 0$ and $\hat{r} > 0$. We can analytically solve for the other two roots, r_3 and r_4, and the parameter $\hat{r}$ by matching the quadratic, cubic, quartic and constant contributions to $r^2 f(r)$. This parametrization is symmetric with respect to $\epsilon \mapsto -\epsilon$. Therefore, the expressions for $(r_3, r_4, \hat{r})$ will involve only even powers of ϵ. In the near extremal limit ($\epsilon \ll 1$), we then approximate f to order $\mathcal{O}(\epsilon^4)$ by

$$f(r) = \frac{1}{\ell^2}\left(\left(\frac{r-\hat{r}}{r}\right)^2 + \left(\frac{\hat{r}\epsilon}{r}\right)^2\right)(r-r_3)(r-r_4)\ , \tag{2.3.6}$$

with

$$(r-r_3)(r-r_4) = \ell^2 + r^2 + 2r\bar{r} + 3\bar{r}^2 - \frac{\ell^2(r+4\bar{r}) + 2\bar{r}^2(r+6\bar{r})}{\ell^2+6\bar{r}^2}\bar{r}\epsilon^2 + \mathcal{O}(\epsilon^4)\ , \tag{2.3.7}$$

and

$$\hat{r} = \bar{r} + \epsilon^2 \frac{\bar{r}}{2\mathcal{C}(\bar{r})}\left(1 + 2\frac{\bar{r}^2}{\ell^2}\right) + \mathcal{O}(\epsilon^4)\ . \tag{2.3.8}$$

Here $\mathcal{C}(r)$ is defined by

$$\mathcal{C}(r) = 6\left(\frac{r}{\ell}\right)^2 + 1\ . \tag{2.3.9}$$

In the region where $r - \bar{r} \ll \bar{r}$ and ϵ is small, we can approximate the metric (2.3.2) as

$$ds^2 = -\mathcal{C}(\bar{r})\left(\left(\frac{r-\bar{r}}{\bar{r}}\right)^2 + \epsilon^2\right)d\tau^2 + \frac{dr^2}{\mathcal{C}(\bar{r})\left(\left(\frac{r-\bar{r}}{\bar{r}}\right)^2 + \epsilon^2\right)} + \bar{r}^2 d\Omega_2^2\ . \tag{2.3.10}$$

By making the following identifications,

$$\rho = \frac{r-\bar{r}}{\epsilon\bar{r}} \quad \text{and} \quad t = \mathcal{C}(\bar{r})\frac{\tau\epsilon}{\bar{r}}\ , \tag{2.3.11}$$

the metric can be brought to global $\mathrm{AdS}_2 \times \mathcal{S}^2$ form

$$ds^2 = \frac{\bar{r}^2}{\mathcal{C}(\bar{r})}\left(-(\rho^2+1)dt^2 + \frac{d\rho^2}{\rho^2+1}\right) + \bar{r}^2 d\Omega_2^2\ . \tag{2.3.12}$$

Following [69], we expect that in the wormhole region the solution is a slight perturbation of the near extremal RN black hole. We make the following gauge choice for our ansatz geometry in the throat

$$ds^2 = \frac{\bar{r}^2}{\mathcal{C}(\bar{r})}\left(-(1+\rho^2+\gamma)dt^2 + \frac{d\rho^2}{1+\rho^2+\gamma}\right) + \bar{r}^2(1+\psi)d\Omega_2^2\ , \tag{2.3.13}$$

where the functions $\psi(\rho)$ and $\gamma(\rho)$ are small fluctuations and $\bar{r}$ is given by (2.3.4). In these coordinates, the stress tensor contribution has the approximate form

$$\langle T^h_{\mu\nu}\rangle \approx -\frac{1}{2\pi^3}\frac{q\lambda(h)}{\bar{r}^2}\mathrm{diag}\left(1, \frac{1}{(1+\rho^2)^2}, 0, 0\right)\ . \tag{2.3.14}$$

The linearized Esintein's equations in this geometry are given by

$$tt: \quad \frac{\zeta}{1+\rho^2} + \psi(\rho) - \rho\psi'(\rho) - (1+\rho^2)\psi''(\rho) = 0 \ , \tag{2.3.15}$$

$$\rho\rho: \quad \frac{\zeta}{1+\rho^2} - \psi(\rho) + \rho\psi'(\rho) = 0 \ , \tag{2.3.16}$$

$$\theta\theta: \quad \frac{4}{\mathcal{C}(\bar{r})}\left(1+3\frac{\bar{r}^2}{\ell^2}\right)\psi(\rho) + \gamma''(\rho) + 2\rho\psi'(\rho) + (1+\rho^2)\psi''(\rho) = 0 \ , \tag{2.3.17}$$

$$\phi\phi: \quad \sin^2(\theta)\left(\frac{4}{\mathcal{C}(\bar{r})}\left(1+3\frac{\bar{r}^2}{\ell^2}\right)\psi(\rho) + \gamma''(\rho) + 2\rho\psi'(\rho) + (1+\rho^2)\psi''(\rho)\right) = 0 \ , \tag{2.3.18}$$

where ζ is a constant given by $\zeta = \frac{4G_N q\lambda(h)}{\pi^2\bar{r}^2}$[8]. Note that the first two equations do not depend on γ. Therefore, we can find an expression for $\psi(\rho)$ by solving the first order equation (2.3.16). This results in

$$\psi(\rho) = \zeta(1+\rho\arctan(\rho)) + c\rho \ , \tag{2.3.19}$$

with c an integration constant. A simple check shows that (2.3.19) also solves the tt component of the Einstein equations (2.3.15). By using the solution for $\psi(\rho)$, we can now use the angular components of the Einstein equations to solve for $\gamma(\rho)$. It turns out that

$$\gamma(\rho) = -\frac{\zeta\left(1+4\frac{\bar{r}^2}{\ell^2}\right)}{\mathcal{C}(\bar{r})}\left(\rho^2 + \rho(3+\rho^2)\arctan(\rho) - \log\left(1+\rho^2\right)\right) + c_1 + \rho c_2 \ , \tag{2.3.20}$$

solves (2.3.17) and (2.3.18). Integration constants can be set to zero by requiring that the geometry is invariant under $\rho \mapsto -\rho$ and by a redefinition of ρ and t.

In the next subsection, we show that there is an overlapping region between the two solutions deep in the RN-AdS throat and construct the full wormhole geometry.

2.3.2 Matching

Intuitively, once the non-local coupling h is turned on, the wormhole is formed and the throat acquires a certain finite length L which we will determine below. Outside this range, the linearized solution found in the previous section will not be valid anymore. In fact, both perturbations ψ and γ increase with the value of ρ, as we approach the wormhole mouth. More precisely, we expect the slightly deformed solution to be valid up to values of ρ for which the term $\zeta\rho^3$ is no longer subleading

[8]Note that we can write q in terms of $\bar{r}$. This results in $\zeta = \frac{4g\lambda(h)}{\pi^2\bar{r}}\sqrt{\frac{G_N\left(1+3\frac{\bar{r}^2}{\ell^2}\right)}{\pi}}$. From this we see that we can let ζ be small at finite h and independent of the ratio between $\bar{r}$ and ℓ.

(since this is the leading order behaviour of γ). In the following, we consider ρ to be large, but $\zeta\rho$ small and fixed, and ζ small. We take the near-horizon limit of (2.3.6)

$$f(r) = \mathcal{C}(\bar{r})\epsilon^2 + \mathcal{C}(\bar{r})\left(\frac{r-\bar{r}}{\bar{r}}\right)^2 - \mathcal{C}\left(\bar{r}\right)\left(\frac{r-\bar{r}}{\bar{r}}\right)\epsilon^2 - 2\left(1+4\frac{\bar{r}^2}{\ell^2}\right)\left(\frac{r-\bar{r}}{\bar{r}}\right)^3 + \cdots \,, \tag{2.3.21}$$

where we have expanded up to third order in ϵ and $\frac{r-\bar{r}}{\bar{r}}$ combined. As a first approximation let us set

$$\rho = \frac{L}{\bar{r}}\frac{r-\bar{r}}{\bar{r}}, \qquad t = \mathcal{C}(\bar{r})\frac{\tau}{L} \,. \tag{2.3.22}$$

In the limit

$$\rho \gg 1 \,, \quad \frac{L}{\bar{r}} \gg 1 \,, \quad \text{and} \quad \frac{r-\bar{r}}{\bar{r}} \ll 1 \,, \tag{2.3.23}$$

equation (2.3.22) matches the order $\mathcal{O}(2)$ of the unperturbed ansatz geometry. Here L is an integration constant that denotes the rescaling between the t and τ coordinates. Furthermore, by considering the relation between ρ and r, one can see that L is a measure up to which we can trust the ansatz; so that ρ has a cutoff at $\rho \sim \frac{L}{\bar{r}}$. By comparing to the matching of the near-extremal Reissner-Nordström black hole given in (2.3.11), we see that L is connected to ϵ through[9]

$$L = \frac{\bar{r}}{\epsilon} \,. \tag{2.3.24}$$

By matching the angular coordinates we see that

$$r^2 = \bar{r}^2(1+\psi(\rho)) \quad \rightarrow \quad \frac{r-\bar{r}}{\bar{r}} = \frac{\psi(\rho)}{2} + \mathcal{O}\left(\psi^2\right) = \frac{\pi\zeta}{4}\rho + \mathcal{O}\left(\zeta^2\right) \,, \tag{2.3.25}$$

where we have expanded $\sqrt{1+\psi(\rho)}$, and in the third equality we used the expansion of $\psi(\rho)$ at large ρ. Using (2.3.22) and (2.3.25) we can find the value for L by examining

$$\rho dt = \mathcal{C}(\bar{r})\frac{r-\bar{r}}{\bar{r}^2}d\tau \quad \Longrightarrow \quad L = \frac{d\tau}{dt}\mathcal{C}(\bar{r}) = \rho\bar{r}\frac{\bar{r}}{r-\bar{r}} = \frac{4\bar{r}}{\pi\zeta} \,. \tag{2.3.26}$$

One can easily see that with this value for L, (2.3.22) and (2.3.25) are consistent with one another. This also gives a relation between the non-local coupling constant h and ϵ. With (2.3.24) and (2.3.26) we see that

$$\epsilon^2 = \frac{\pi^2\zeta^2}{16} = \frac{G_N g^2\lambda^2(h)}{\pi^3\bar{r}^2}\left(1+3\frac{\bar{r}^2}{\ell^2}\right) = \frac{G_N^2 q^2\lambda^2(h)}{\pi^2\bar{r}^4} \,. \tag{2.3.27}$$

[9]Recall that ϵ encodes how "far" from extremality the near-extremal black hole metric is.

The matching of the time component of the geometry is discussed in Appendix C. In this appendix we show that the equations above give a consistent matching between the Reissner-Nordström geometry and the deformed $AdS_2 \times S^2$. A final comment we make concerning the matching is that the deformation γ gives a correction to the range of the radial coordinate, which in turn leads to a correction to the stress tensor. However, this correction is of order ζ, and therefore will not influence the matching[10]. The full wormhole geometry with the two regimes is schematically shown in Fig. 2.2.

An important fact to notice about the wormhole solution we find is that there are three independent parameters: the charge, the non-local coupling and the AdS length by which the solution is determined. As soon as these three parameters are fixed, there is a unique, static and spherically symmetric wormhole geometry that solves Einstein's equations. At radii below the cutoff the geometry is that of deformed $\mathrm{AdS}_2 \times \mathcal{S}^2$. As ρ increases, the geometry smoothly interpolates to a near-extremal Reissner-Nordström black hole in AdS_4. This black hole is characterized by its charge r_e, while its mass is given by

$$M_{WH} = M_{\text{ext}} + \Delta M, \tag{2.3.28}$$

with

$$M_{\text{ext}} = \frac{\bar{r}}{G_N} + \frac{2\bar{r}^3}{G_N \ell^2}, \quad \text{and} \quad \Delta M = -\frac{\bar{r}\epsilon^2}{2G_N}\mathcal{C}\left(\bar{r}\right) = -\frac{g^2\lambda^2(h)}{2\pi^3\bar{r}}\left(1 + 3\frac{\bar{r}^2}{\ell^2}\right)\mathcal{C}(\bar{r})\ , \tag{2.3.29}$$

where M_{ext} is the mass of an extremal black hole.

Since it is not very pleasant to have a factor of g in this formula, we use the definitions to rewrite this as

$$\Delta M = -\frac{G_N q^2 \lambda^2(h)}{2\pi^2 \bar{r}^3}\mathcal{C}\left(\bar{r}\right) \sim -\frac{q\lambda(h)\mathcal{C}\left(\bar{r}\right)}{\bar{r}}\zeta\ . \tag{2.3.30}$$

Therefore, the black hole is indeed near-extremal, with mass just below the extremal mass. Coming from infinity, as an observer approaches the wormhole mouth, the observer would experience getting closer and closer to a naked singularity. All of a sudden, the wormhole throat opens up and she traverses through the wormhole reaching the other side safely.

In the limit $\ell \gg r_e$, where the AdS radius is larger than the radii of the throats.

[10]The correction can be calculated by considering $\Delta x = \int_{-\infty}^{\infty} \frac{dy}{g_{yy}}$, with y the holographic coordinate, resulting in $\Delta x = \pi\left(1 + \zeta f(\bar{r})\right)$, for some function f. Since we consider ζ to be small, the matching is consistent. If we had taken this correction into account the stress tensor would have been given by $\langle T^h_{\mu\nu}\rangle = \frac{1}{\Delta x}\frac{q\lambda(h)}{2\pi^2 R^2}\mathrm{diag}\left(1,1,0,0\right)$.

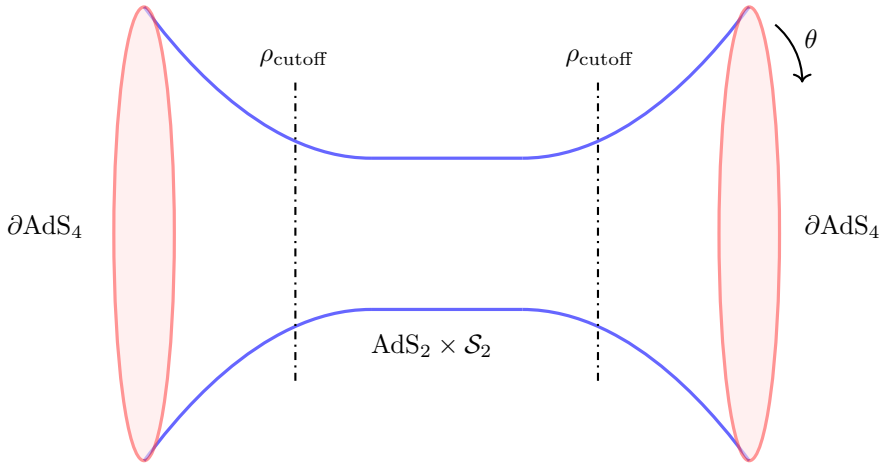

Figure 2.2: Wormhole geometry: In the throat region the metric has the $\text{AdS}_2 \times \mathcal{S}^2$ form (2.3.12) up to the cutoff located at $\rho \sim L/\bar{r}$. Around this point, where the limits (2.3.23) are satisfied, the geometry smoothly interpolates to near-extremal Reissner-Nordström black holes in AdS_4.

The change in the mass due to the non-local coupling has the form

$$\Delta M = -\frac{G_N q^2 \lambda^2(h)}{2\pi^2 r_e^3} \,, \tag{2.3.31}$$

which has the same scaling as the binding energy, relative to the the energy of two disconnected extremal black holes, coming from the wormhole throat in the asymptotically flat case [69].

2.3.3 Non-linear solution

One might be concerned that the solution presented in the previous subsection only exists in the linearized analysis. We will proceed to find a similar solution to the full Einstein's equations. The geometry ansatz we will consider is the following

$$ds^2 = \frac{\bar{r}^2}{\mathcal{C}(\bar{r})}\left(-f(\rho)dt^2 + \frac{d\rho^2}{f(\rho)}\right) + R^2(\rho)d\Omega_2^2 \,, \tag{2.3.32}$$

$\rho \in [0, \pm\infty)$, $t \in (-\infty, \infty)$ and we have assumed the extremal value for the radius in the overall factor. The non-zero components of the Einstein equations can be

written as

$$
\begin{aligned}
tt: \quad & \frac{3\bar{r}^2 f(\rho)}{\mathcal{C}(\bar{r})\ell^2} - \frac{\pi G_N q^2 \bar{r}^2 f(\rho)}{g^2 \mathcal{C}(\bar{r}) R^4(\rho)} + \frac{4 G_N q \lambda(h)}{\pi^2 R^2(\rho)} + \frac{\bar{r}^2 f(\rho)}{\mathcal{C}(\bar{r}) R^2(\rho)} \\
& - \frac{f(\rho) f'(\rho) R'(\rho)}{R(\rho)} - \frac{f^2(\rho) R'^2(\rho)}{R^2(\rho)} - \frac{2 f^2(\rho) R''(\rho)}{R(\rho)} = 0 \ , \qquad (2.3.33) \\
\rho\rho: \quad & - \frac{3\bar{r}^2}{\mathcal{C}(\bar{r})\ell^2 f(\rho)} + \frac{\pi G_N q^2 \bar{r}^2}{g^2 \mathcal{C}(\bar{r}) f(\rho) R^4(\rho)} + \frac{4 G_N q \lambda(h)}{\pi^2 f^2(\rho) R^2(\rho)} \\
& - \frac{\bar{r}^2}{\mathcal{C}(\bar{r}) f(\rho) R^2(\rho)} + \frac{f'(\rho) R'(\rho)}{f(\rho) R(\rho)} + \frac{R'^2(\rho)}{R^2(\rho)} = 0 \ , \qquad (2.3.34) \\
\theta\theta: \quad & - \frac{\pi G_N q^2}{g^2 R^2(\rho)} - \frac{3 R^2(\rho)}{\ell^2} + \frac{\mathcal{C}(\bar{r}) R(\rho) f'(\rho) R'(\rho)}{\bar{r}^2} \\
& + \frac{\mathcal{C}(\bar{r}) R^2(\rho) f''(\rho)}{2\bar{r}^2} + \frac{\mathcal{C}(\bar{r}) f(\rho) R(\rho) R''(\rho)}{\bar{r}^2} = 0 \ , \qquad (2.3.35) \\
\phi\phi: \quad & \sin^2(\theta) \left(- \frac{\pi G_N q^2}{g^2 R^2(\rho)} - \frac{3 R^2(\rho)}{\ell^2} + \frac{\mathcal{C}(\bar{r}) R(\rho) f'(\rho) R'(\rho)}{\bar{r}^2} \right) \\
& + \sin^2(\theta) \left(\frac{\mathcal{C}(\bar{r}) R^2(\rho) f''(\rho)}{2\bar{r}^2} + \frac{\mathcal{C}(\bar{r}) f(\rho) R(\rho) R''(\rho)}{\bar{r}^2} \right) = 0 \ . \qquad (2.3.36)
\end{aligned}
$$

These differential equations depend on three independent physical parameters of the form

$$
\frac{G_N q^2}{g^2 \ell^2}, \quad \frac{G_N q \lambda(h)}{\ell^2}, \quad \text{and} \quad \ell \ . \qquad (2.3.37)
$$

Since both functions f and R appear in the differential equations with two derivatives, there will be four integration constants. By requiring the solution to be symmetric around $\rho = 0$ we fix two of those. Requiring this $\mathbb{Z}_2$ symmetry is equivalent to setting $f'(0) = R'(0) = 0$. Furthermore we have the freedom to rescale the time coordinate. This allows us to pick $f(0) = 1$. Now the constraint equation (2.3.34) fixes $R(0)$ in terms of $f(0)$. By these choices all integration constants are then fixed. Also note that due to spherical symmetry whenever the $\theta\theta$ equation is solved, the $\phi\phi$ equation is automatically satisfied. With the integration constants as mentioned, we can now solve the tt and $\theta\theta$ equation numerically. The results of solving the non-linear Einstein equations are shown in Figures 2.3 and 2.4. In order to compare with the linearized results, we pick the integration constants so that the non-linear and linear solutions agree at $\rho = 0$. We should note however that the non-linear solution makes sense for other parameter values and integration constants as well. We expect the linear and non-linear results to agree up to $|\rho| \sim \rho_{\text{cutoff}} = \frac{L}{\bar{r}}$. As a final comment note that, as can be seen from Figure 2.3, for large ρ the numerical solution behaves as $R(\rho) \sim \left(\frac{L}{\bar{r}}\right)^{-1} |\rho|$, which is precisely what we expect in light of equation (2.3.22) and by the fact that away from the wormhole we expect the $\mathcal{S}^2$ radius to be equal to r.

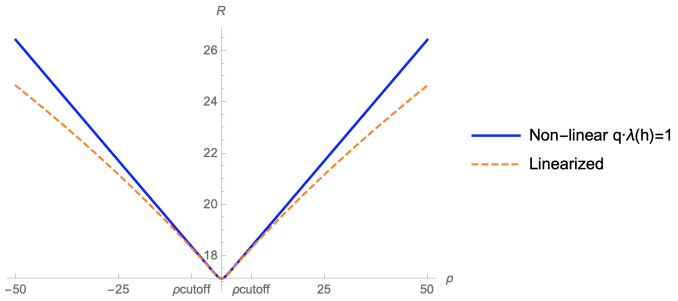

Figure 2.3: Solutions of $R(\rho)$ with parameters $\frac{G_N q^2}{g^2 \ell^2} = 0.01$, $\frac{G_N q \lambda(h)}{\ell^2} = 0.001$, and $\ell = 100$. The initial condition is $R(0) = 17$. For these parameters we expect agreement up to $\rho_{\text{cutoff}} = 7.2$. We see that for larger ρ the linear solution starts to deviate.

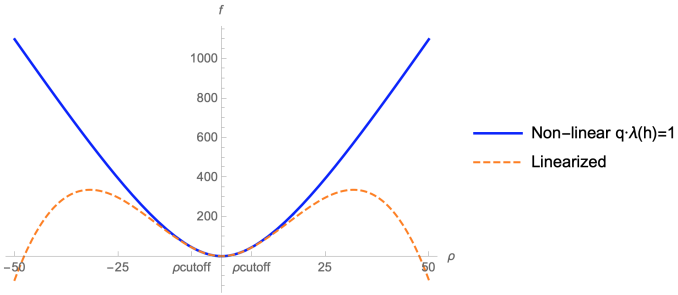

Figure 2.4: Solutions of $f(\rho)$ with parameters $\frac{G_N q^2}{g^2 \ell^2} = 0.01$, $\frac{G_N q \lambda(h)}{\ell^2} = 0.001$, and $\ell = 100$. The initial condition is $R(0) = 17$. For these parameters we expect agreement up to $\rho_{\text{cutoff}} = 7.2$. We see that for larger ρ the linear solution starts to deviate, and even becomes negative. Of course, in this region the RN AdS black hole dominates.

2.4 Thermodynamics

This section contains a calculation of the on-shell Hamiltonian of the wormhole solution. We propose a Hamiltonian and show that the wormhole solution is the ground state for a region of parameter space. Furthermore we give a qualitative discussion of the thermodynamic stability of the wormhole solution in the (grand) canonical ensemble.

2.4.1 Hamiltonian ground state

We expect the wormhole geometry presented in the previous section to be dual to the asymptotic field theories in some particular entangled state. In particular, it should be dual to the ground state of a certain local Hamiltonian whose ground state is approximately the thermofield double state with chemical potential [68,74].

From the gravity point of view, given the set of boundary conditions, Einstein's equations fill in the bulk geometry smoothly. We will consider three solutions with the same boundary conditions at zero temperature: the wormhole, two disconnected black holes and empty AdS. Depending on the values of $\lambda(h)$ and μ, there is a dominant saddle. For concreteness we will focus on the symmetric case where the total magnetic charge is $Q := Q_R = -Q_L$ and the mass is $M := M_R = M_L$. Of course, less symmetric cases can also be considered but we believe they will not dramatically modify the presented results.

In a general covariant theory, the on-shell Hamiltonian can be computed as a boundary integral as follows

$$H[\zeta] = \int_{\partial\Sigma} d^2x\sqrt{\sigma}u^\alpha\zeta^\beta T_{\alpha\beta} \ , \quad T_{\alpha\beta} := \frac{2}{\sqrt{-\gamma}}\frac{\delta S}{\delta\gamma^{\alpha\beta}} \ , \tag{2.4.1}$$

where $T_{\alpha\beta}$ is the Brown-York stress tensor[11], u^α is the unit normal to a constant time hypersurface, ζ^β is the flow vector and $\sqrt{\sigma}$ is the volume element of the boundary at fixed time. The energy of a gravitational solution is associated to time-translation symmetry, *i.e.,* , to the Killing vector $\zeta = \partial_\tau$.

The wormhole solution presented in the last section is a solution to the action with interacting term

$$S_{\text{int}} = ih\int d^3x\sqrt{-\gamma}\left(\bar{\Psi}_-^R\Psi_+^L + \bar{\Psi}_+^L\Psi_-^R\right) \ . \tag{2.4.2}$$

[11]In order to avoid IR divergences in AdS, we need to include counterterms in the purely gravitational part of the action (2.2.1). In d=3, they result in a modified stress tensor $T_{\alpha\beta} = K_{\alpha\beta} - K\gamma_{\alpha\beta} - \frac{2}{\ell}\gamma_{\alpha\beta} - \ell G_{\alpha\beta}$, where $G_{\alpha\beta}$ is the Einstein tensor computed on the boundary induced metric $\gamma_{\alpha\beta}$ [81].

The interacting part of the boundary stress tensor then has the form

$$T_{\alpha\beta} := \frac{2}{\sqrt{-\gamma}}\frac{\delta S_{\rm int}}{\delta \gamma^{\alpha\beta}} = ih\gamma_{\alpha\beta}\left(\bar{\Psi}^R_- \Psi^L_+ + \bar{\Psi}^L_+ \Psi^R_-\right) \ . \tag{2.4.3}$$

The metric close to the AdS_4 boundary at $r \to \infty$ and the time-like unit vector are of the form

$$ds^2 = -f(r)d\tau^2 + \frac{dr^2}{f(r)} + r^2 d\Omega_2^2 \quad \text{and} \quad u = \sqrt{f}d\tau \ . \tag{2.4.4}$$

The $\mathbb{Z}_2$ symmetry along the radial direction allows us to define a notion of gravitational energy by applying the formula (2.4.1) at the asymptotic AdS boundaries

$$H_{\rm int} := H[\zeta^\tau] = -ihr^2\sqrt{f}\int d^2\Omega \left(\bar{\Psi}^R_- \Psi^L_+ + \bar{\Psi}^L_+ \Psi^R_-\right) \ . \tag{2.4.5}$$

At this point we need to evaluate the bulk spinors close to the asymptotic boundary. We can achieve this by evaluating the scaling factor close to the boundary[12]

$$\begin{aligned}\bar{\Psi}^R_- \Psi^L_+ &= \frac{e^{-\sigma}}{R^2}\left[(\psi^R\otimes\eta)^\dagger \mathcal{P}_- \gamma^1 \mathcal{P}_+ \left(\psi^L\otimes\eta\right)\right] \\ &= \frac{\mathcal{C}(\bar{r})}{Lr^2\sqrt{f}}\left[(\psi^R\otimes\eta)^\dagger \mathcal{P}_- \gamma^1 \mathcal{P}_+ \left(\psi^L\otimes\eta\right)\right] \ ,\end{aligned} \tag{2.4.6}$$

and a similar expression for $\bar{\Psi}^L_+ \Psi^R_-$. We then find

$$H_{\rm int} = -ih\mathcal{C}(\bar{r})\frac{\epsilon}{\bar{r}}\int d^2\Omega \left[(\psi^R\otimes\eta)^\dagger \mathcal{P}_- \gamma^1 \mathcal{P}_+ \left(\psi^L\otimes\eta\right) + (\psi^L\otimes\eta)^\dagger \mathcal{P}_+ \gamma^1 \mathcal{P}_- \left(\psi^R\otimes\eta\right)\right] \ . \tag{2.4.7}$$

We can compute the semi-classical interacting Hamiltonian in the state defined in (2.2.36) by computing the following expectation value

$$\langle H_{\rm int}\rangle = -ih\mathcal{C}(\bar{r})\frac{\epsilon}{\bar{r}}\int d^2\Omega \left[\langle(\psi^R\otimes\eta)^\dagger \mathcal{P}_- \gamma^1 \mathcal{P}_+ \left(\psi^L\otimes\eta\right)\rangle + \langle(\psi^L\otimes\eta)^\dagger \mathcal{P}_+ \gamma^1 \mathcal{P}_- \left(\psi^R\otimes\eta\right)\rangle\right] \ . \tag{2.4.8}$$

We can evaluate the boundary integral by taking first the angular spinors on-shell. The correlators involved in (2.4.8) can be computed perturbatively in the limit where $\lambda(h) \sim h$. They are explicitly given in Appendix D. Finally, we obtain the result[13]

$$\langle H_{\rm int}\rangle = \mathcal{C}(\bar{r})\frac{\epsilon}{\bar{r}}\frac{2qh}{\pi}\left(-1 + \frac{4h}{\pi}\right) = 4\Delta M + \mathcal{O}\left(h^3\right) \ , \tag{2.4.9}$$

[12] In the RN background (2.4.4), far away from the horizon the metric is conformaly flat. The relation between the coordinates is $t = \frac{\tau}{L}\mathcal{C}(\bar{r})$, and $x = \int dr \frac{1}{L}\frac{1}{f(r)}\mathcal{C}(\bar{r})$, and the conformal factor equals $e^{2\sigma} = \left(\frac{L}{\mathcal{C}(\bar{r})}\right)^2 f$.

[13] Note that in the second equal sign we only take into account the terms up to order h^2, even though the expression in the middle contains a third order term. This is done to compare to the results of the previous section, which included terms up to second order.

with ΔM given by (2.3.29). In order to get the total wormhole energy, we need to add the energy asssociated to the non-interacting parts, *i.e.,* , of two near-extremal RN black holes

$$\langle H\rangle_{WH} = 2M_{WH} + 4\Delta M - 2\mu Q = 2M_{ext} + 6\Delta M - 2\mu Q \ , \tag{2.4.10}$$

where M_{ext} is the black hole extremal mass and Q the extremal charge. In this equation, we have taken into account the change in energy due to the chemical potential μ for the asymptotic charges. This is similar to the electric case [82].

Now that we understand the energy of the wormhole geometry, we would like to investigate whether it is the ground state of some Hamiltonian. We propose the following *local boundary Hamiltonian*

$$H = H_L + H_R - \frac{ih}{\ell}\int d\Omega_2 \left(\bar{\mathbf{\Psi}}^R_- \mathbf{\Psi}^L_+ + \bar{\mathbf{\Psi}}^L_+ \mathbf{\Psi}^R_-\right) + \mu(Q_L - Q_R) \ , \tag{2.4.11}$$

where H_L and H_R are the Hamiltonians associated to the boundary dual of the two identical original systems, and again we take into account the change in energy due to the chemical potential μ for the asymptotic charges. It is important to notice that equation (2.4.11) is an expression written purely in terms of boundary data. In particular, we have defined the boundary spinors, denoted as $\mathbf{\Psi}$, by removing the scaling factor defined in (2.2.19), so that

$$\Psi_\pm = R^{-\frac{3}{2}}\mathbf{\Psi}_\pm \ . \tag{2.4.12}$$

Note that the interacting term is inspired by (2.4.2), which in terms of the boundary data can be written as

$$S_{int} = \frac{ih}{\ell}\int d\tau d\Omega_2 \left(\bar{\mathbf{\Psi}}^R_- \mathbf{\Psi}^L_+ + \bar{\mathbf{\Psi}}^L_+ \mathbf{\Psi}^R_-\right) . \tag{2.4.13}$$

The Hamiltonian determines the time-evolution with respect to the asymptotic time defined in (2.4.4). Note that the total charge of the field theories is conserved as a consequence of a global symmetry.

Next, we consider the expectation value of the Hamiltonian for the different phases. First of all note that the expectation value of (2.4.11) is precisely equal to (2.4.10) for the wormhole solution, since that is the primary reason for the definition of (2.4.11). Secondly, note that the empty AdS geometry has a vanishing Hamiltonian. Finally, we note that for the disconnected black holes, the interaction term of the Hamiltonian does not contribute to the energy. This can be seen from the fact that we can Wick rotate the RN black hole solution, after which the geometry is conformal to the disk. However, the conformal factor vanishes if the black hole

is extremal. Since the correlators on the disk must be finite, the total contribution of the interacting part of the Hamiltonian must indeed be equal to zero.

The difference between the wormhole and the extremal black holes phases is given by

$$\langle H\rangle_{\text{2BH}} - \langle H\rangle_{\text{WH}} > 0 \ . \tag{2.4.14}$$

It is easy to see that $\langle H\rangle_{\text{2BH}}$ has a minimum at the point

$$\bar{r} = \frac{\ell}{\sqrt{3\pi}}\sqrt{\frac{\mu^2}{m_p^2} - \pi} \ , \quad \text{for} \quad \frac{\mu^2}{m_p^2} > \pi \ , \tag{2.4.15}$$

for which $\langle H\rangle_{\text{2BH}} < \langle H\rangle_{\text{Vacuum}} = 0$ (see Figure 2.5). Then, *the wormhole phase (where it exists) dominates the ground state for values of the chemical potential* $\mu > \mu_c$. The complete phase diagram is shown in Figure 2.6. We see that the point $(h = 0, \mu = \mu_c)$ is actually a *triple point* where the three different phases meet. Intuitively, empty AdS is the dominant saddle for very small values of h, for which the wormhole has not been formed yet, and μ so that the charge contribution is negligible. For $h < 0$ and $\mu > \mu_c$, the black holes phase is the dominant saddle. Alternatively, for positive values of the coupling and $\mu > \mu_c$, the wormhole phase will be the ground state of (2.4.11).

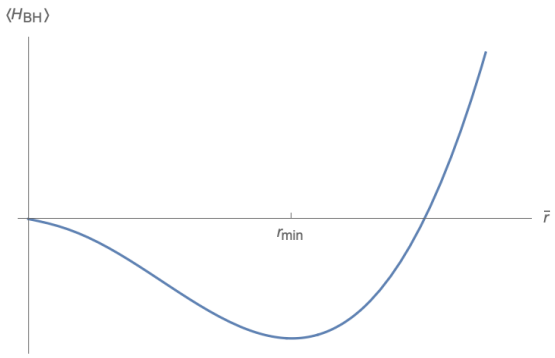

Figure 2.5: Expectation value of the Hamiltonian (2.4.11) in the two-disconnected black holes phase for different values of $\bar{r}$. The minimum is located at r_{min}, which is given in (2.4.15).

2.4.2 Stability

We briefly discuss possible instabilities of the solution. When considering scalar fields in a Reissner-Nördstrom AdS background there are instabilities that lead to hairy black holes. These instabilities can be understood, for near-extremal

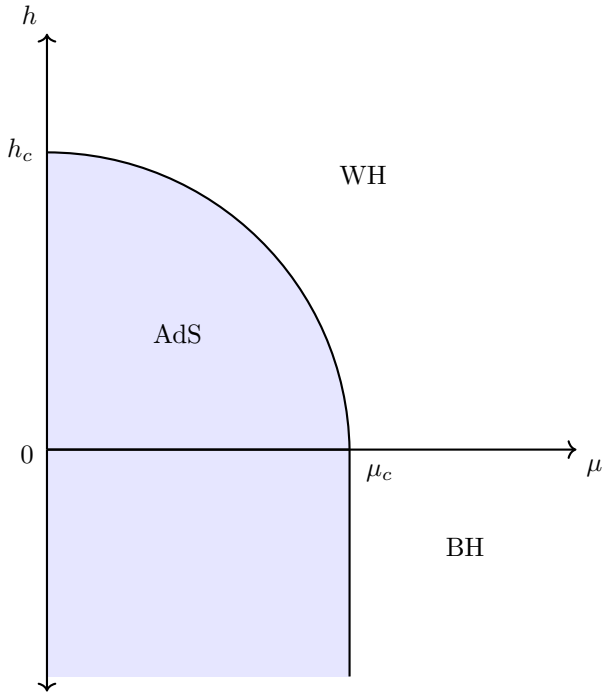

Figure 2.6: Diagram that shows the ground state of the Hamiltonian (2.4.11) for different values of h and μ. Empty AdS is the dominant contribution at the origin up to the critical values $h_c = \frac{\bar{r}^2}{G_N q}\sqrt{\frac{2\pi}{3\mathcal{C}}\left(1+\frac{2\bar{r}^2}{\ell^2}\right)}$ and $\mu_c = m_p\sqrt{\pi}$ where the wormhole phase becomes the ground state. The point ($h = 0$, $\mu = \mu_c$) is a triple point where the three phases meet. For negative values of h, there is a competition between the empty AdS and the black holes phases. Note that depending on the mass of the monopoles in the theory there could be a region in the diagram where the ground state is AdS with monopoles.

black holes, as originating from the difference between the Breitenlöhner Freedman bounds for AdS_2 and AdS_4; fields that are allowed tachyons in the asymptotic AdS_4 spacetime lead to instabilities in the AdS_2 near-horizon region. Even though intuitively similar arguments would lead to fermionic instabilities, no evidence for the existence of fermionic hairy black holes has been found [83]. Since the argument crucially depends on the fact that there is an asymptotic AdS_2 geometry, we expect the same result to hold for the wormhole phase.

Besides investigating whether the wormhole solution is the ground state of the Hamiltonian (2.4.11), one could also wonder whether it is the thermodynamically favored phase in one of the standard thermodynamic ensembles. We must couple the two CFT's in order for a wormhole solution to exist; if signals can cross from one boundary to the other in the bulk, it must be possible to transfer information between the CFT's [62].

Before coupling the CFT's, each CFT has a global $U(1)$ symmetry with an associated charge conservation. After coupling the theories, charge can flow from one to the other, so only a single $U(1)$ survives. In our conventions, the conserved charge us $Q_L + Q_R$. In our conventions, the wormhole solution has $Q_L = -Q_R$. One can picture magnetic field lines threading the wormhole, so this convention is natural. Therefore, the conserved charge for the wormhole is $Q_L + Q_R = 0$. In the standard construction of thermodynamic ensembles, one can only turn on a chemical potential for this conserved charge. The term $\mu(Q_L - Q_R)$ appearing in our Hamiltonian looks like a chemical potential, but it is not really, because $Q_L - Q_R$ is not conserved: it does not commute with the interaction term in the Hamiltonian.

One can ask whether the wormhole dominates one of the standard thermodynamic ensembles at zero temperature; for example, consider the canonical ensemble. The different phases that should be compared are the following: empty AdS, two black holes, the wormhole solution.

The free energy is

$$F = E - TS \ , \tag{2.4.16}$$

in the canonical ensemble. At zero temperature, the wormhole phase will have free energy equal to $F = 2M_{WH}$, while empty AdS has a vanishing free energy. Therefore, empty AdS dominates the ensemble.

Finally, one could consider other ensembles in the hope of finding an ensemble in which the wormhole solution dominates. One candidate is the grand canonical ensemble, with potential given by

$$\Phi = E - TS - \mu Q. \tag{2.4.17}$$

However, the wormhole phase has a conserved charge $Q = Q_L + Q_R = 0$. Therefore, adding a term proportional to Q will not change the potential of the wormhole phase. Because of this it can never dominate the ensemble. The only thing that we have achieved by changing ensembles is that there can be even more phases with a lower potential than the wormhole. Note that it is not very clear how to interpret magnetic charges (and how to fix them) in the different ensembles. The electromagnetic duality suggests they should be treated in the same way as electric charges, but in the standard AdS/CFT context black holes with different electric charges are different states in the same theory, while black holes with different magnetic charges live in different theories. Presumably one can make a choice when imposing boundary conditions for the gauge field analogous to the standard vs alternate quantization for other light fields, and this choice determines whether electric or magnetic states live in the same theory. It would be interesting to understand this better, since our setup depends on the magnetic charges, but this subtlety is mostly orthogonal to our work here.

To summarize: the wormhole appears to be a stable solution that corresponds to the ground state of our Hamiltonian. However, it does not seem to arise as the dominant phase of one of the standard thermodynamic ensembles with chemical potential.

2.5 Discussion

We have found an eternal traversable wormhole in a four-dimensional AdS background. This geometry is a solution to the Einstein-Hilbert gravity action with negative cosmological constant, a $U(1)$ gauge field and massless fermions charged under the gauge field. To open up the wormhole we need negative energy, which we acquire by coupling the CFT's living on the two boundaries of the spacetime.

By calculating the backreaction of the negative energy on the geometry, we find a static traversable wormhole geometry with no horizons or singularities. This wormhole is dual to the ground state of a simple Hamiltonian for two coupled holographic CFT's. The parameters in the Hamiltonian are the chemical potential, the coupling strength, and the central charge. The wormhole dominates in some region of parameter space, while disconnected geometries dominate other regions.

Working in the semi-classical approximation, the authors of [62] proved that there are no traversable wormholes that preserve Poincaré invariance along the boundary field theory directions in more than two spacetime dimensions. The geometry found in this work evades this result because our solution is not Poincaré invariant.

There are a number of interesting future directions.

Traversable Wormholes in the lab; energy gap. One possible application of our results is to build traversable wormholes in the lab by implementing our interacting Hamiltonian and allowing the system to cool to the ground state. For this process to be efficient, it is important the energy gap between the ground state and the first excited state is not too small.

It would be interesting to carefully calculate the gap in this system. A rough estimate can be obtained by calculating the maximum redshift. Black holes have infinite redshift near the horizon and therefore support excitations with arbitrarily small energy in the semi-classical limit.

Looking back at our 'matching' section, we see that the black hole geometry is valid down to

$$r - \bar{r} \sim \epsilon L \sim \bar{r} \ . \tag{2.5.1}$$

At this location, the redshift is $f(r) \sim \mathcal{C}(\bar{r})$. Inside this matching radius, the geometry is $\mathrm{AdS}_2 \times S_2$. The relative redshift between the middle of the wormhole and the matching surface is

$$\frac{f_{\mathrm{match}}}{f_0} \sim \rho^2_{\mathrm{match}} \sim \frac{1}{\epsilon^2} \ . \tag{2.5.2}$$

Combining these results, and restoring units using the AdS radius, our guess is

$$\mathrm{Gap} \sim \frac{\mathcal{C}(\bar{r})\epsilon^2}{\ell} \ . \tag{2.5.3}$$

This result looks concerningly small due to the ϵ^2; however, $\mathcal{C}(r) = 1 + 6\bar{r}^2/\ell^2$ is large for large black holes. We leave a fuller discussion and more reliable calculation for the future.

RG flow. Our bulk analysis is made convenient by the Weyl invariance of the massless fermions, which correspond to boundary operators of particular dimensions. If we think of the interaction term as an interaction in a single CFT, this term appears to be exactly marginal. It would be interesting to understand whether higher order corrections change the scaling dimension of this interaction, or more generally to understand the RG flow of our system.

Supersymmetry. Related to the RG flow, it would add a degree of theoretical control to realize the initial extremal black hole as a BPS state in a supersymmetric theory. Accomplishing this requires embedding our simple $U(1)$ theory in a theory with more conserved charges [84–87].

CFT state. In the related construction of Cottrell et al [74], the state of the dual CFT was identified with the thermofield double state, while the bulk geometry was not under semiclassical control. In this paper, we have constructed a controlled traversable wormhole, but have not calculated the quantum state of the CFT in boundary variables. One may expect that it is a thermofield double type state, but note that the wormhole is a zero temperature solution, so it cannot be exactly the TFD. On the other hand, the bulk geometry clearly looks like a slightly superextremal Reissner Nordstrom black hole away from the wormhole mouth, giving a clear hint regarding the CFT state.

Multi-mouth wormholes. In the present work, we focused on asymptotically AdS_4 two-mouth traversable wormhole geometries. It might be interesting to extend our results and explore in the future the possibility of fourth dimensional multi-mouth wormholes similar to those studied in [66, 67]. In particular, the results of this paper might be used to understand explicitly the role played by multiparty entanglement in the wormhole's traversability.

Information transfer. Moreover, it would be interesting to investigate the amount of information that can be sent through this type of wormhole, in a similar fashion as in [38, 58, 63].

Replica wormholes. Finally, it has been found that two dimensional eternal traversable wormhole geometries contribute to the fine-grained entropy in the context of islands in de Sitter spacetime [88] (see also [89,90]). It would be interesting to understand whether more general set-ups in higher dimensions can be described with similar methods to those employed in this paper.

A Appendices

Propagators

In this appendix we present the results for the propagators. Below, we show the derivation of (2.2.37)

$$\begin{aligned}
\langle \psi_+^\dagger(x_-)\psi_+(x'_-)\rangle &= \left\langle \sum_{k,j\in\mathbb{Z}} \frac{1}{\pi}\alpha_k^\dagger\alpha_j e^{i\omega_j x'_- - i\omega_k x_-} \right\rangle \\
&= \left\langle \sum_{k,j\in\mathbb{Z}_{\geq 0}} \frac{1}{\pi}\alpha_k^\dagger\alpha_j e^{i\omega_j x'_- - i\omega_k x_-} \right\rangle \\
&= \left\langle \sum_{k,j\in\mathbb{Z}_{\geq 0}} \frac{1}{\pi}(\delta_{k,j}-\alpha_j\alpha_k^\dagger) e^{i\omega_j x'_- - i\omega_k x_-} \right\rangle \\
&= \sum_{j\in\mathbb{Z}_{\geq 0}} \frac{1}{\pi} e^{i\omega_j(x'_- - x_-)} \\
&= \sum_{j\in\mathbb{Z}_{\geq 0}} \frac{1}{\pi} e^{i\left(\frac{2j+1}{2}\right)(x'_- - x_-)} \left(1+(-1)^j\frac{2i\lambda(h)}{\pi}(x'_- - x_-)\right) + \mathcal{O}\left((x'_- - x_-)^2\right) \\
&= \frac{1}{\pi}\frac{e^{\frac{i}{2}(x'_- - x_-)}}{1-e^{i(x'_- - x_-)}} + \frac{e^{\frac{i}{2}(x'_- - x_-)}}{1+e^{i(x'_- - x_-)}}\frac{2i\lambda(h)}{\pi^2}(x'_- - x_-) + \mathcal{O}\left((x'_- - x_-)^2\right) \ .
\end{aligned} \tag{A.1}$$

The rest of the propagators can be derived in a similar fashion. We present the results

$$\langle \psi_-^\dagger(x_+)\psi_-(x'_+)\rangle = \frac{1}{\pi}\frac{e^{\frac{i}{2}(x'_+ - x_+)}}{1-e^{i(x'_+ - x_+)}} + \frac{e^{\frac{i}{2}(x'_+ - x_+)}}{1+e^{i(x'_+ - x_+)}}\frac{2i\lambda(h)}{\pi^2}(x'_+ - x_+) + \mathcal{O}\left((x'_- - x_-)^2\right) \ , \tag{A.2}$$

$$\langle \psi_+^\dagger(x_-)\psi_-(x'_+)\rangle = -\frac{1}{\pi}\frac{e^{\frac{i}{2}(x'_+-x_-)}}{1+e^{i(x'_+-x_-)}} - \frac{e^{\frac{i}{2}(x'_+-x_-)}}{1-e^{i(x'_+-x_-)}}\frac{2i\lambda(h)}{\pi^2}(x'_+-x_-) + \mathcal{O}\left((x'_- - x_-)^2\right) , \tag{A.3}$$

and

$$\langle \psi_-(x_+)\psi_+(x'_-)\rangle = \langle \psi_-(x_+)\psi_-(x'_+)\rangle = \langle \psi_+(x_-)\psi_+(x'_-)\rangle = 0 . \tag{A.4}$$

B Stress tensor

In this appendix, we show the calculation of the stress tensor. First of all note that we can average over the angular directions by taking the spherical components on-shell in equation (2.2.38). Since the spherical components are normalized such that $\int d^2\Omega\ \bar{\eta}^m \eta^n = \delta_{m,n}$, averaging over the angular directions results in a factor of $\frac{1}{4\pi}$. Using this and point-splitting, the first line of (2.2.38) becomes

$$\begin{aligned}\langle T_{11}\rangle &= \lim_{\substack{t'\to t\\ x'\to x}} \frac{1}{4\pi}\sum_{m,n}\int d^2\Omega \frac{i}{2R^2}\left(\partial'_t-\partial_t\right)\left(\langle \psi_+^{m\dagger}(x_-)\psi_+^n(x'_-)\rangle + \langle \psi_-^{m\dagger}(x_+)\psi_-^n(x'_+)\rangle\right)\eta^{m\dagger}\eta^n \\ &= \lim_{\substack{t'\to t\\ x'\to x}} \frac{qi}{8\pi R^2}\left(\partial'_t-\partial_t\right)\left(\langle {\psi_+}^\dagger(x_-)\psi_+(x'_-)\rangle + \langle \psi_-^\dagger(x_+)\psi_-(x'_+)\rangle\right)\ . \end{aligned} \tag{B.1}$$

The renormalized $\langle T_{11}\rangle$ is found by subtracting the $h=0$ contribution from the $h\neq 0$ expression as follows

$$\begin{aligned}\langle T_{11}\rangle &= \langle T_{11}^{h\neq 0}\rangle - \langle T_{11}^{h=0}\rangle \\ &= \lim_{\substack{t'\to t\\ x'\to x}} \frac{qi}{8\pi R^2}\left(\partial'_t-\partial_t\right)\left(\frac{e^{\frac{i}{2}(x'_- - x_-)}}{1+e^{i(x'_- - x_-)}}\frac{2i\lambda(h)}{\pi^2}(x'_- - x_-) + \frac{e^{\frac{i}{2}(x'_+ - x_+)}}{1+e^{i(x'_+ - x_+)}}\frac{2i\lambda(h)}{\pi^2}(x'_+ - x_+\right) \\ &= \lim_{\substack{t'\to t\\ x'\to x}} \frac{qi}{8\pi R^2}\left(\frac{4i\lambda(h)}{\pi^2}+\frac{3i\lambda(h)}{2\pi^2}\left((t'-t)^2+(x'-x)^2\right)\right) \\ &= -\frac{q\lambda(h)}{2\pi^3 R^2}\ , \end{aligned} \tag{B.2}$$

where we have omitted combined factors of $(t'-t)$ and $(x'-x)$ to higher orders. Similarly, we find that the rest of the renormalized components of the stress tensor are given by

$$\langle T_{22}\rangle = -\frac{q\lambda(h)}{2\pi^3 R^2}, \quad \text{and} \quad \langle T_{33}\rangle = \langle T_{44}\rangle = 0\ . \tag{B.3}$$

It is easy to see that this contribution to the stress tensor is traceless

$$\langle T_\mu{}^\mu\rangle = g^{\mu\nu}\langle T_{\mu\nu}\rangle = e^{-2\sigma}\left(\frac{q\lambda(h)}{2\pi^3 R^2}-\frac{q\lambda(h)}{2\pi^3 R^2}\right) = 0\ . \tag{B.4}$$

We can also check that the stress tensor is conserved. We will need the following components of $\nabla_\mu \langle T_{\rho\nu} \rangle$

$$\begin{aligned}
\nabla_x \langle T_{xx} \rangle &= \partial_x \langle T_{xx} \rangle - \Gamma^\rho_{xx} \langle T_{\rho x} \rangle - \Gamma^\rho_{xx} \langle T_{x\rho} \rangle \\
&= \frac{q\lambda(h) R'}{\pi^3 R^3} + \frac{q\lambda(h)\sigma'}{\pi^3 R^2}, \\
\nabla_t \langle T_{tx} \rangle &= \partial_t \langle T_{tx} \rangle - \Gamma^\rho_{tt} \langle T_{\rho x} \rangle - \Gamma^\rho_{tx} \langle T_{x\rho} \rangle \\
&= \frac{q\lambda(h)\sigma'}{\pi^3 R^2}, \\
\nabla_\theta \langle T_{\theta x} \rangle &= \partial_\theta \langle T_{\theta x} \rangle - \Gamma^\rho_{\theta\theta} \langle T_{\rho x} \rangle - \Gamma^\rho_{\theta x} \langle T_{x\rho} \rangle \\
&= -\frac{q\lambda(h) R' e^{-2\sigma}}{2\pi^3 R}, \\
\nabla_\phi \langle T_{\phi x} \rangle &= \partial_\phi \langle T_{\phi x} \rangle - \Gamma^\rho_{\phi\phi} \langle T_{\rho x} \rangle - \Gamma^\rho_{\phi x} \langle T_{x\rho} \rangle \\
&= -\frac{q\lambda(h) R' e^{-2\sigma} \sin^2(\theta)}{2\pi^3 R}\ ,
\end{aligned}$$

so that

$$\begin{aligned}
\nabla_\mu \langle T^\mu_{\ \nu} \rangle =& g^{\mu\rho} \nabla_\mu \langle T_{\rho\nu} \rangle \\
=& g^{xx} \nabla_x \langle T_{xx} \rangle + g^{tt} \nabla_t \langle T_{tx} \rangle + g^{\theta\theta} \nabla_\theta \langle T_{\theta x} \rangle + g^{\phi\phi} \nabla_\phi \langle T_{\phi x} \rangle \\
=& e^{-2\sigma} \left(\frac{q\lambda(h) R'}{\pi^3 R^3} + \frac{q\lambda(h) h \sigma'}{\pi^3 R^2} \right) \qquad \text{(B.5)} \\
& - e^{-2\sigma} \frac{q\lambda(h)\sigma'}{\pi^3 R^2} - \frac{1}{R^2} \frac{q\lambda(h) R' e^{-2\sigma}}{2\pi^3 R} - \frac{1}{R^2 \sin^2(\theta)} \frac{q\lambda(h) R' e^{-2\sigma} \sin^2(\theta)}{2\pi^3 R} \\
=& 0. \qquad \text{(B.6)}
\end{aligned}$$

As a final check one can show that the t, x component of the stress tensor is indeed equal to zero. First note that T_{12} is equal to

$$T_{12} = \frac{i}{2R^2} \left(\psi^\dagger_+ \partial_- \psi_+ - \psi^\dagger_- \partial_+ \psi_- - \partial_- \psi^\dagger_+ \psi_+ + \partial_+ \psi^\dagger_- \psi_- \right) \otimes \eta^\dagger \eta. \qquad \text{(B.7)}$$

Using point-splitting this becomes

$$\begin{aligned}
\langle T_{12} \rangle =& \lim_{\substack{t' \to t \\ x' \to x}} \frac{1}{4\pi} \sum_{m,n} \int d^2\Omega \frac{i}{2R^2} \Big(\partial'_- \langle \psi^{m\dagger}_+(x_-) \psi^n_+(x'_-) \rangle - \partial_- \langle \psi^{m\dagger}_+(x_-) \psi^n_+(x'_-) \rangle \\
& \qquad - \partial'_+ \langle \psi^{m\dagger}_-(x_+) \psi^n_-(x'_+) \rangle - \partial_+ \langle \psi^{m\dagger}_-(x_+) \psi^n_-(x'_+) \rangle \Big) \eta^{m\dagger} \eta^n \\
=& \lim_{\substack{t' \to t \\ x' \to x}} \frac{qi}{8\pi R^2} \Big(\partial'_- \langle \psi^\dagger_+(x_-) \psi_+(x'_-) \rangle - \partial_- \langle \psi^\dagger_+(x_-) \psi_+(x'_-) \rangle \\
& \qquad - \partial'_+ \langle \psi^\dagger_-(x_+) \psi_-(x'_+) \rangle - \partial_+ \langle \psi^\dagger_-(x_+) \psi_-(x'_+) \rangle \Big)\ , \qquad \text{(B.8)}
\end{aligned}$$

and we see that

$$
\begin{aligned}
\langle T_{12}\rangle =&\langle T_{12}^{h\neq 0}\rangle - \langle T_{12}^{h=0}\rangle \\
=&\lim_{\substack{t'\to t\\ x'\to x}} \frac{qi}{8\pi R^2}\Big(\partial'_- \frac{e^{\frac{i}{2}(x'_- - x_-)}}{1+e^{i(x'_- - x_-)}}\frac{2\lambda(h)i}{\pi^2}(x'_- - x_-) - \partial_- \frac{e^{\frac{i}{2}(x'_- - x_-)}}{1+e^{i(x'_- - x_-)}}\frac{2\lambda(h)i}{\pi^2}(x'_- - x_-) \\
&\quad - \partial'_+ \frac{e^{\frac{i}{2}(x'_+ - x_+)}}{1+e^{i(x'_+ - x_+)}}\frac{2\lambda(h)i}{\pi^2}(x'_+ - x_+) - \partial_+ \frac{e^{\frac{i}{2}(x'_+ - x_+)}}{1+e^{i(x'_+ - x_+)}}\frac{2\lambda(h)i}{\pi^2}(x'_+ - x_+)\Big) \\
&\quad + \mathcal{O}\left((x'_- - x_-)^2\right) + \mathcal{O}\left((x'_+ - x_+)^2\right) \\
=&0\ .
\end{aligned}
\tag{B.9}
$$

C Matching

Let us turn to the time component of the metrics. At large ρ we can expand $\gamma(\rho)$ in the following way

$$\gamma(\rho) = \frac{\zeta}{\mathcal{C}(\bar{r})}\left(1+4\frac{\bar{r}^2}{\ell^2}\right)\left(-\frac{\pi}{2}\rho^3 - \frac{3\pi}{2}\rho + 2\log(\rho)\right) + \cdots \ . \tag{C.1}$$

In order to match the cubic term in ρ to the $\left(\frac{r-\bar{r}}{\bar{r}}\right)^3$ term in (2.3.21) we will consider the following limit. We consider ρ to be large, but $\zeta\rho$ small and fixed. In this limit ψ is still given by (2.3.25). Furthermore, from (2.3.27) we see that we should consider ϵ to be of order ζ. This limit corresponds to expanding f at small $\frac{r-\bar{r}}{\bar{r}}$, but even smaller $\zeta \propto \epsilon$. More precisely, compared to (2.3.21) we still expand in $\frac{r-\bar{r}}{\bar{r}}$ up to third order. However, we only consider ϵ up to zeroth order

$$f(r) = \mathcal{C}(\bar{r})\left(\frac{r-\bar{r}}{\bar{r}}\right)^2 - 2\left(1+4\frac{\bar{r}^2}{\ell^2}\right)\left(\frac{r-\bar{r}}{\bar{r}}\right)^3 + \mathcal{O}\left(\left(\frac{r-\bar{r}}{\bar{r}}\right)^4\right) \ . \tag{C.2}$$

We should now match the expansion (C.2) to the following expression, where we will assume to be in the limit discussed above

$$\begin{aligned}\frac{\bar{r}^2}{\mathcal{C}(\bar{r})}(1+\rho^2+\gamma(\rho))\frac{dt^2}{d\tau^2} &= \mathcal{C}(\bar{r})\left(\rho^2 - \frac{\pi}{2}\rho^3\frac{\zeta}{\mathcal{C}(\bar{r})}\left(1+4\frac{\bar{r}^2}{\ell^2}\right)\right)\frac{1}{\rho^2}\left(\frac{r-\bar{r}}{\bar{r}}\right)^2 \\ &= \mathcal{C}(\bar{r})\left(\frac{r-\bar{r}}{\bar{r}}\right)^2 - \frac{\pi}{2}\rho\left(\frac{r-\bar{r}}{\bar{r}}\right)^2\zeta\left(1+4\frac{\bar{r}^2}{\ell^2}\right) \\ &= \mathcal{C}(\bar{r})\left(\frac{r-\bar{r}}{\bar{r}}\right)^2 - 2\left(1+4\frac{\bar{r}^2}{\ell^2}\right)\left(\frac{r-\bar{r}}{\bar{r}}\right)^3, \end{aligned} \tag{C.3}$$

where in the third line we used (2.3.25). We see that we recover (C.2) up to third order.

D Correlators in $\langle H_{\text{int}} \rangle$

In this appendix, we show explicitly the equal-time correlators involved in the computation of the semi-classical interacting Hamiltonian in terms of the $2D$ propagators presented in Appendix A. Note that in Appendix A, the propagators are expanded in $x - x'$, while here we need the location of the fields to approach opposing boundaries. However, the expressions obtained are still valid if we take h small, and expand in h instead. The equal-time correletors present in the Hamiltonian are given by[1]

$$\begin{aligned}\langle H_{\text{int}} \rangle &\supset -ih\mathcal{C}(\bar{r})\frac{\epsilon}{\bar{r}}\int d^2\Omega \langle \bar{\Psi}_-^R \Psi_+^L \rangle \\ &= -\frac{ih\epsilon}{2\bar{r}}\mathcal{C}(\bar{r})\int d^2\Omega \left(\langle -\psi_+^{R\dagger}\psi_+^L \rangle + i\langle \psi_+^{R\dagger}\psi_-^L \rangle + i\langle \psi_-^{R\dagger}\psi_+^L \rangle + \langle \psi_-^{R\dagger}\psi_-^L \rangle \right) \eta_-^\dagger \eta_- \\ &= \frac{qh\epsilon}{\pi\bar{r}}\mathcal{C}(\bar{r})\left(-1 + \frac{4h}{\pi}\right) + \mathcal{O}\left(h^4\right) \ , \end{aligned} \tag{D.1}$$

and

$$\begin{aligned}\langle H_{\text{int}} \rangle &\supset -ih\mathcal{C}(\bar{r})\frac{\epsilon}{\bar{r}}\int d^2\Omega \langle \bar{\Psi}_+^L \Psi_-^R \rangle \\ &= -\frac{ih\epsilon}{2\bar{r}}\mathcal{C}(\bar{r})\int d^2\Omega \left(\langle \psi_+^{L\dagger}\psi_+^R \rangle + i\langle \psi_+^{L\dagger}\psi_-^R \rangle + i\langle \psi_-^{L\dagger}\psi_+^R \rangle - \langle \psi_-^{L\dagger}\psi_-^R \rangle \right) \eta_-^\dagger \eta_- \\ &= \frac{qh\epsilon}{\pi\bar{r}}\mathcal{C}(\bar{r})\left(-1 + \frac{4h}{\pi}\right) + \mathcal{O}\left(h^4\right) \ . \end{aligned} \tag{D.2}$$

[1] Note that we include higher orders than we need for the computation in the main text.

3 Virasoro Entanglement Berry Phases

3.1 Introduction

A particular goal of holography is to understand the emergence of geometry from the boundary conformal field theory. Recent applications of quantum information theory in holography have given a means of directly probing geometry of the bulk, and thus have provided a promising avenue for addressing this question.

One geometrical application of entanglement is an auxiliary space for holography known as kinematic space, which can be defined as the space of pairs of spacelike points in a CFT_d [91, 92]. Perturbations of entanglement entropy are seen to propagate as fields on this space [93]. For CFT_2, kinematic space can additionally be obtained from the set of entanglement entropies associated to intervals [94]. While fixed by the asymptotic conformal symmetry, kinematic space provides a tool for the reconstruction of bulk geometry in certain sufficiently symmetrical and controlled settings. For instance, it reconstructs geometry for locally AdS_3 spacetimes [95]. It also probes the geometry only outside of entanglement shadow regions that are inaccessible to spacelike geodesics [96,97]. This auxiliary space is a symplectic manifold, specifically it is a particular coadjoint orbit of the conformal group [98].

The drawback here is of course the reliance on symmetries and special geometries. Is it possible to use entanglement to probe more general geometries? To this end, transport for 2d kinematic space was generalized to a parallel transport process for the modular Hamiltonian [28, 32].[1] In this setup, there is an associated Berry connection on kinematic space that computes lengths of curves in the bulk. More generally, a modular Berry connection can be shown to relate

[1] For approaches to general reconstruction using null surfaces rather than spacelike extremal surfaces, see [99–101]. To move beyond entanglement shadow regions and geodesic barriers [102] one could also use timelike geodesics as probes. These are dual to circuit complexity as defined by the Nielsen geometric approach. They describe an auxiliary symplectic geometry which is also a coadjoint orbit of the conformal group, just a different one than kinematic space [103].

frames for CFT algebras associated to different states and subregions. Entanglement provides a connection that sews together nearby entanglement wedges and probes the geometry near the extremal surface. This connection builds spacetime from entanglement, reminiscent of the ER=EPR proposal [39]. While the modular Hamiltonian admits a particularly simple, local description only in special cases, the parallel transport of modular Hamiltonians is true more generally, and its bulk description relies only on leading order in $1/N$ and sufficient smoothness of the extremal surface.

The parallel transport of modular Hamiltonians has been studied in the setting where the interval shape is varied, which connects to kinematic space [91]. Shape-changing parallel transport has also been applied to study cases in holography where the modular chaos bound is saturated, which is governed by a certain algebra of modular scrambling modes that generate null deformations close to the extremal surface [104]. We are interested in generalizing beyond the case where the shape or interval location is varied, to consider modular parallel transport governed by a change of global *state* (see also [105] for a similar approach). For instance, one could imagine acting on a CFT on the cylinder by a large diffeomorphism contained in the Virasoro algebra. This would modify the algebra of operators on the interval. The redundancy by certain symmetries known as *modular zero modes* which change the algebra but leave physical observables fixed results in a connection and non-trivial parallel transport, even in the case where the interval remains fixed. A general modular transport problem would consist of an amalgamation of these two kinds of parallel transport, with a simultaneous modification of both the state and interval shape.

Ultimately, we consider special transformations which do not lie in the Virasoro algebra as typically defined since they are not analytic, rather they vanish at the interval endpoints and are non-differentiable at these points. The reason for this is technical: to uniquely isolate the zero mode contribution it is necessary to have a decomposition into kernel and image of the adjoint action of the modular Hamiltonian. As we explain in Appendix C, this is not possible for the Virasoro algebra. This is a subtlety that, to our knowledge, has not been previously studied. For a large class of transformations which obey certain properties, we derive a general expression for the Berry curvature in Appendix B. We also explain how these non-standard vector fields have a simple interpretation as plane waves in the hyperbolic black hole geometry using the map of Casini, Huerta and Myers [106].

We define a suitable algebra of vector fields on the circle constructed from wave packets of these eigenstates. Much as similar group-theoretic parallel transport problems are governed by the geometry of symplectic manifolds known as coadjoint orbits, here that is the case as well. We show that the Berry curvature for state-

changing parallel transport is equal to the Kirillov-Kostant symplectic form on an orbit associated to this algebra of vector fields.

State-changing parallel transport can also be related to bulk geometry. This has the advantage of accessing different geometrical data in the bulk, compared to the setting where only the interval shape is varied. We find that the Berry curvature for a fixed interval and changing state computes the symplectic form for a Euclidean conical singularity geometry obtained from the backreaction of a cosmic brane, subject to a suitable principal value prescription for regulating divergences near the interval endpoint. To match the curvature, we must impose Dirichlet boundary conditions at the location of the extremal surface. We interpret this as describing (and defining) a symplectic form associated to the entanglement wedge. In the discussion, we connect to earlier work on the holographic interpretation of the Berry curvature, and comment on the relation to the entanglement wedge symplectic form in the case of operator-based parallel transport.

Modular parallel transport, either in the case of a changing shape or a changing state, is a parallel transport of *operators* and density matrices. It is distinct from existing algebraic applications of parallel transport of *states*, which for instance transform under unitary representations of a symmetry group. As part of this work we hope to clarify some of the differences, as well as various applications of each. In particular, we both review how kinematic space for CFT_2 can be understood in the language of operator-based parallel transport in Section 3.2.1, while also providing a new derivation of this same kinematic space using state-based parallel transport in Appendix A. This gives two different ways of viewing the same problem, both utilizing group theory, reminiscent of the 'Heisenberg' versus 'Schrödinger' pictures for quantum mechanics.

This chapter will be organized as follows. We begin in Section 3.2 by giving a summary of both state and operator-based parallel transport, and providing a few examples of each. In Section 3.3, we derive the boundary parallel transport process for transformations that diagonalize the adjoint action and compute the curvature in an example. We go into further detail in Section 3.4 about the algebraic structure and the connection to coadjoint orbits. In Section 3.5, we present our proposal for the bulk dual using the symplectic form for Euclidean conical singularity solutions created from the backreaction of a cosmic brane. We end with a discussion about some subtleties and suggest future research directions. In Appendix A, we provide a derivation of kinematic space using state-based parallel transport, and in Appendix B we derive a general expression for the curvature for operator-based parallel transport, which applies for any algebra. Finally, in Appendix C we discuss some subtleties about diagonalization of the adjoint action

for the Virasoro algebra.

3.2 Geometric Berry phases

Geometric phases can arise in quantum mechanics when a Hamiltonian depends continuously on certain parameters, such as an external magnetic field. This results in a state that differs from the starting state by a phase under a closed path in parameter space. Several generalizations of this notion have recently arisen in studies of conformal field theory and holography, relying for instance on the fact that entanglement can act as a connection that relates the Hilbert spaces of different subsystems.

The applications to holography utilize group-based generalizations of the familiar geometric phases of quantum mechanics. In this section, we will review the tools that are relevant, making a distinction between two different approaches for group-based parallel transport depending on whether it is applied to states (a Schrödinger-type picture) or density matrices (a Heisenberg approach). Before moving on to new results, we give some examples of how these different approaches have so far been applied to holography.

3.2.1 States

We begin by describing the parallel transport of states that transform under a unitary representation of a group (see [107] for applications to the Virasoro group). The basic idea is to generalize beyond a path in a space of parameters, as in quantum mechanics, to a path in a group representation. A gauge connection can be defined relating different tangent spaces along the path. If some unitaries in the representation act trivially on a starting state, this constitutes a redundancy by which the state may not return to itself under a closed path through the group manifold.

Specifically, consider a group G with Lie algebra $\mathfrak{g}$, and a unitary representation $\mathcal{D}$ which acts on a Hilbert space $\mathcal{H}$. Take a state $|\phi\rangle \in \mathcal{H}$ that is an eigenstate of all elements in a 'stabilizer' subalgebra $\mathfrak{h} \subset \mathfrak{g}$, or equivalently it is left invariant up to a phase under the action of the corresponding subgroup $H \subset G$. Let $U(\gamma(t)) \in \mathcal{D}$ with $\gamma(t) \in G$, $t \in [0, T]$ be a continuous path through this representation, which corresponds to a continuous path of states $|\phi(t)\rangle = U(\gamma(t))\,|\phi\rangle$. The states $|\phi(t)\rangle$ for all $\gamma(t)$ are often called generalized coherent states, and they parametrize the coset space G/H [108, 109].

The Berry connection is defined as

$$A = i\,\langle\phi(t)|\,d\,|\phi(t)\rangle = i\,\langle\phi|\,U^{-1}dU\,|\phi\rangle \ , \tag{3.2.1}$$

where d is the exterior derivative on the group manifold, and we have used $U^\dagger = U^{-1}$ since the representation is unitary. The connection is just $A = i \langle\phi| \mathcal{D}(\Theta) |\phi\rangle$ with Θ the Maurer-Cartan form associated to the group, $\Theta(\dot\gamma(t)) = \frac{d}{d\tau}\big|_{\tau=t} [\gamma(t)^{-1}\gamma(\tau)]$. Under action by an element of the stabilizer subgroup, the state changes by a phase $|\phi(t)\rangle \to e^{i\alpha} |\phi(t)\rangle$. The connection then transforms as a gauge field, $A \to A - d\alpha$.

The associated Berry curvature is

$$F = dA \ , \tag{3.2.2}$$

and the geometric phase is defined as

$$\theta(\gamma) = \int_\gamma A \ . \tag{3.2.3}$$

This phase is in general gauge dependent, but is gauge invariant when the path γ is closed. In this case, we can write

$$\theta(\gamma) = \oint_\gamma A \ = \int_{B|\partial B=\gamma} F \ , \tag{3.2.4}$$

where in the last line we have used Stokes' theorem to convert this to the flux of the Berry curvature over any surface B with boundary γ. This measures the phase picked up by the state $|\phi\rangle$ under a closed trajectory through the group representation.

Similar techniques are relevant in the study of Nielsen complexity, which describes the geometry of the space of states related by unitaries, starting from a given reference state. A specific path through unitaries is known as a 'circuit.' In conformal field theory, one can choose a reference state such as a primary that is invariant under a subset of the conformal symmetry. Defining the complexity further requires a notion of distance between states. Certain choices have relations to the Berry connection or curvature of state-based parallel transport [103,110–115] (for the application of similar mathematical structures to a description of other definitions for complexity, see [116, 117]).

Another application arises in a subfield of holography known as 'kinematic space,' which studies the geometric properties of the space of spacelike pairs of points in a CFT$_d$ and their role in probing the geometry of the bulk anti-de Sitter (AdS) spacetime [91–94]. It was demonstrated that certain bilocal operators in a CFT pick up phases under a parallel transport that displaces the location of the spacelike points where they are evaluated. In the bulk AdS spacetime this was shown to compute the length of a curve traced out by geodesics limiting to these point pairs

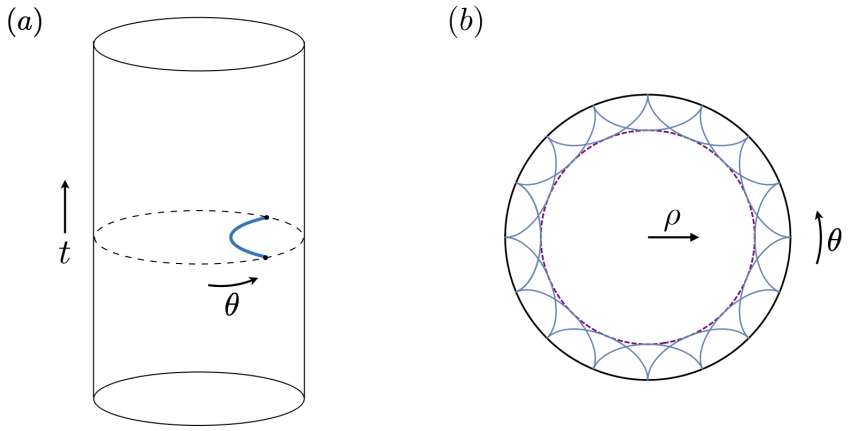

Figure 3.1: (a) Kinematic space can be defined as the space of pairs of spacelike separated points in a CFT, which are in correspondence with bulk minimal area spacelike geodesics ending on these points. The blue curve is one such geodesic, in the special case that the endpoints lie on the same time slice. (b) The parallel transport of operators in kinematic space can be related to lengths in the bulk AdS spacetime. Depicted here is a constant time slice of anti-de Sitter spacetime. Pairs of points on the boundary define bulk geodesics (blue, solid curves). As the interval position is varied, these trace out an envelope in the bulk (dashed purple circle). The length of this envelope is directly related to the Berry phase associated to the boundary parallel transport of bilocal operators evaluated at the endpoints [28].

on the boundary (see Figure 3.1) [28]. As we show in Appendix A, these results for kinematic space can be understood using the language of state-based parallel transport.

3.2.2 Density matrices

Consider a subregion A on a time slice of a CFT. Associated to this region is an algebra of operators $\mathcal{A}_A$. Assuming some short distance cutoff, the state is described by a reduced density matrix ρ_A, obtained from tracing the full state over the complement $\bar{A}$ of A. From this we can define the modular Hamiltonian H_{mod} through $\rho_A = e^{-H_{\text{mod}}}/(\text{tr } e^{-H_{\text{mod}}})$. The modular Hamiltonian encodes information about the entanglement properties of the state. It will be formally useful to refer to the 'complete' modular Hamiltonian $H_{\text{mod,A}} - H_{\text{mod},\bar{\text{A}}}$. We will often drop the subscript A, and additionally allow the modular Hamiltonian to depend on some parameter $H_{\text{mod}}(\lambda)$. This could for instance encode changes in the size of region A as was studied in [28,32], or a change of state as we describe in the next section.

The physical data associated to A is not the set of operators in $\mathcal{A}$, but rather their expectation values. As such, there can be symmetries, i.e, transformations which act on the algebra while leaving no imprint on measurable quantities. We define a *modular zero mode* Q_i as a Hermitian operator that commutes with the modular Hamiltonian,

$$[Q_i, H_{\text{mod}}] = 0 \ . \tag{3.2.5}$$

The modular zero mode can be exponentiated to the unitary

$$V = e^{-i\sum_i s_i Q_i} \ . \tag{3.2.6}$$

Under the flow $\mathcal{O} \to V^\dagger \mathcal{O} V$, the expectation values of algebra elements are left unchanged while taking the algebra to itself. The transformation by modular zero modes therefore constitutes a kind of gauge redundancy.

Given an operator, it is often useful to separate the zero mode part out from a contribution that is non-ambiguous. In the finite-dimensional case, we can compute the zero mode contribution by using the projection operator

$$P_0[\mathcal{O}] = \sum_{E,q_i,q_i'} |E,q_i\rangle \langle E,q_i| \, \mathcal{O} \, |E,q_i'\rangle \langle E,q_i'| \ , \tag{3.2.7}$$

where $|E,q_i\rangle$ are simultaneous eigenstates of H_{mod} and Q_i. Note that later we will be working with an infinite-dimensional algebra, where this formula no longer applies. We will show how to define an appropriate projection relevant for that situation in Section 3.3.

The zero mode frame redundancy leads to a Berry transport problem for operators. Imagine a process that modifies the algebra $\mathcal{A}_A$ depending on a parameter λ, for instance by changing the interval A or the state. We start by diagonalizing the modular Hamiltonian,

$$H_{\text{mod}} = U^\dagger \Delta U \ , \tag{3.2.8}$$

where Δ is a diagonal matrix of eigenvalues. H_{mod}, U and Δ are functions of λ that vary along the path. Taking the derivative gives the 'parallel transport equation,'

$$\dot{H}_{\text{mod}} = [\dot{U}^\dagger U, H_{\text{mod}}] + U^\dagger \dot{\Delta} U \ , \tag{3.2.9}$$

where $\dot{\cdot} = \partial_\lambda$. The first term on the right-hand side lies in the image of the adjoint action, $[\cdot, H_{\text{mod}}]$. The second term encodes the change of spectrum under the parallel transport. It is a zero mode since it commutes with the modular Hamiltonian, in other words, it lies in the kernel of the adjoint action. We will assume that there is a unique decomposition into the image and kernel of the adjoint action, so that the entire zero mode contribution can be isolated from the

second term: $P_0[\dot{H}_{\rm mod}] = U^\dagger \dot{\Delta} U$. For a discussion of subtleties associated with this assumption for the Virasoro algebra, see Appendix C.

This equation exhibits a redundancy due to the presence of modular zero modes. For instance, the modular Hamiltonian together with Eq. (3.2.9) could be equally well expressed in terms of $U \to \tilde{U} = UV$ where V given by Eq. (3.2.6) is generated by a modular zero mode. Instead of Eq. (3.2.8) this gauge choice leads to

$$H_{\rm mod} = V^\dagger U^\dagger \Delta U V \ . \tag{3.2.10}$$

A reasonable choice for fixing this ambiguity is to impose that

$$P_0[\partial_\lambda \tilde{U}^\dagger \tilde{U}] = 0 \ . \tag{3.2.11}$$

Since V preserves the zero mode space, $P_0[V^\dagger \dot{U}^\dagger U V] = V^\dagger P_0[\dot{U}^\dagger U] V$ from Eq. (3.2.7). Likewise, $\dot{V}^\dagger V$ is a modular zero mode from Eq. (3.2.6), so it projects to itself. Thus, this condition reduces to

$$-V^\dagger \dot{V} + V^\dagger P_0[\dot{U}^\dagger U] V = 0 \ , \tag{3.2.12}$$

where we have used $\dot{V}^\dagger V = -V^\dagger \dot{V}$ since V is unitary. We therefore obtain a more familiar expression for parallel transport of the operator V,

$$(\partial_\lambda - \Gamma)\, V = 0 \ , \tag{3.2.13}$$

where

$$\Gamma = P_0[\dot{U}^\dagger U] \tag{3.2.14}$$

is a Berry connection that encodes information about how the zero mode frame changes as we vary the modular Hamiltonian. It transforms as $\Gamma \to V^\dagger \Gamma V - V^\dagger \dot{V}$ under $U \to UV$. After performing the parallel transport around a closed loop, $\dot{U}^\dagger U$ has a definite value by Eq. (3.2.11). However, U itself may differ by a modular zero mode,

$$U(\lambda_f) = U(\lambda_i) e^{-i \sum_i \kappa_i Q_i} \ . \tag{3.2.15}$$

Here, $\lambda_f = \lambda_i$ are the endpoints of a closed path. The coefficients κ_i contain information about the loop.

There is also a curvature, F, associated to this parallel transport process. We can evaluate the curvature by performing parallel transport around a small loop. Here, 'small' means that we replace the derivatives with infinitesimal transformations. We can think of the operator $S_{\delta\lambda} = \tilde{U}^\dagger \delta_\lambda \tilde{U}$ as a generator of parallel transport. It transforms as a gauge field

$$S_{\delta\lambda} \to V^\dagger S_{\delta\lambda} V + V^\dagger \delta_\lambda V \tag{3.2.16}$$

under a change of modular frame $\tilde{U} \to \tilde{U}V$ and satisfies $P_0[S_{\delta\lambda}] = 0$ by Eq. (3.2.11). The curvature F associated to this gauge field is what we call the *modular Berry curvature*. It can be represented in the usual way by performing two consecutive infinitesimal transformations $\lambda_i \to \lambda_i + \delta_1\lambda$, followed by $\lambda_i + \delta_1\lambda \to \lambda_i + \delta_1\lambda + \delta_2\lambda$. Doing the same with $(1 \leftrightarrow 2)$ and taking the difference gives a closed loop with

$$F = (1 + S_{\delta_2\lambda}(\lambda_i + \delta_1\lambda))(1 + S_{\delta_1\lambda}(\lambda_i)) - (1 \leftrightarrow 2) \ . \tag{3.2.17}$$

Here, we use that the holonomy operator along the line $[\lambda_i, \lambda_i + \delta\lambda]$ is given by

$$\exp\left(\int_{\lambda_i}^{\lambda_i+\delta\lambda} \tilde{U}^\dagger \delta_\lambda \tilde{U}\right) = 1 + S_{\delta\lambda}(\lambda_i) \ . \tag{3.2.18}$$

In Appendix B, we will derive a general expression for the curvature, Eq. (3.2.17), and we apply it in Section 3.3 to the case of state-changing parallel transport.

Example: Shape-changing parallel transport

As an example, we will review how this framework for parallel transport of operators can be applied to a parallel transport process of the modular Hamiltonian intervals whose location is varied in the CFT vacuum. This reduces to the study of kinematic space, which we see can also be described using state-based parallel transport in Appendix A.

We consider our subregion A to be an interval on a fixed time slice of the CFT with endpoints located at θ_L and θ_R. Generalizing to subregions with endpoints which are not in the same time slice is straightforward. The modular Hamiltonian associated to A can be written in terms of $\mathfrak{sl}(2,\mathbb{R})$ generators as

$$H_{\text{mod}} = s_1 L_1 + s_0 L_0 + s_{-1} L_{-1} \ . \tag{3.2.19}$$

Here, we have omitted the $\bar{L}$ operators for simplicity. The coefficients in Eq. (3.2.19) depend on θ_L, θ_R and can be determined by requiring that the generator keeps the interval fixed. Explicitly, they are given by

$$s_1 = \frac{2\pi \cot\left(\frac{\theta_R - \theta_L}{2}\right)}{e^{i\theta_R} + e^{i\theta_L}} \ , \quad s_0 = -2\pi \cot\left(\frac{\theta_R - \theta_L}{2}\right) \ , \quad s_{-1} = \frac{2\pi \cot\left(\frac{\theta_R - \theta_L}{2}\right)}{e^{-i\theta_R} + e^{-i\theta_L}} \ . \tag{3.2.20}$$

In case of A extending along half the interval, taking for example $\theta_R = -\theta_L = \pi/2$, the modular Hamiltonian can be found from Eq. (3.2.20) to be $H_{\text{mod}} = \pi(L_1 + L_{-1})$.

We now construct a one-parameter family of modular Hamiltonians by changing the shape of the interval. The simplest trajectory is given by just changing one of the endpoints, e.g., taking the parameter $\lambda = \theta_L$. The change in modular

Hamiltonian is now captured by the parallel transport equation Eq. (3.2.9), which in this case reads

$$\delta_{\theta_L} H_{\text{mod}} = [S_{\delta\theta_L}, H_{\text{mod}}] \ . \tag{3.2.21}$$

We can solve Eq. (3.2.21) for the shape-changing parallel transport operator $S_{\delta\theta_L}$ by first diagonalizing the action of the modular Hamiltonian

$$[H_{\text{mod}}, V_\mu] = i\mu V_\mu \ , \tag{3.2.22}$$

with $\mu \in \mathbb{R}$. It is not difficult to see that the following operators are solutions

$$V_{-2\pi} = \partial_{\theta_L} H_{\text{mod}} \ , \quad V_0 = H_{\text{mod}} \ , \quad V_{2\pi} = \partial_{\theta_R} H_{\text{mod}} \ , \tag{3.2.23}$$

with $\mu = -2\pi, 0, 2\pi$ respectively. The operators $V_{2\pi}$ and $V_{-2\pi}$ saturate the modular chaos bound [104]. Importantly, notice that this class of deformations is characterized by imaginary eigenvalues in Eq. (3.2.22). The generator of modular parallel transport therefore takes the form

$$S_{\delta\theta_L} = -\frac{i}{2\pi} \partial_{\theta_L} H_{\text{mod}} \ . \tag{3.2.24}$$

For this particular operator Eq. (3.2.11) is automatically satisfied, since it can be written as the commutator of H_{mod}. Similarly, one can show that $S_{\delta\theta_R} = \frac{i}{2\pi}\partial_{\theta_R} H_{\text{mod}}$. Then, using Eq. (3.2.17) one can compute the modular Berry curvature for this shape-changing transport to be

$$F = [S_{\delta\theta_L}, S_{\delta\theta_R}] = -\frac{i}{4\pi} \frac{H_{\text{mod}}}{\sin^2\left(\frac{\theta_R - \theta_L}{2}\right)} \ . \tag{3.2.25}$$

In particular, applying the projection P_0 to this expression does not change it, as the curvature is proportional to a zero mode. In Appendix A, we rederive the result in Eq. (3.2.25) from the point of view of kinematic space. The curvature, Eq. (3.2.25), is simply the volume form on kinematic space.

3.3 State-changing parallel transport

Let us apply the formalism above to a parallel transport process that modifies not the location of the entangling interval, but rather the state of the system. For definiteness, we work on the AdS_3 cylinder with a choice of time slice in the boundary CFT_2.

Consider a change of state by acting by an element $\xi(z)$ of $\text{Diff}(S^1)$, starting from the vacuum of AdS_3. The operator that implements this is

$$X_\xi = \frac{1}{2\pi i} \oint \xi(z) T(z)\, dz \ , \tag{3.3.1}$$

where $T(z)$ is the stress tensor of the boundary CFT. In particular, the diffeomorphism $\xi(z) = z^n$ is implemented by the usual Virasoro mode operator $X_{z^n} = L_{n-1}$.

Under such a general transformation, the modular Hamiltonian H_{mod} associated to some interval on the boundary transforms as

$$\delta_\xi H_{\text{mod}} = [X_\xi, H_{\text{mod}}] \ . \tag{3.3.2}$$

Notice that this is just the parallel transport equation, Eq. (3.2.9), minus the zero mode piece.

Now imagine computing the curvature, Eq. (3.2.17), by taking the parallel transport along a small square, i.e., first performing a transformation ξ_1 followed by a transformation ξ_2, then subtracting the opposite order. The result for the curvature is derived in Appendix B and is given by

$$F = P_0([X_{\xi_1}, X_{\xi_2}]) \ , \tag{3.3.3}$$

where P_0 projects to the zero mode of its argument, and the operators X_{ξ_i} are assumed to have no zero modes themselves. We note that while we focus here on CFT_2, this is a quite general result that applies to any parallel transport process of the form Eq. (3.3.2). Eq. (3.3.3) together with its application in an explicit example constitute the main results of this section.

The projection operator in Eq. (3.3.3) is defined by the property that it gives a nonzero answer when evaluated on the modular Hamiltonian (and in general, any other operators that commute with it). Meanwhile, it evaluates to zero on any other operators, which we have assumed take the form $[\cdot, H_{\text{mod}}]$ in the decomposition Eq. (3.2.9). It is possible to construct the projection explicitly in cases where the modular Hamiltonian is known, for instance in our case of CFT_2. Let θ be the spatial boundary coordinate on a constant time slice. The modular Hamiltonian for an interval of angular radius α centered around $\theta = 0$ on the cylinder is [118, 119]

$$H_{\text{mod}} = \int_{-\alpha}^{\alpha} d\theta \, \frac{\cos\theta - \cos\alpha}{\sin\alpha} \, T_{00}(\theta) \ . \tag{3.3.4}$$

Here, the units are chosen so that the stress energy tensor is dimensionless, $T_{00} \sim -c/12$ in the vacuum on the cylinder, with $T_{00}(\theta) \equiv -(T(\theta) + \overline{T}(\theta))$.

It will be useful to work in planar coordinates. We consider the conformal transformation

$$z = e^{i\theta} \tag{3.3.5}$$

to map the cylinder to the plane (with radial ordering). In particular, the interval $[-\alpha, \alpha]$ in the θ-coordinate is mapped to the circle arc with opening angle 2α in

the z-plane. The stress tensor transforms as

$$T(\theta) = \left(\frac{\partial z}{\partial \theta}\right)^2 T(z) + \frac{c}{12}\{z, \theta\} \ , \tag{3.3.6}$$

where the Schwarzian derivative is defined by

$$\{z, \theta\} = \frac{z'''}{z'} - \frac{3}{2}\left(\frac{z''}{z'}\right)^2 \ . \tag{3.3.7}$$

Applying the transformation Eq. (3.3.5), we find that the modular Hamiltonian on the plane is given by

$$H_{\text{mod}} = \frac{1}{i}\oint_{|z|=1} \frac{\frac{1}{2}(1+z^2) - z\cos\alpha}{\sin\alpha} T(z)\, dz \ . \tag{3.3.8}$$

Notice that in Eq. (3.3.8) we have converted to the *complete* modular Hamiltonian by integrating over the full range of coordinates instead of $[-\alpha, \alpha]$. The reason is that an integration over the full circle allows for an expansion of quantities in terms of Virasoro modes. Moreover, we have conveniently subtracted the vacuum energy of the cylinder in going from Eq. (3.3.4) to Eq. (3.3.8) and only kept the holomorphic part of the stress tensor.

For simplicity, we will take $\alpha = \pi/2$ so that the interval extends along half of the cylinder (from $z = -i$ to $z = i$ in the Euclidean plane). The generalization to intervals with arbitrary α is straightforward. With this convention the modular Hamiltonian simplifies to

$$H_{\text{mod}} = \frac{1}{2i}\oint (1+z^2) T(z)\, dz \ . \tag{3.3.9}$$

We can also express this in terms of the Virasoro modes on the plane,

$$L_n = \frac{1}{2\pi i}\oint z^{n+1} T(z) dz \ \ , \tag{3.3.10}$$

which satisfy the Virasoro algebra

$$[L_m, L_n] = (m-n)L_{m+n} + \frac{c}{12} m(m^2-1)\delta_{m+n,0} \ . \tag{3.3.11}$$

Then, Eq. (3.3.9) can be re-expressed as

$$H_{\text{mod}} = \pi(L_{-1} + L_1) \ . \tag{3.3.12}$$

In the following, it will be useful to write formulae in terms of the diffeomorphism ξ directly, rather than in terms of the corresponding operator X_ξ. In particular,

we identify the modular Hamiltonian H_{mod} with the vector field $\xi(z) = \pi(1+z^2)$, as follows from Eq. (3.3.9). Moreover, if we take an operator of the form

$$X_\xi = \frac{1}{2\pi i} \oint \xi(z) T(z)\, dz \ , \tag{3.3.13}$$

the commutator with H_{mod} can also be expressed in ξ directly. Using Eqs. (3.3.9) and (3.3.13), applying the OPE

$$T(w)T(z) = \frac{c/2}{(z-w)^4} + \frac{2T(w)}{(z-w)^2} + \frac{\partial T(w)}{z-w} + ... \tag{3.3.14}$$

and integrating by parts we find

$$[H_{\text{mod}}, X_\xi] = \frac{1}{2i} \oint \left[2z\xi(z) - (1+z^2)\xi'(z)\right] T(z)\, dz \ . \tag{3.3.15}$$

Applying several integration by parts directly onto Eq. (3.3.9), the term proportional to the central charge identically vanishes in this case.

To implement Eq. (3.3.3) for the modular Berry curvature one needs to define the operator P_0 which projects onto the zero mode. Following the general prescription in Section 3.2.2, one would like to decompose an arbitrary operator X into the image and the kernel of the adjoint action of H_{mod},

$$X = \kappa H_{\text{mod}} + [H_{\text{mod}}, Y] \ , \tag{3.3.16}$$

where κ is the zero mode that needs to be extracted. However, it turns out that there is a subtlety associated with the above decomposition in the case of the Virasoro algebra. In general, there are operators which are neither in the kernel, nor in the image of the adjoint action[2], which leads to an ambiguity in the definition of the zero mode projection P_0. We refer to Appendix C for a discussion of these issues in the case of the Virasoro algebra. For this reason, we will consider a different class of transformations, i.e., those which diagonalize the adjoint action of the modular Hamiltonian H_{mod} (see [120] where a similar diagonalization in terms of so-called modular eigenmodes was considered). Therefore, we start from the eigenvalue equation

$$[H_{\text{mod}}, X_\lambda] = \lambda X_\lambda \ , \tag{3.3.17}$$

where we have used the short-hand notation $X_\lambda \equiv X_{\xi_\lambda}$ for the operator associated to the transformation ξ_λ. Using Eq. (3.3.15) it is not difficult to see that Eq. (3.3.17) is solved by

$$\xi_\lambda(z) = \pi(1+z^2)\left(\frac{1-iz}{z-i}\right)^{-i\lambda/2\pi} \ . \tag{3.3.18}$$

[2]For finite-dimensional vector spaces this is not the case if the kernel and image are disjoint, as follows from a simple dimension counting. In the infinite-dimensional set-up the situation is more complicated, e.g., one can write down linear maps which are injective but not surjective.

In particular, we see that the operator with eigenvalue zero, $\lambda = 0$, is the modular Hamiltonian itself, as one would expect from Eq. (3.3.17). Notice that the solutions in Eq. (3.3.18) go to zero at the endpoints of the interval:

$$\xi_\lambda(z) \to 0 \quad \text{as} \quad z \to \pm i \ . \tag{3.3.19}$$

The eigenfunctions of H_{mod} therefore correspond to the transformations which change the state, but not the location of the boundary interval. They are not analytic at $z = \pm i$,[3] so strictly speaking they are not part of the Virasoro algebra (defined in the usual way as the space of smooth vector fields on the circle). However, they seem to be the natural transformations to consider in this context. We will refer to them as *state-changing* transformations as opposed to the shape-changing transformations in Section 3.2.2.

From Eq. (3.3.17) combined with the Jacobi identity, these eigenfunctions form an algebra with commutation relations

$$[X_\lambda, X_\mu] = (\lambda - \mu) X_{\lambda+\mu} \ , \tag{3.3.20}$$

which defines a continuous version of the Virasoro algebra[4] with generators X_λ labeled by a continuous parameter $\lambda \in \mathbb{R}$. Note that in the following we are leaving out the central extension (so strictly speaking we are working with a continuous version of the Witt algebra). We will return to discuss how to include the central extension in Section 3.3.3.

It is natural to define the transformations in Eq. (3.3.18) to have support only on the subregion A. In the case at hand, this makes all the contour integrals collapse to integrals over the semicircle from $-i$ to i, e.g., the $\lambda = 0$ eigenfunction does not correspond to the *complete* modular Hamiltonian, but simply to the half-sided one. The state-changing vector fields, which might look unfamiliar in terms of the z-coordinate, take a more familiar form when we map the entanglement wedge to a hyperbolic black hole geometry using [106].

This can be seen in the following way. Starting with the boundary CFT_d on the Euclidean cylinder $\mathbb{R} \times S^{d-1}$ with metric

$$ds^2 = dt_E^2 + d\theta^2 + \sin^2\theta \ d\Omega_{d-2}^2 \ , \tag{3.3.21}$$

we consider a fixed sphere at $t_E = 0$, $\theta = \theta_0$. We can apply the following conformal

[3] Note that due to Eq. (3.3.19), it is valid to apply a single integration by parts. Thus, Eq. (3.3.15) is maintained.

[4] A Virasoro algebra with continuous index also appears in the context of the so-called dipolar quantization of 2d CFT [121, 122] which is related to the sine-square deformation [123, 124], as well as in the study of non-equilibrium flows in CFT [125].

transformation considered in [106]:

$$\begin{aligned} \tanh t_E &= \frac{\sin\theta_0 \sin\tau}{\cosh u + \cos\theta_0 \cos\tau} \ , \\ \tan\theta &= \frac{\sin\theta_0 \sinh u}{\cos\theta_0 \cosh u + \cos\tau} \ , \end{aligned} \tag{3.3.22}$$

which conformally maps the causal development of the sphere to the hyperbolic geometry $\mathbb{R} \times \mathbb{H}^{d-1}$ given by

$$ds^2 = \Omega^2 \left(d\tau^2 + du^2 + \sinh^2 u \ d\Omega_{d-2}^2 \right) \ , \tag{3.3.23}$$

with conformal factor

$$\Omega^2 = \frac{\sin^2\theta_0}{(\cosh u + \cos\theta_0 \cos\tau)^2 - \sin^2\theta_0 \sin^2\tau} \ . \tag{3.3.24}$$

Taking $d = 2$ and $\theta_0 = \pi/2$ for the half interval entangling surface, the transformation Eq. (3.3.22) at the $\tau = 0$ (or equivalently $t_E = 0$) time slice reduces simply to

$$\tan\theta = \sinh u \ . \tag{3.3.25}$$

Written in terms of the coordinate $z = e^{i\theta}$ this leads to

$$e^u = \frac{1 - iz}{z - i} \ . \tag{3.3.26}$$

Recall that the boundary region A corresponds to $|z| = 1$ and $-\pi/2 \leq \arg(z) \leq \pi/2$ in the plane, so it is mapped to $u \in \mathbb{R}$. Moreover, the components of the vector field transform according to

$$\xi_\lambda(z) \frac{\partial}{\partial z} = \xi_\lambda(u) \frac{\partial}{\partial u} \tag{3.3.27}$$

with

$$du = -2i \frac{dz}{1 + z^2} \ , \tag{3.3.28}$$

so that the transformations take the simple form

$$\xi_\lambda(u) = -2\pi i \, e^{-i\lambda u/2\pi} \ . \tag{3.3.29}$$

Hence, we find that the state-changing transformations, when written in terms of the u-variable, are simply plane wave solutions with frequency $\lambda/2\pi$ in this black hole background. Therefore, they are natural objects to consider in this geometry.

We can reintroduce both the right- and the left-movers by replacing $u \to u + i\tau$ in Eq. (3.3.26), so that z is allowed to take values in the half plane $\mathrm{Re}\, z \geq 0$ (the

radial direction in the z-plane corresponds to time evolution in τ). Eq. (3.3.27) is therefore modified according to

$$\xi_\lambda(z)\frac{\partial}{\partial z} = \xi_\lambda(u+i\tau)\left(\frac{\partial}{\partial u} - i\frac{\partial}{\partial \tau}\right) , \quad \xi_\lambda(\bar{z})\frac{\partial}{\partial \bar{z}} = -\xi_\lambda(-u+i\tau)\left(\frac{\partial}{\partial u} + i\frac{\partial}{\partial \tau}\right) . \tag{3.3.30}$$

By setting $\lambda = 0$ and adding the right- and left-moving contributions, we see that the modular Hamiltonian indeed acts by time translation in the black hole geometry:

$$H_{\text{mod}} \sim \frac{\partial}{\partial \tau} . \tag{3.3.31}$$

Working in the algebra associated to the eigenfunctions of H_{mod}, we do have a unique decomposition of the form Eq. (3.3.16): one simply decomposes an arbitrary operator into eigenoperators, which have either $\lambda = 0$ or $\lambda \neq 0$. Given such a decomposition it is easy to write down an operation which extracts the zero mode κ, namely a linear functional P_0 which satisfies[5]

$$P_0(H_{\text{mod}}) \sim \delta(0) , \quad P_0([H_{\text{mod}}, Y]) = 0 . \tag{3.3.32}$$

In the u-coordinate such a functional can be written as

$$P_0(X_\xi) = \lim_{\Lambda\to\infty} \frac{i}{2\pi}\int_{-\Lambda}^{\Lambda} \xi(u)\, du . \tag{3.3.33}$$

Using the coordinate change Eq. (3.3.28), we can represent the projection in the z-coordinate as

$$P_0(X_\xi) = \lim_{\Lambda\to\infty} \frac{i}{2\pi}\int_{-\Lambda}^{\Lambda} \xi(u)\, du = \frac{1}{\pi}\int_{-i}^{i} \frac{\xi(z)}{(1+z^2)^2}\, dz . \tag{3.3.34}$$

When applied to the eigenfunctions of H_{mod} the projection becomes

$$P_0(X_\lambda) = \lim_{\Lambda\to\infty} 2\pi\int_{-\Lambda}^{\Lambda} e^{i\lambda u}\, du = 4\pi^2\delta(\lambda) , \tag{3.3.35}$$

which is a standard representation of the Dirac delta function. To show that P_0 vanishes on commutators of the form $[H_{\text{mod}}, Y]$, it suffices to remark that one can take Y to satisfy $[H_{\text{mod}}, Y] = \lambda Y$ with $\lambda \neq 0$ without loss of generality. This shows that Eq. (3.3.33) defines a good projection operator in the sense of Eq. (3.3.32). Unlike for the case of the ordinary Virasoro algebra treated in Section C, there is no ambiguity in the resulting projection.

[5]For technical reasons we set $P_0(H_{\text{mod}}) \sim \delta(0)$, instead of $P_0(H_{\text{mod}}) \sim 1$ as one might have naively expected. This results from the plane-wave normalizability of the eigenfunctions, Eq. (3.3.29). It ensures the modular Berry curvature is finite when evaluated on wave packets in Section 3.3.1.

3.3.1 Example

We now have all the ingredients to compute the curvature in an explicit example. We consider a general perturbation of the form

$$z' = z + \epsilon\, \xi(z) + \mathcal{O}(\epsilon^2) \ , \tag{3.3.36}$$

where $\xi(z)$ is a wave packet

$$\xi(z) = \frac{1}{2\pi} \int_{-\infty}^{\infty} c(\lambda) \xi_\lambda(z)\, d\lambda \ , \tag{3.3.37}$$

with $\xi_\lambda(z)$ defined in Eq. (3.3.18). We start by obtaining the correction to the transformed modular Hamiltonian upon acting with Eq. (3.3.36). Let us expand both the modular Hamiltonian and the parallel transport operator to first order in the small parameter ϵ:

$$H'_{\text{mod}} = H^{(0)} + \epsilon\, H^{(1)} + \mathcal{O}(\epsilon^2) \ , S = S^{(0)} + \epsilon\, S^{(1)} + \mathcal{O}(\epsilon^2) \ . \tag{3.3.38}$$

Using that $z = z' - \epsilon \xi(z') + \mathcal{O}(\epsilon^2)$, one can expand the transformed H_{mod} to order $\mathcal{O}(\epsilon^2)$. One finds that $H^{(0)} = H_{\text{mod}}$ is the original modular Hamiltonian, while the correction is given by

$$H^{(1)} = -\frac{1}{2i} \oint \left[2z\xi(z) - (1+z^2)\xi'(z) \right] T(z)\, dz \ . \tag{3.3.39}$$

Here, we have neglected the Schwarzian contribution for simplicity. It will be treated separately in Section 3.3.3. We now expand the parallel transport equation

$$\delta H_{\text{mod}} = [S, H_{\text{mod}}] \tag{3.3.40}$$

to first order in ϵ. This gives two separate equations:

$$0 = [S^{(0)}, H^{(0)}] \ , \quad H^{(1)} = [S^{(0)}, H^{(1)}] + [S^{(1)}, H^{(0)}] \ . \tag{3.3.41}$$

Solving Eq. (3.3.41) for the correction $S^{(1)}$ to the parallel transport operator gives the solution

$$S^{(0)} = 0 \ , S^{(1)} = X_\xi \ . \tag{3.3.42}$$

Both $S^{(0)}$ and $S^{(1)}$ are defined up to a zero mode, meaning that one can add to it an extra operator Q for which $[Q, H_{\text{mod}}] = 0$ (e.g., the modular Hamiltonian itself) and the parallel transport equation would still be satisfied.

To compute the curvature we need to consider two different parallel transport operators S_1 and S_2 which we take to be defined according to the transformations

$$\xi_1(z) = \frac{1}{2\pi} \int_{-\infty}^{\infty} c_1(\lambda) \xi_\lambda(z)\, d\lambda \ , \quad \xi_2(z) = \frac{1}{2\pi} \int_{-\infty}^{\infty} c_2(\lambda) \xi_\lambda(z)\, d\lambda \ , \tag{3.3.43}$$

respectively. After projecting out their zero modes, we take the commutator and project to the zero modes again to obtain the value of the curvature component. Therefore, we need to compute

$$[S_1^{(1)} - \kappa_1 H^{(0)}, S_2^{(1)} - \kappa_2 H^{(0)}] \ , \tag{3.3.44}$$

where $\kappa_i = P_0(S_i)$, is the zero mode coefficient of the parallel transport operator S_i. We can split Eq. (3.3.44) into terms that we can treat separately. Notice that the term proportional to $[H^{(0)}, H^{(0)}]$ is zero and can be removed. Moreover, the definition of the projection operator immediately implies

$$P_0([S_1^{(1)}, H^{(0)}]) = P_0([S_2^{(1)}, H^{(0)}]) = 0 \ . \tag{3.3.45}$$

To evaluate the last commutator we use the commutation relations in Eq. (3.3.20) to obtain

$$[S_1^{(1)}, S_2^{(1)}] = \frac{1}{4\pi^2} \int_{-\infty}^{\infty} \int_{-\infty}^{\infty} (\lambda_1 - \lambda_2) c_1(\lambda_1) c_2(\lambda_2) X_{\lambda_1+\lambda_2} \, d\lambda_1 d\lambda_2 \ . \tag{3.3.46}$$

Applying the projection operator sets $\lambda_1 = -\lambda_2$, so that we find

$$P_0([S_1^{(1)}, S_2^{(1)}]) = 2 \int_{-\infty}^{\infty} \lambda \, c_1(\lambda) c_2(-\lambda) \, d\lambda \ . \tag{3.3.47}$$

Therefore, the final result for the modular Berry curvature associated to the state-changing transport problem is given by

$$F = 2 \int_{-\infty}^{\infty} \lambda \, c_1(\lambda) c_2(-\lambda) \, d\lambda \ . \tag{3.3.48}$$

Note that the curvature appropriately vanishes when two perturbations lie along the same direction, $c_1(\lambda) = c_2(\lambda)$. If we take the modes to be peaked at the eigenfunctions $\xi_{\lambda_i}(z)$ themselves, $c_i(\lambda) = \delta(\lambda - \lambda_i)$, the above formula reduces to

$$F = (\lambda_1 - \lambda_2)\delta(\lambda_1 + \lambda_2) \ , \tag{3.3.49}$$

which is a local formula in terms of the parameters λ_i.

3.3.2 Lie algebra

To diagonalize the adjoint action, we saw that we must work with a continuous version of the Virasoro algebra. Viewed in terms of vector fields on the circle, we must consider non-smooth vector fields on the circle, Eq. (3.3.18), which have support only along the interval. When mapped to the real line, these are just plane waves, Eq. (3.3.29). In the last section, we performed parallel transport using wave

packets constructed out of these eigenfunctions. In terms of the coordinates on the real line,

$$\xi(u) = \frac{1}{2\pi}\int_{-\infty}^{\infty} c(\lambda)\xi_\lambda(u)d\lambda \ . \tag{3.3.50}$$

Now we would like to be more precise about the sense in which the corresponding vector fields form a Lie algebra. This amounts to imposing extra conditions on $c(\lambda)$ for these to form a closed algebra, along with any other desirable properties.

The simplest choice would be to demand that the $\xi(u)$ be smooth. Then, since the smoothness of functions is preserved under pointwise multiplication, the corresponding vector fields $\xi(u)\partial_u$ will form a closed algebra. However, an arbitrary $\xi(u)$ will not necessarily have finite zero mode projection, nor will there necessarily exist a natural definition for a dual space. To define sensible wave packets we will impose two additional requirements:

- There is a notion of Fourier transform that maps the space to itself,
- The $\xi(u)$ are integrable. This means that the projection, Eq. (3.3.33), is finite, and this property is preserved under commutation of the vector fields $\xi(u)\partial_u$. It also allows us to define a dual space in terms of distributions.

To accomplish this, it is convenient to work with wave packets $\xi(u)$ that are *Schwartz functions*. These are smooth, bounded functions whose derivatives are also all bounded: $|u^\alpha \partial^\beta \xi(u)| < \infty$ for all $\alpha, \beta > 0$. In other words, they rapidly go to zero as $u \to \pm\infty$, faster than any reciprocal power of u. This definition excludes for example polynomials, but includes polynomials weighted by an exponential $e^{-c|u|^2}$ for $c \in \mathbb{R}$. By the Leibniz rule, the Schwartz space $\mathcal{S}$ is closed under pointwise multiplication, thus the corresponding vector fields form a closed Lie algebra. We denote $\mathcal{S}$ for the space of Schwartz functions and $\mathfrak{s}$ for the corresponding algebra of vector fields.

Since these functions are integrable, it is natural to define a dual space $\mathcal{S}'$ consisting of linear functionals $T : \mathcal{S} \to \mathbb{C}$, in terms of distributions:

$$T[\xi(u)] = \int_{-\infty}^{\infty} \xi(u)T(u)du \ . \tag{3.3.51}$$

A pairing between Schwartz functions and dual elements can be defined from this as $\langle T, \xi\rangle \equiv T[\xi(u)]$. Likewise, there is also a dual space $\mathfrak{s}^*$ consisting of linear functionals on $\mathfrak{s}$, the algebra of vector fields. This is inherited from the dual space $\mathcal{S}'$, i.e., it consists of the space of distributions evaluated on Schwartz functions. There is a pairing $\langle\cdot,\cdot\rangle$ between $\mathfrak{s}$ and $\mathfrak{s}^*$ which descends from the pairing on $\mathcal{S}$ and $\mathcal{S}'$.

Notice that, evaluated on the wave packets Eq. (3.3.50), the projection operator Eq. (3.3.33)

$$P_0 : \xi(u) \mapsto 2\pi c(0) \tag{3.3.52}$$

is a linear functional, and thus it is an element of the dual space. The pairing is given by $\langle P_0, \xi\rangle = P_0(\xi) = 2\pi c(0)$.

In the coordinates on the circle, recall that this dual element can be expressed from Eq. (3.3.34) as

$$P_0 : \xi(z) \mapsto \frac{1}{\pi}\int dz \frac{\xi(z)}{(1+z^2)^2} \ . \tag{3.3.53}$$

Notice that this dual element is not a smooth quadratic form on the circle as is typically considered in treatments of the dual space of the Virasoro algebra, but rather a more general distribution that involves singularities at $z = \pm i$[6]. A standard definition of the dual space is an attempt to get a space that is roughly the same size as the algebra itself. For infinite-dimensional spaces the formal dual is much larger and one needs some additional structure, e.g., that of a Hilbert space, to limit it.

We emphasize that there is considerable freedom in these definitions. A different choice would amount to taking a different set-up for varying the state in the parallel transport process. Our definitions allow us to perform parallel transport using wavefunctions that are 'physical' in the sense of being Fourier transformable and integrable. The existence of a natural dual space also allows for contact with a geometrical picture in terms of coadjoint orbits, which we describe in the next section.

3.3.3 Central extension

We have so far only considered changing the state with a transformation of the circle. When the transformations are diffeomorphisms on the circle, the group $\mathrm{Diff}(\mathrm{S}^1)$ gets centrally extended to the full Virasoro group, $\mathrm{Diff}(\mathrm{S}^1) \times \mathbb{R}$. Here we are considering a continuous version of the Virasoro generated by the transformations, Eq. (3.3.18). For the central extension, we proceed in direct analogy with the Virasoro case. In the following, the vector fields $\xi(z)$ should be understood to

[6] In the usual discussion of the Virasoro algebra the dual space is identified with the space of smooth quadratic differentials. Formally, one could argue that distributions such as $\delta(z - z_0)$ and $\delta'(z - z_0)$ are also part of some suitably defined notion of the dual space. Indeed, they define linear functionals

$$\xi \mapsto \xi(z_0) \ , \quad \xi \mapsto -\xi'(z_0) \ , \tag{3.3.54}$$

which evaluate a function (or its derivative) at some point z_0. The projection operator P_0 in Eq. (3.3.53), when integrated over the full circle and properly regularized, can be regarded in this fashion. See Appendix C for more details, for example, Eqs. (C.29) - (C.31).

have non-zero support only between $z = \pm i$, so that this is the only part of the integral over the full circle that contributes.

We consider pairs (ξ, α), where ξ is a vector field of the form Eq. (3.3.18), which diagonalizes the adjoint action, and $\alpha \in \mathbb{R}$. The Lie bracket is defined as

$$[(\xi,\alpha),(\chi,\beta)] = \left(-[\xi,\chi], -\frac{1}{48\pi}\oint dz\,(\xi(z)\chi'''(z) - \xi'''(z)\chi(z))\right) , \tag{3.3.55}$$

where $[\xi, \chi] := \xi\chi' - \chi\xi'$ is the commutator of vector fields. This is identical to the commutators for the Virasoro algebra, with the only difference being that we integrate only over half the circle, and also consider transformations ξ which are not smooth at the endpoints. In terms of the operators X_λ, this extends the algebra in Eq. (3.3.20) to

$$[\bar{X}_{\bar{\lambda}}, \bar{X}_{\bar{\mu}}] = (\bar{\lambda} - \bar{\mu})\bar{X}_{\bar{\lambda}+\bar{\mu}} + \frac{c}{12}\bar{\lambda}(\bar{\lambda}^2 + 1)\delta(\bar{\lambda} + \bar{\mu}) . \tag{3.3.56}$$

where we have defined rescaled barred variables through $X_\lambda = -2\pi\bar{X}_\lambda, \lambda = -2\pi\bar{\lambda}$ to bring this to a form that more closely resembles the usual Virasoro algebra with discrete labels.

One often introduces a new generator, denoted by c, which commutes with all other elements in the algebra, to write

$$(\xi, \alpha) = \xi(z)\partial_z - i\alpha c . \tag{3.3.57}$$

By definition, the central element c commutes with H_{mod}, i.e., $[H_{\text{mod}}, c] = 0$. Therefore, we can think about the central element as another zero mode in the parallel transport problem.

Luckily, the situation for the central element is simpler than for the modular Hamiltonian itself. From the form of H_{mod}, Eq. (3.3.12), and the algebra, Eq. (3.3.55), we see that the central element c does not appear in commutators of the form $[H_{\text{mod}}, X]$. Therefore, the projection onto the coefficient of c is simply given by the linear functional

$$(\xi, \alpha) \to \alpha . \tag{3.3.58}$$

One way to include the information of the central term is to make the Berry curvature give a $U(1)\times U(1)$-valued number (organized in terms of an extra element which we take to be c). More precisely, we define the zero mode projection operator P_0^c, which depends on c, by

$$P_0^c((X_\xi, \alpha)) = P_0(X_\xi) - \alpha c . \tag{3.3.59}$$

The first term is the usual zero mode, while the second term keeps track of the central zero mode. It is easy to see how the result for the Berry curvature gets

modified. Using Eq. (3.3.3) with P_0^c instead of P_0, we see that the formula for the Berry curvature is given by

$$F = P_0([X_{\xi_1}, X_{\xi_2}]) + \frac{c}{48\pi}\oint dz\ (\xi_1(z)\xi_2'''(z) - \xi_1'''(z)\xi_2(z)) \ . \tag{3.3.60}$$

As a consistency check, we can go back to our example in Section 3.3.1 and consider the contribution from the Schwarzian term in Eq. (3.3.39). Expanding the parallel transport equation, we need to solve

$$H^{(1)} = [S^{(1)}, H^{(0)}] \ , \tag{3.3.61}$$

where the change in the modular Hamiltonian due to the Schwarzian derivative to first order is given by

$$H^{(1)}_{\text{Schw}} = \frac{c}{24i}\oint dz(1+z^2)\xi'''(z) \ , \tag{3.3.62}$$

having used that $\{z', z\} = \epsilon\xi''' + \mathcal{O}(\epsilon^2)$. On the full circle, applying three integration by parts, this is just $H^{(1)}_{\text{Schw}} = 0$ (equivalently, no diffeomorphism has $\xi''' = z^{-1}$ or z^{-3} which would give a pole). The situation is a bit more subtle on the half circle, since due to non-differentiability at the endpoints it is no longer valid to apply integration by parts multiple times. However, it is still the case that none of the eigenfunctions, Eq. (3.3.18), have $\xi''' = z^{-1}$ or z^{-3}, and so the Schwarzian contribution vanishes. Thus, in either case the solution to Eq. (3.3.61) with the new Lie bracket Eq. (3.3.55) is still given by $S^{(1)} = X_\xi$. The extra contribution to the commutator $[S_1^{(1)}, S_2^{(1)}]$ due to the central charge is indeed given by Eq. (3.3.60).

Note while it is not possible to apply integration by parts multiple times on Eq. (3.3.62) for the half circle, we have *defined* the central extension as the version that obeys integration by parts three times. This is because we have chosen the antisymmetric combination for the central charge part in Eq. (3.3.55). As a result, our bracket respects the properties of the commutator, $[X_\xi, X_\chi] = -[X_\chi, X_\xi]$. Likewise, one can check that the Jacobi identity is satisfied. Given elements $(\xi,\alpha),(\chi,\beta),(\rho,\gamma)$ which satisfy the algebra Eq. (3.3.55), we have

$$\begin{aligned}&[(\xi,\alpha),[(\chi,\beta),(\rho,\gamma)]] + [(\chi,\beta),[(\rho,\gamma),(\xi,\alpha)]] + [(\rho,\gamma),[(\xi,\alpha),(\chi,\beta)]] \\ &\quad = \left(0, -\frac{1}{48\pi}\oint\left([\chi,\rho]\,\xi^{(3)} + [\rho,\xi]\,\chi^{(3)} + [\xi,\chi]\,\rho^{(3)}\right)\right) \ .\end{aligned} \tag{3.3.63}$$

We can see this is identically zero by integrating each term by parts once onto the commutator, which vanishes at the interval endpoints by Eq. (3.3.19) so that there is no boundary contribution. These properties are sufficient to ensure the consistency of the central extension.

3.4 Coadjoint orbit interpretation

Various versions of the parallel transport problem we consider exhibit connections to the geometry of symplectic manifolds known as coadjoint orbits. For the state-based parallel transport summarized in Section 3.2.1 applied to the Virasoro algebra, connections to coadjoint orbits were described in [107]. In Appendix A, we additionally explain how to use state-based parallel transport to obtain coadjoint orbits of $SO(2,1)$, which describe kinematic space [98]. We will begin by reviewing the notion of coadjoint orbits, and then we explain how our operator-based parallel transport can be related to the geometry of orbits.

Consider a Lie group G with Lie algebra $\mathfrak{g}$. Let $\mathfrak{g}^*$ be the dual space, i.e., the space of linear maps $T : \mathfrak{g} \to \mathbb{C}$. This defines an invariant pairing $\langle T, X\rangle \equiv T(X)$ for $X \in \mathfrak{g}, T \in \mathfrak{g}^*$. The group G acts on the algebra $\mathfrak{g}$ through the adjoint action,

$$\mathrm{Ad}_g(X) = \frac{d}{d\lambda}\left(ge^{\lambda X}g^{-1}\right)\Big|_{\lambda=0} \ , g \in G,\ X \in \mathfrak{g}\ . \tag{3.4.1}$$

For matrix groups such as $SO(2,1)$, which we consider in Appendix A, Eq. (3.4.1) is just $\mathrm{Ad}_g(X) = gXg^{-1}$.

The adjoint action of the algebra on itself can be defined from this as

$$\mathrm{ad}_X(Y) = \frac{d}{d\rho}\left(\mathrm{Ad}_{e^{\rho X}}(Y)\right)\big|_{\rho=0} = [X,Y]\ , X, Y \in \mathfrak{g}\ . \tag{3.4.2}$$

The adjoint action descends to an action on the dual space. This *coadjoint action* ad^*_X on $\mathfrak{g}^*$ is defined implicitly through

$$\langle \mathrm{ad}^*_X z, Y\rangle = \langle z, \mathrm{ad}_X Y\rangle\ \ , z \in \mathfrak{g}^*,\ X, Y \in \mathfrak{g}\ . \tag{3.4.3}$$

For a given $T \in \mathfrak{g}^*$, the orbit $\mathcal{O}_T = \{\mathrm{ad}^*_X(T)\,|\,X \in \mathfrak{g}\}$ generated by the coadjoint action is known as a *coadjoint orbit*.

Let x_1, x_2 be coadjoint vectors tangent to the orbit $\mathcal{O}_T$, and let X_1, X_2 be the adjoint vectors that are dual to these through the invariant pairing. Then, the *Kirillov-Kostant symplectic form* associated to this orbit is [126–129]

$$\omega(x_1, x_2) = \langle T, [X_1, X_2]\rangle\ . \tag{3.4.4}$$

This is manifestly anti-symmetric and G-invariant. It is also closed and nondegenerate [126], and hence it defines a symplectic structure on $\mathcal{O}_T$. Thus, coadjoint orbits are naturally symplectic manifolds. For matrix groups, the algebra and dual space are isomorphic through the Cartan-Killing form, which is non-degenerate in this case. It suffices to consider an orbit of the adjoint action, and these generate

symplectic manifolds. This is the setting of Appendix A. We emphasize that in the general case this is not true and one must work in the dual space.

It will be useful to review the case of the Virasoro group, along with a suitable generalization given by the algebra described in Sections 3.3.2 and 3.3.3 that applies to our case of interest. Recall that the Virasoro group consists of $\mathrm{Diff}(\mathrm{S}^1)$ together with its central extension, $\widehat{\mathrm{Diff}(\mathrm{S}^1)} = \mathrm{Diff}(\mathrm{S}^1) \times \mathbb{R}$. For our problem, we are considering a continuous version of the ordinary Virasoro algebra, with a central extension described in Section 3.3.3. In either case, the formulae will be the same, with the difference that in the second scenario the vector fields ξ should be understood to be non-differentiable at the interval endpoints, with vanishing support outside the interval. Thus, in the latter case all integrals should be understood to cover only the range of the interval rather than the full circle.

For either algebra we consider elements $\xi(z)\partial_z - i\alpha c$ where $\xi(z)\partial_z$ is a vector field on the circle (smooth for Virasoro, and of the form Eq. (3.3.18) for its generalization) and $\alpha \in \mathbb{R}$ is a parameter for the central extension, generated by the algebra element c. The only non-trivial commutators are

$$[\xi_1(z)\partial_z, \xi_2(z)\partial_z] = -(\xi_1\xi_2' - \xi_1'\xi_2)\partial_z + \frac{ic}{48\pi}\oint dz\,(\xi_1\xi_2''' - \xi_1'''\xi_2)\ . \tag{3.4.5}$$

In the Virasoro case, using $L_n = z^{n+1}\partial_z$ the bracket Eq. (3.3.55) indeed leads to the usual form of the Virasoro algebra, Eq. (3.3.11).

For both algebras we can define a pairing between an adjoint vector (ξ, α) and a coadjoint vector (T, β) given by

$$\langle (T,\beta), (\xi,\alpha)\rangle = -\left[\oint dz\, T(z)\xi(z) + \alpha\beta\right]. \tag{3.4.6}$$

Now consider algebra elements $X_{\xi_1} = (\xi_1, \alpha_1)$ and $X_{\xi_2} = (\xi_2, \alpha_2)$, and let x_{ξ_1}, x_{ξ_2} be the corresponding dual elements. The Kirillov-Kostant symplectic form through dual element (T, β) is

$$\omega(x_{\xi_1}, x_{\xi_2}) = \langle (T,\beta), [X_{\xi_1}, X_{\xi_2}]\rangle = \oint dz\left[T(\xi_1\xi_2' - \xi_1'\xi_2) + \frac{\beta}{48\pi}(\xi_1\xi_2''' - \xi_1'''\xi_2)\right]. \tag{3.4.7}$$

Focusing now on the case of our non-smooth generalization of the Virasoro algebra, we can define the coadjoint orbit $\mathcal{O}_{T_*}$ through the unorthodox element $T_* = (P_0, c)$ of the dual space defined by the projection operator, Eq. (3.3.52), together with its central extension c in the full algebra. Again considering elements x_{ξ_1}, x_{ξ_2} in

the dual space that correspond to algebra elements X_{ξ_1}, X_{ξ_2} through the pairing, and using Eq. (3.3.34), this becomes

$$\omega(x_{\xi_1}, x_{\xi_2}) = \langle T_*, [X_{\xi_1}, X_{\xi_2}]\rangle = P_0([X_{\xi_1}, X_{\xi_2}]) + \frac{c}{48\pi}\oint dz\,[(\xi_1\xi_2''' - \xi_1'''\xi_2)] \ . \tag{3.4.8}$$

This is precisely Eq. (3.3.60) for the curvature. Thus, the modular Berry curvature for state-changing parallel transport is now related to the symplectic form on this orbit.

What is the holographic bulk interpretation of such a non-standard orbit? We will argue that the corresponding geometry is related to the backreaction of a cosmic brane.

3.5 Bulk phase space interpretation

A Berry curvature for pure states constructed from Euclidean path integrals was shown to be equal to the integral of the bulk symplectic form over a Cauchy slice extending into the bulk in [130, 131] (see also [132]). The notion of Uhlmann holonomy is one particular generalization of Berry phases to mixed states, and it was argued in [105] that its holographic dual is the integral of the bulk symplectic form over the entanglement wedge. However, the arguments for arriving at this result for Uhlmann holonomy are purely formal, and to the best of our knowledge this identification has not been worked out in an explicit example. The derivation also lacks a precise definition for the entanglement wedge symplectic form, which we will provide.

In this section, we will comment on a possible bulk interpretation of the modular Berry curvature for state-changing parallel transport. We will see that the result for the curvature that we obtained in the previous sections is closely related to an integral of a bulk symplectic form on a geometry with a conical singularity. See [15, 133–136] for a related discussion of this geometry.

3.5.1 The conical singularity geometry

We consider a Euclidean geometry obtained through the backreaction of a codimension-2 brane homologous to the boundary interval A. This leads to a family of Euclidean bulk solutions, which we denote by $\mathcal{M}_n$, where n is a function of the tension of the brane [133]:

$$\mathcal{T}_n = \frac{n-1}{4nG} \ . \tag{3.5.1}$$

In the limit $n \to 1$, the cosmic brane becomes tensionless and settles on the location of the the usual RT surface associated to the entangling region, but for non-zero

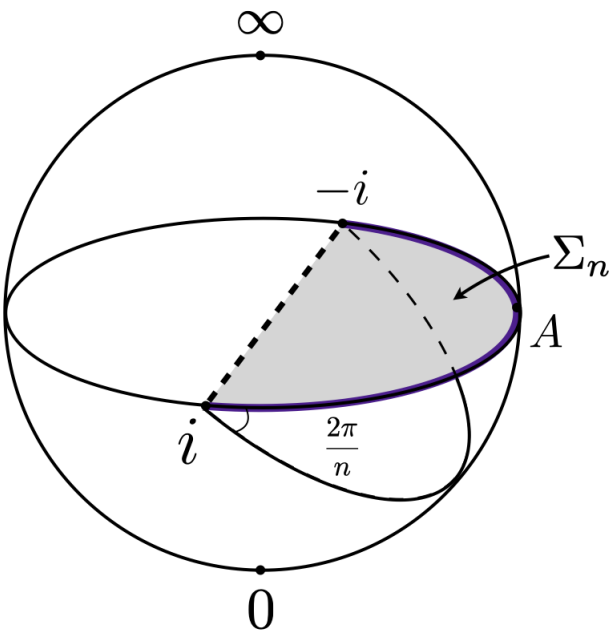

Figure 3.2: The conical singularity geometry $\mathcal{M}_n$ and entanglement wedge region Σ_n corresponding to the boundary region A. The thick striped line corresponds to the cosmic brane extending from $-i$ to i. The backreaction process creates a conical singularity of opening angle $2\pi/n$.

tension the brane backreacts on the geometry. The resulting geometries $\mathcal{M}_n$ are used in the context of the holographic computation of Rényi entropies S_n in the boundary CFT, and we will argue that these are also relevant for a holographic interpretation of the modular Berry curvature.

Let us first examine the boundary dual of the backreaction process. Inserting a cosmic brane which anchors the boundary at z_1 and z_2 corresponds to the insertion of twist fields $\mathcal{O}_n$ in the CFT at z_1 and z_2 [135]. The field $\mathcal{O}_n(z)$ is a (spinless) conformal primary of dimension [137]

$$\Delta_n = \frac{c}{12}\left(n - \frac{1}{n}\right) \ . \tag{3.5.2}$$

We use the fact that the cosmic brane can be computed as a correlation function of $\mathbb{Z}_n$ twist operators $\mathcal{O}_n, \mathcal{O}_{-n}$ in the boundary theory [133, 135].

Geometrically, we can think about the twist field as creating a conical singularity at the insertion point. Let us denote the two-dimensional geometry obtained

from $\mathcal{O}_n(z_1), \mathcal{O}_{-n}(z_2)$ by $\mathcal{B}_n$. We are interested in the stress tensor profile on the boundary of the backreacted geometry, which by this reasoning is given by the stress tensor on the plane in the background of two twist fields:

$$\langle T(z)\rangle_{\mathcal{B}_n} = \frac{\langle T(z)\mathcal{O}_n(z_1)\mathcal{O}_{-n}(z_2)\rangle_{\mathbb{C}}}{\langle \mathcal{O}_n(z_1)\mathcal{O}_{-n}(z_2)\rangle_{\mathbb{C}}} \ . \tag{3.5.3}$$

Using the general form of the three-point function in a CFT in terms of conformal dimensions, it now follows that $T(z)$ has poles of order two at z_1 and z_2 respectively.

To describe the geometry $\mathcal{M}_n$ explicitly, we consider the complex plane with coordinate z which is flat everywhere except for two conical singularities at $z = z_1$ and $z = z_2$. The singular points are assumed to have a conical deficit of magnitude

$$\Delta\varphi = 2\pi\left(1 - \frac{1}{n}\right). \tag{3.5.4}$$

We can use a uniformizing function $f(z)$ to map the z-plane with conical singularities to the smooth covering space, which we denote by $\widetilde{\mathcal{B}}_n$, which is a complex plane with coordinate z' defined by

$$z' = f(z) = \left(\frac{z - z_1}{z - z_2}\right)^{\frac{1}{n}} \ . \tag{3.5.5}$$

This maps $z_1 \to 0$ and $z_2 \to \infty$ so that the interval between z_1 and z_2 goes to the positive real axis $[0, \infty)$. The power of $\frac{1}{n}$ removes the conical singularity by gluing the n sheets of the z-plane together, each represented by a wedge of opening angle $\frac{2\pi}{n}$.

In terms of the coordinate z' we extend $\widetilde{\mathcal{B}}_n$ into the bulk by introducing a 'radial' coordinate w' with metric of the form

$$ds^2 = \frac{dw'^2 + dz'd\bar{z}'}{w'^2} \ . \tag{3.5.6}$$

Here, we restrict the range of z' by the identification $z' \sim e^{2\pi i/n}z'$, as this represents a fundamental domain $\widetilde{\mathcal{B}}_n/\mathbb{Z}_n$ in the covering space. The bulk coordinate approaches the boundary in the limit $w' \to 0$. The metric in Eq. (3.5.6) is a wedge of three-dimensional hyperbolic space $\mathbb{H}^3$. We now use the following transformation:

$$w' = w\frac{1}{N}\sqrt{f'(z)\bar{f}'(\bar{z})} \ , \quad z' = f(z) - w^2\frac{1}{N}\frac{f'(z)\bar{f}''(\bar{z})}{2\bar{f}'(\bar{z})} \ , \tag{3.5.7}$$

where $f(z)$ is defined in Eq. (3.5.5) and

$$N = 1 + w^2\frac{f''(z)\bar{f}''(\bar{z})}{4f'(z)\bar{f}'(\bar{z})} \ . \tag{3.5.8}$$

This transformation reduces to the conformal transformation in Eq. (3.5.5) when we go to the boundary $w \to 0$. The metric in the new coordinates reads

$$ds^2 = \frac{dw^2}{w^2} + \frac{1}{w^2}\left(dz - w^2\frac{6}{c}\bar{T}(\bar{z})d\bar{z}\right)\left(d\bar{z} - w^2\frac{6}{c}T(z)dz\right) \ , \tag{3.5.9}$$

where

$$T(z) = \frac{c}{12}\{f(z), z\} = \frac{c}{24}\left(1 - \frac{1}{n^2}\right)\frac{(z_1 - z_2)^2}{(z - z_1)^2(z - z_2)^2} \ , \tag{3.5.10}$$

with a similar expression holding for the anti-holomorphic component of the stress tensor $\bar{T}(\bar{z})$. The metric Eq. (3.5.9) falls into the class of Bañados geometries [138], and $T(z)$ has the interpretation of the expectation value of the stress tensor in the boundary CFT on $\mathcal{B}_n$. Therefore, Eq. (3.5.10) agrees with the expression, Eq. (3.5.3), in terms of twist fields. The formula for $T(z)$ can also be seen more directly from the way the stress tensor in a CFT transforms under a conformal transformation. Starting from the vacuum stress tensor in the z'-coordinate, $T(z') = 0$, and applying Eq. (3.5.5), the transformation picks up precisely the Schwarzian contribution in Eq. (3.5.10).

We can also give a description for these geometries in the language of Chern-Simons (CS) theory. It is known that Euclidean AdS_3 can be described by two copies of a Chern-Simons theory with gauge connections $A, \bar{A}$ valued in $\mathfrak{sl}(2, \mathbb{C})$, and where the Chern-Simons coupling is related to Newton's constant by $k = (4G_3)^{-1}$ [139]. We can expand these connections (with complex coefficients) over $\mathfrak{sl}(2, \mathbb{R})$ generators $L_0, L_\pm$ satisfying $[L_0, L_\pm] = \mp L_\pm$, $[L_+, L_-] = 2L_0$. In an explicit two-dimensional representation of the algebra, these are

$$L_0 = \frac{1}{2}\begin{pmatrix} 1 & 0 \\ 0 & -1 \end{pmatrix} \ , \quad L_+ = \begin{pmatrix} 0 & 0 \\ -1 & 0 \end{pmatrix} \ , \quad L_- = \begin{pmatrix} 0 & 1 \\ 0 & 0 \end{pmatrix} \ . \tag{3.5.11}$$

We can then describe the geometries, Eq. (3.5.9), using the connections

$$A = \frac{1}{2w}\begin{pmatrix} dw & -2\,dz \\ w^2\frac{12}{c}T(z)\,dz & -dw \end{pmatrix}, \qquad \bar{A} = -\frac{1}{2w}\begin{pmatrix} dw & w^2\frac{12}{c}\bar{T}(\bar{z})\,d\bar{z} \\ -2\,d\bar{z} & -dw \end{pmatrix} \ . \tag{3.5.12}$$

Each metric in this family of solutions corresponds to a choice of gauge connections, Eq. (3.5.12), with the same $T(z), \bar{T}(\bar{z})$ through the relation $ds^2 = \frac{1}{2}\mathrm{tr}((A - \bar{A})^2)$.

It will be useful to extract the radial dependence in Eq. (3.5.12) by using a suitable gauge transformation

$$A = bab^{-1} + bdb^{-1} \ , \bar{A} = b^{-1}\bar{a}b + b^{-1}db \ , \tag{3.5.13}$$

with gauge parameters

$$a = \begin{pmatrix} 0 & -dz \\ \frac{6}{c}T(z)\,dz & 0 \end{pmatrix} , \quad \bar{a} = \begin{pmatrix} 0 & -\frac{6}{c}\bar{T}(\bar{z})\,d\bar{z} \\ d\bar{z} & 0 \end{pmatrix} , \quad b(w) = \begin{pmatrix} \frac{1}{\sqrt{w}} & 0 \\ 0 & \sqrt{w} \end{pmatrix} . \tag{3.5.14}$$

3.5.2 Symplectic form

We now turn our attention to the bulk symplectic form. It is useful to work in the Chern-Simons formulation of three-dimensional gravity. For a similar discussion of the symplectic structure of 3d gravity in this setting, especially as pertains to the connection to coadjoint orbits, see [140–143].

The CS action with CS coupling k and gauge connection A is given by

$$S_{\rm CS} = \int \mathcal{L}_{\rm CS} = \frac{k}{4\pi}\int {\rm tr}\left(A\wedge dA + \frac{2}{3}A\wedge A\wedge A\right) . \tag{3.5.15}$$

We would like to evaluate the symplectic form. Taking the variation of the action for a single copy gives

$$\delta\mathcal{L}_{\rm CS} = \frac{k}{2\pi}{\rm tr}\left(\delta A\wedge F\right) + d\Theta \tag{3.5.16}$$

in terms of field strength $F = dA + A\wedge A$, and where $\Theta = \frac{k}{4\pi}{\rm tr}(A\wedge\delta A)$. The symplectic form for CS theory on some spatial region Σ is then given by

$$\omega = \int_\Sigma \delta\Theta = \frac{k}{4\pi}\int_\Sigma {\rm tr}(\delta_1 A\wedge\delta_2 A) . \tag{3.5.17}$$

In the following, we will assume that Σ is topologically a disk, i.e., it has a single boundary but no singularities in the interior. The symplectic form is a two-form on the space of classical solutions satisfying $F = 0$. Because we are working with a disk which admits no nontrivial cycles, a variation δA which leaves this condition invariant is of the form

$$\delta A = d_A\zeta \equiv d\zeta + [A,\zeta] \tag{3.5.18}$$

for some gauge transformation ζ, as follows from $\delta F = d_A\delta A = d_A^2\zeta = 0$.

We now consider the symplectic form for such a transformation. Using the identity

$${\rm tr}\left([A,\zeta]\wedge\delta A\right) = -{\rm tr}\left(\zeta\wedge[A,\delta A]\right) \tag{3.5.19}$$

and integrating by parts we obtain

$$\begin{aligned}\omega &= \frac{k}{4\pi}\int_\Sigma {\rm tr}(d_A\zeta\wedge\delta A) = \frac{k}{4\pi}\oint_{\partial\Sigma}{\rm tr}(\zeta\wedge\delta A) - \frac{k}{4\pi}\int_\Sigma {\rm tr}(\zeta\wedge d_A\delta A)\\ &= \frac{k}{4\pi}\oint_{\partial\Sigma}{\rm tr}(\zeta\wedge\delta A) .\end{aligned} \tag{3.5.20}$$

From Eq. (3.5.20) we see that the symplectic form ω is localized at the boundary of Σ.

Suppose that $\partial\Sigma$ lies in the asymptotic boundary of the geometry, in the $w = 0$ plane, and that we have gauged away the radial dependence. Using the explicit form of the connections, Eqs. (3.5.12) and (3.5.14), we can evaluate the symplectic form in Eq. (3.5.20). We see that the field variation can be expressed in terms of the stress tensor as

$$\delta A = \frac{6}{c}\begin{pmatrix} 0 & 0 \\ \delta T & 0 \end{pmatrix} dz \ . \tag{3.5.21}$$

It is also possible to solve Eq. (3.5.18) for δT. Decomposing ζ over the $\mathfrak{sl}(2,\mathbb{R})$ generators as $\zeta = \zeta_- L_{-1} + \zeta_0 L_0 + \zeta_+ L_1$ and using the form of the gauge field in Eq. (3.5.14), one can compute $d_A\zeta$. Matching with Eq. (3.5.21) gives a solution of the form

$$\delta T = \frac{c}{12}\xi''' + 2T\xi' + \partial T\xi \ , \tag{3.5.22}$$

where we have written $\xi \equiv -\zeta_-$ for the component of the gauge transformation associated to the L_{-1} generator. This is the usual stress tensor transformation law. From the form of the gauge transformation and the variation δA in Eq. (3.5.18), and using the Brown-Henneaux relation $(4G_3)^{-1} = c/6$ combined with the gravitational value for the CS coupling, we find that

$$\omega = \frac{1}{4\pi}\oint_{\partial\Sigma} dz\, \xi \wedge \delta T \ . \tag{3.5.23}$$

Using Eq. (3.5.22) the symplectic form becomes

$$\omega = \frac{1}{4\pi}\oint_{\partial\Sigma} dz \left(\frac{c}{12}\xi \wedge \xi''' + 2T\, \xi \wedge \xi'\right). \tag{3.5.24}$$

Plugging in two diffeomorphisms ξ_1 and ξ_2, the final result for the symplectic form reads:

$$\omega = \frac{1}{2\pi}\oint_{\partial\Sigma} dz \left(T\left(\xi_1\xi_2' - \xi_2\xi_1'\right) + \frac{c}{24}\left(\xi_1\xi_2''' - \xi_2\xi_1'''\right)\right) \ . \tag{3.5.25}$$

When the stress tensor $T(z) = T$ is a constant, Eq. (3.5.25) is reminiscent of the Kirillov-Kostant symplectic form on the coadjoint orbit $\mathrm{Diff}(\mathrm{S}^1)/\mathrm{U}(1)$ (or $\mathrm{Diff}(\mathrm{S}^1)/\mathrm{SL}(2,\mathbb{R})$ for the vacuum stress tensor) of the Virasoro group $\widehat{\mathrm{Diff}(\mathrm{S}^1)}$ with central charge c. However to match onto the Berry curvature, Eq. (3.3.3), with the zero mode projection Eq. (3.3.34), we must consider a non-constant vacuum stress tensor. In fact the the stress tensor profile that reproduces the correct projection is of the form Eq. (3.5.10). In other words, the zero mode projection for the parallel transport process is implemented by integrating against the stress-tensor expectation value in the presence of two twist fields. We will now argue

more precisely that in order to match the modular Berry curvature we need to consider a non-standard orbit corresponding to the conical singularity geometry described in Section 3.5.1.

3.5.3 Contour prescription

Let us return to the Euclidean geometry $\mathcal{M}_n$, which is obtained from the backreaction of a cosmic brane with tension $\mathcal{T}_n$. We showed that the stress tensor profile at the boundary is given by Eq. (3.5.10). Let us now restrict to transformations which leave the interval at the boundary fixed. This corresponds to Dirichlet boundary conditions $\delta A = 0$ at the cosmic brane.

We consider the symplectic form

$$\omega_n = \frac{k}{4\pi} \int_{\Sigma_n} \mathrm{tr}(\delta_1 A \wedge \delta_2 A) \ , \tag{3.5.26}$$

supported on some region Σ_n which corresponds to the entanglement wedge in the geometry $\mathcal{M}_n$, see Figure 3.2. The subscript in the symplectic form indicates that it depends on n. The entanglement wedge has two boundary components:

$$\partial\Sigma_n = \gamma_n \cup \mathrm{Brane}_n \ , \tag{3.5.27}$$

where γ_n is the entangling region at the asymptotic boundary extending between z_1 and z_2 and Brane_n is the cosmic brane anchored at those points. In Section 3.5.2, we have seen that the bulk symplectic form localizes to the boundary of Σ_n (using that the region is topologically trivial), because $\mathrm{tr}(\delta_1 A \wedge \delta_2 A) = d\eta$ is an exact form with $\eta = \mathrm{tr}(\xi \wedge \delta A)$. The expression for ω_n therefore reduces to a boundary term of the form

$$\omega_n = \frac{k}{4\pi} \left[\int_{\gamma_n} \eta + \int_{\mathrm{Brane}_n} \eta \right] \ . \tag{3.5.28}$$

The contribution at the cosmic brane vanishes due to the boundary conditions we put on the field variations there, i.e., $\delta A = 0$ at Brane_n. We are therefore left with the integral over the entangling region γ_n at the asymptotic boundary. There, η takes the form

$$k\,\eta = \xi \wedge \delta T = \frac{c}{12} \left(\xi_1 \xi_2''' - \xi_2 \xi_1''' \right) + 2\,T[\xi_1, \xi_2] \ , \tag{3.5.29}$$

in terms of the boundary stress tensor profile T of the geometry $\mathcal{M}_n$. Plugging in Eq. (3.5.10) with $z_1 = i$ and $z_2 = -i$, we find that

$$\omega_n = \frac{c}{12\pi} \left(1 - \frac{1}{n^2} \right) \int_{\gamma_n} \frac{[\xi_1, \xi_2]}{(z^2+1)^2}\, dz + \frac{c}{48\pi} \int_{\gamma_n} \left(\xi_1 \xi_2''' - \xi_2 \xi_1''' \right) dz \ . \tag{3.5.30}$$

Note that the integrand is singular at the endpoints of the integration region γ_n. Therefore, we should implement some kind of regularization procedure for the integral to avoid the twist field insertion points. A standard choice would be the *principal value* prescription, where we excise a small ball of size ϵ around each of the singularities located at the endpoints of γ_n. After computing the integral, we take $\epsilon \to 0$. The resulting expression for ω_n is UV divergent ($\omega_n \sim \log \epsilon$).

In the limit $n \to 1$ the first term in Eq. (3.5.30) vanishes. This is expected, since as the cosmic branes becomes tensionless the geometry reduces to pure AdS_3, for which the bulk symplectic form is identically zero (up to the central charge term). To extract a non-zero answer from ω_n, we first take a derivative with respect to n and define

$$\omega \equiv \lim_{n\to 1} \frac{\partial}{\partial n} \frac{\omega_n}{k} \ . \tag{3.5.31}$$

This corresponds to studying the first order correction of the backreaction process. The appearance of the operator $\lim_{n\to 1} \partial_n$ is not unfamiliar in the context of computing entanglement entropy using Euclidean solutions with conical singularties of the form $\mathcal{M}_n$[7]. Eq. (3.5.31) is our proposal for the bulk symplectic form associated to the entanglement wedge, and we will now show that it matches the modular Berry curvature.

To make the connection with the boundary computation, we rewrite the integral over the entangling region in terms of the variable u defined in Eq. (3.3.26). Notice that the unit semicircle $-\pi/2 \leq \arg(z) \leq \pi/2$ is mapped to the line $u \in [-\infty, \infty]$, since $z = 1$ goes to $u = 0$. In particular, the points $u = \pm\Lambda$ correspond to

$$z = \frac{1 + ie^{\pm\Lambda}}{e^{\pm\Lambda} + i} \sim e^{\pm i\left(\frac{\pi}{2} - \epsilon\right)} \ , \tag{3.5.32}$$

if we identify Λ with the UV regulator by $\Lambda = -\log \frac{\epsilon}{2}$, in the limit $\Lambda \to \infty, \epsilon \to 0$. In the limit $\Lambda \to \infty$, the endpoints go to $z \to \pm i$ along the unit circle, so Eq. (3.5.32) is precisely the principal value prescription for γ_n.

Moreover, under the transformation in Eq. (3.3.26) the integration measure changes as Eq. (3.3.28). Therefore, we can represent the integral over the entangling region γ_n in terms of the u-variable as

$$\frac{1}{\pi} \int_{-i}^{i} \frac{\xi(z)}{(1+z^2)^2}\, dz = \lim_{\Lambda\to\infty} \frac{i}{2\pi} \int_{-\Lambda}^{\Lambda} \xi(u)\, du \ , \tag{3.5.33}$$

which is precisely the projection operator $P_0(X_\xi)$ in Eq. (3.3.33). Thus, we can

[7] In fact, the entanglement entropy S associated to the subregion A can be computed by the formula $S = -\lim_{n\to 1} \partial_n \log Z_n$, where $\log Z_n \sim -I\left[\mathcal{M}_n\right]$ is the classical action evaluated on the conical singularity geometry $\mathcal{M}_n$.

rewrite the symplectic form ω_n as

$$\omega_n = \frac{c}{12}\left(1 - \frac{1}{n^2}\right) P_0([X_{\xi_1}, X_{\xi_2}]) + \frac{c}{48\pi}\int_{-i}^{i} (\xi_1 \xi_2''' - \xi_2 \xi_1''')\, dz \ . \tag{3.5.34}$$

Taking the derivative with respect to n and setting $n \to 1$ according to Eq. (3.5.31) gives the final result:

$$\omega = P_0([X_{\xi_1}, X_{\xi_2}]) \ , \tag{3.5.35}$$

which agrees with the curvature F in Eq. (3.3.3). Notice that the information about the central zero mode discussed in Section 3.3.3 is also contained in ω_n: it simply corresponds to taking $\lim_{n\to 1} \omega_n$ directly.

3.6 Discussion

We have considered the case of boundary parallel transport of a fixed interval under a change in global state, which is in contrast to the situation considered in [32] where the state is held fixed while the interval location is varied. However, a general parallel transport process will change both the state and the location of the interval. In such a situation, the curvature will contain cross-terms between the X_λ's of Eq. (3.3.33) and the V_μ's of Section 3.2.2. Both are eigenoperators of the adjoint action of the modular Hamiltonian, $[H_{\text{mod}}, X_\lambda] = \lambda X_\lambda$ and $[H_{\text{mod}}, V_\mu] = i\mu V_\mu$, but notice that the eigenvalue of the X_λ's is real while that of V_μ is purely imaginary. By the Jacobi identity, the commutator $[X_\lambda, V_\mu]$ will have an eigenvalue that is the sum of the two, thus it has both a real and imaginary part. This is never zero, which means $[X_\lambda, V_\mu]$ does not have a zero mode. The curvature, Eq. (3.3.3), is given by the projection onto this zero mode, which means that computed in these directions that mix changes of state and interval location, it must vanish. Thus, it appears to be sufficient to consider state and interval location-based transport separately.

In the bulk, we have demonstrated an abstract connection between state-changing parallel transport of boundary intervals and a certain family of Euclidean bulk solutions. The holographic dual of the modular Berry curvature was argued to be an entanglement wedge symplectic form on this geometry. This is similar in spirit to the results of [130,131], but in the case of mixed states. However, a direct phase space interpretation of this symplectic form in Lorentzian signature is not so obvious. Associating a phase space, i.e., a solution space of a proper initial value problem, to an entanglement wedge involves some subtleties, e.g., the possibility of edge modes [144–146] and boundary ambiguities at the RT surface that must be fixed by a suitable choice of boundary conditions. Possibly, one could exploit the relation to the hyperbolic black hole and identify the relevant phase space with

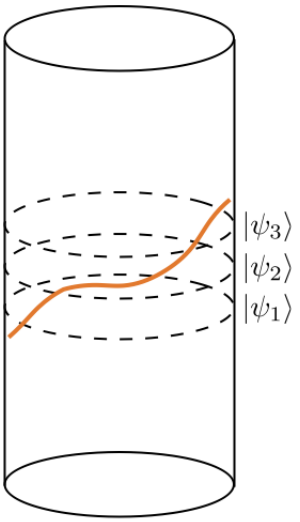

Figure 3.3: An example of a time-dependent geometry limiting to different boundary states $|\psi_i\rangle$ at each time. Could the Berry phase associated to state-dependent parallel transport compute the length of a curve (such as the thick orange curve) in such a geometry?

the one associated to the (outside of the) black hole. This would lead to geometric setup for which the Lorentzian continuation is more well-behaved. In particular, this approach requires a further study of the choice of boundary conditions that are natural to put at the horizon.

It would also be interesting to explore a bulk description within a single Lorentzian geometry. For instance, one could imagine constructing a time-dependent geometry by gluing together certain slowly varying time-independent geometries that are each dual to different boundary states. Since this will not in general give an on-shell solution, one could try to turn on suitable sources on the boundary as a function of time, in such a way that time evolution under the modified Hamiltonian (with sources) provides precisely the sequence of states under consideration. In such a situation, one could look for a corresponding on-shell bulk solution with modified asymptotics. It would be interesting to explore whether the Berry phase associated to state-changing parallel transport computes a length within a time-dependent geometry (see Figure 3.3).

Additionally, it would be interesting to explore further the connections to Uhlmann holonomy described in [105]. This is a version of parallel transport constructed from purification of density matrices subject to certain maximization conditions

on transition probabilities. Through appropriate insertion of stress tensors at the boundary, this is claimed in [147–150] to describe the shape-changing transport problem considered in Section 3.2.2. In this setting, the Berry curvature associated to a parallel transport process that changes the state was argued to be dual to the symplectic form of the entanglement wedge. While similar in spirit to much of this work, it would be interesting to further study the relation to our work in the context of key differences, such as the need for diagonalizing the adjoint action and the use of non-smooth vector fields.

The problem we study also has relevance for thermalization in 2d CFT. For example, the Krylov complexity contains information about operator growth in quantum chaotic systems. Roughly speaking, this is given by counting the operators that result under nested commutators with respect to a 'Hamiltonian' of the system. In [151], the Krylov complexity was studied for the case where this Hamiltonian takes the form of Eq. (3.3.12), using an oscillator representation of the Virasoro algebra. This is similar to the modular Berry transport process we have considered, with the exception again of the use of non-smooth vector fields.

In studying operator-based parallel transport, we uncovered some subtleties regarding the diagonalization of the adjoint action for arbitrary Virasoro generators (an explanation of these issues was given in Appendix C). For this reason we considered a set of certain non-smooth vector fields on the circle, Eq. (3.3.18), which explicitly diagonalize the adjoint action so that the curvature results of Appendix B may be applied. It would be interesting to further study this issue. For instance, we found that the adjoint action could not be diagonalized over the usual Virasoro algebra, defined as the set of smooth vector fields on the circle.[8] Instead, we saw that the set of generators not expressible as $[H_{\text{mod}}, X]$ was dimension three, larger than the dimension of the kernel (which is in this case one-dimensional and generated by H_{mod}). Furthermore, there was an ambiguity in the non-zero mode piece. One could ask whether it is possible to consider parallel transport generated by elements of the usual Virasoro algebra, and perhaps resolve the ambiguities in the decomposition by taking a suitable choice of norm. Along these lines, one could consider only Virasoro algebra elements that are contained within physical correlators. It would be interesting to apply techniques from algebraic quantum field theory to see if this eliminates some of the ambiguities we have encountered.

To properly diagonalize the adjoint action we were led to consider vector fields on the circle that are non-differentiable on the endpoints of the interval. These

[8] This is actually not uncommon in the case of infinite-dimensional vector spaces. For example, when one tries to diagonalize the derivative operator on the space of polynomial functions one naturally finds exponential functions, which are not part of the original space. The non-analyticities we found should be regarded in the same way.

form a continuous version of the Virasoro algebra. Our Berry curvature can be understood formally as the Kirillov-Kostant symplectic form on an orbit associated to this algebra. It would be interesting to conduct a more rigorous study of this algebra and its central extension. It is also worth noting that we considered a dual space of distributions on the circle, which is larger than the set of smooth quadratic differentials considered in the classification of [126]. For this reason, the orbits we consider differ considerably from known Virasoro orbits since the associated representative, Eq. (3.3.53), is not a quadratic form on the circle. To our knowledge, such orbits have not been studied before in the literature. We have identified at least one physical implication of such unconventional orbits, and thus it would be interesting to revisit the classification of Virasoro orbits using more general duals.

A Kinematic space example

We will now describe a version of the state-based parallel transport summarized in Section 3.2.1, which reproduces some of the results from kinematic space for CFT_2 on a time-slice. As we saw in Section 3.2.2, the parallel transport process for kinematic space could also be derived in the operator-based transport language. In this way of formulating the problem, the geometrical description of kinematic space in terms of coadjoint orbits [98] is more readily transparent.

We will start by setting up some geometry that is relevant for this problem. Consider the group $SL(2,\mathbb{R})$. Its Lie algebra $\mathfrak{sl}(2,\mathbb{R})$ consists of generators t_μ, $\mu = 0,1,2$ satisfying the commutation relations $[t_\mu, t_\nu] = \epsilon_{\mu\nu}{}^{\rho} t_\rho$, where the indices are raised by a metric η_{ab} with signature $(-,+,+)$. We will make use of an explicit finite-dimensional representation by 2×2 matrices given by

$$t_0 = \frac{1}{2}\begin{pmatrix} 0 & 1 \\ -1 & 0 \end{pmatrix} \ , \quad t_1 = \frac{1}{2}\begin{pmatrix} 0 & 1 \\ 1 & 0 \end{pmatrix} \ , \quad t_2 = \frac{1}{2}\begin{pmatrix} 1 & 0 \\ 0 & -1 \end{pmatrix} \ . \tag{A.1}$$

This basis will be most convenient for the calculation of the Berry curvature. It can be easily expressed in terms of the basis used in Section 3.5 as $t_0 = \frac{1}{2}(L_- + L_+), t_1 = \frac{1}{2}(L_- - L_+), t_2 = L_0$.

Now consider embedding coordinates (X^0, X^1, X^2) describing 3-dimensional Minkowski spacetime with metric

$$ds^2 = -(dX^0)^2 + (dX^1)^2 + (dX^2)^2 \ . \tag{A.2}$$

Recall that $SL(2,\mathbb{R})/\mathbb{Z}_2 \cong SO(2,1)$. A convenient parametrization for the algebra $\mathfrak{sl}(2,\mathbb{R})$ is given through the isomorphism to Mink_3:

$$\frac{1}{2}\begin{pmatrix} X^2 & X^1 + X^0 \\ X^1 - X^0 & -X^2 \end{pmatrix} \leftrightarrow (X^0, X^1, X^2) \ . \tag{A.3}$$

The reason to express $\mathfrak{sl}(2,\mathbb{R})$ in this way is that the coadjoint orbits of the Lie group can be realized geometrically in Minkowski space. Any element of $\mathfrak{sl}(2,\mathbb{R})$

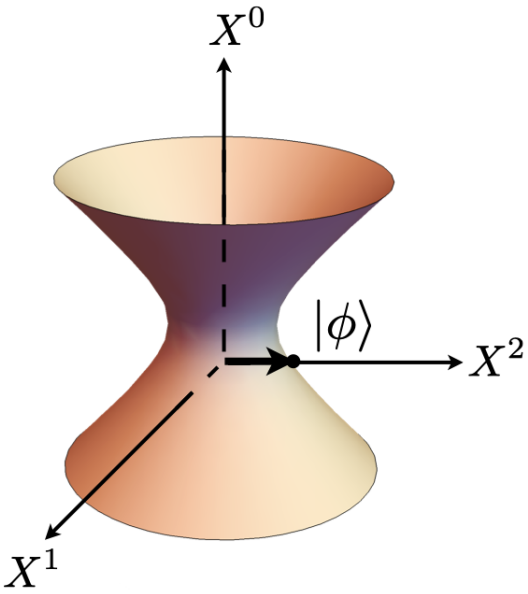

Figure A.1: The dS_2 hyperboloid describing kinematic space, which is a coadjoint orbit of $SO(2,1)$. The arrow points to a special point that corresponds to the coherent state $|\phi\rangle$.

lies in one of three conjugacy classes (up to an overall factor ± 1). These can be classified by the value of $\epsilon \equiv |\mathrm{tr}(g)|/2$ where $g \in SL(2,\mathbb{R})$: $\epsilon < 1$ is elliptic, $\epsilon = 1$ is parabolic and $\epsilon > 1$ is hyperbolic.

We will assume that our representative is in the diagonal class

$$\Lambda = \mathrm{diag}(\lambda, -\lambda)/2 \tag{A.4}$$

with $\lambda \in \mathbb{R}$. Since $|\mathrm{tr}(e^{\Lambda})|/2 > 1$ for all λ, this is a hyperbolic element. Other choices lead to different orbits.

Consider a general group element

$$g = \begin{pmatrix} a & b \\ c & d \end{pmatrix} \in SL(2,\mathbb{R}) \ , \tag{A.5}$$

with $a, b, c, d \in \mathbb{R}$ and $ad - bc = 1$. The coadjoint orbit is generated by the adjoint action of Λ with arbitrary g,

$$g \cdot \Lambda \cdot g^{-1} = \begin{pmatrix} \frac{\lambda}{2}(bc + ad) & -\lambda ab \\ \lambda cd & -\frac{\lambda}{2}(bc + ad) \end{pmatrix} \ . \tag{A.6}$$

The determinant is constant along the orbit, $\det(g \cdot \Lambda \cdot g^{-1}) = -\lambda^2/4$. Applying the map to Minkowski space, Eq. (A.3), this results in the condition

$$-(X^0)^2 + (X^1)^2 + (X^2)^2 = \lambda^2 \ . \tag{A.7}$$

This is the defining equation of a single-sheeted hyperboloid with radius λ. Take the embedding coordinates

$$\begin{aligned} X^0 &= \lambda \cot t \ , \\ X^1 &= \lambda \csc t \cos\theta \ , \\ X^2 &= \lambda \csc t \sin\theta \ . \end{aligned} \tag{A.8}$$

These satisfy Eq. (A.7) and from Eq. (A.2) result in the induced metric

$$ds^2 = \lambda^2 \csc^2 t(-dt^2 + d\theta^2) \ . \tag{A.9}$$

This is just the metric on $\mathrm{dS}_2 \simeq SO(1,2)/SO(1,1)$. We saw that this describes the coadjoint orbit passing through the representative, Eq. (A.4).

The coadjoint orbit can be thought of as a fiber bundle whose base space is $SO(1,2)/SO(1,1)$ and its fiber is $SO(1,1)$. We want to consider an appropriate section of the fiber bundle. The discussion below follows closely [107]. Using the embedding coordinate Eq. (A.8) and the map Eq. (A.3), we obtain the constraints

$$\begin{aligned} 2\mathrm{tr}(g\,\Lambda\,g^{-1}\,t_0) &= -X_0 = -\lambda \cot t \ , \\ 2\mathrm{tr}(g\,\Lambda\,g^{-1}\,t_1) &= X_1 = \lambda \cos\theta \csc t \ , \\ 2\mathrm{tr}(g\,\Lambda\,g^{-1}\,t_2) &= X_2 = \lambda \sin\theta \csc t \ . \end{aligned} \tag{A.10}$$

Solving this system of equations, Eq. (A.10), we obtain

$$b = -\frac{\cot t + \cos\theta \csc t}{2a} \ , \quad c = \frac{a(1 - \sin\theta \csc t)}{\cot t + \cos\theta \csc t} \ , \quad d = \frac{1 + \sin\theta \csc t}{2a} \ . \tag{A.11}$$

We have the freedom to impose $a = 1$, in which case the expressions somewhat simplify. Applying this back to Eq. (A.5), we obtain a section $g : \mathrm{dS}_2 \to SL(2,\mathbb{R})$ for the bundle given by

$$g = \begin{pmatrix} 1 & -\frac{1}{2}(\cos t + \cos\theta)\csc t \\ \tan\left(\frac{t-\theta}{2}\right) & \frac{1}{2}(1 + \csc t \sin\theta) \end{pmatrix} \ . \tag{A.12}$$

Notice that g reduces to the identity for $t = \theta = \pi/2$ which corresponds to the point of intersection of the hyperboloid with the axis labeled by the t_2 generator.

Now we will apply some of these tools to the problem of state-based parallel transport for the group $SL(2,\mathbb{R})$, with the aim of describing kinematic space.

Recall that to define a state-based Berry phase it is necessary to choose a suitable 'Hamiltonian' with an eigenstate $|\phi\rangle$ that serves as the base state for the parallel transport process. The 'Hamiltonian' is one which generates a specified subgroup of $SL(2,\mathbb{R})$, which we interpret as a flow in time. The state is acted on by group elements in a unitary representation, which we denote by $\mathcal{D}(g)$, $\mathcal{D}(u)$ for $g \in SL(2,\mathbb{R}), u \in \mathfrak{sl}(2,\mathbb{R})$. In the coadjoint orbit language, eigenstates of subalgebras of the symmetry algebra are known as *coherent states*. Specifically, we will choose our Hamiltonian to be t_2, which generates an $\mathfrak{so}(1,1)$ subalgebra. This exponentiates to the hyperbolic group element

$$\mathcal{J} = e^{\eta t_2/2} \tag{A.13}$$

with $\eta \in \mathbb{R}$. Taking $X \to \mathcal{J} X \mathcal{J}^{-1}$ using the isomorphism, Eq. (A.3), we see the adjoint action with respect to $\mathcal{J}$ acts geometrically as

$$X^0 \to X^0 \cosh(\eta/2) + X^1 \sinh(\eta/2) \ , \tag{A.14}$$

$$X^1 \to X^0 \sinh(\eta/2) + X^1 \cosh(\eta/2) \ , \tag{A.15}$$

$$X^2 \to X^2 \ , \tag{A.16}$$

in other words, it acts as a boost with rapidity $-\eta/2$ in the $X^0 - X^1$ direction in embedding space.

We define our coherent state through the condition that the boost leaves it invariant up to a phase,

$$\mathcal{D}(\mathcal{J})\,|\phi\rangle = e^{i\eta\zeta}\,|\phi\rangle \ \ , \mathcal{D}(t_2)\,|\phi\rangle = 2\zeta\,|\phi\rangle \ \ , \tag{A.17}$$

with $\zeta \in \mathbb{R}$ since $\mathcal{D}(\mathcal{J})$ is assumed to be unitary and $\mathcal{D}(t_2)$ Hermitian in the representation. By a theorem of Perelomov [108] (see also [109]), coherent states are in one-to-one correspondence with points on an orbit. Our state $|\phi\rangle$ corresponds to the point $(0,0,1)$ on the dS_2 hyperboloid that is left fixed by the action of the boost (see Figure A.1). It is geometrically simple to see that the action of the other generators t_0, t_1 do not leave this point invariant, which corresponds to the statement that $|\phi\rangle$ is not also an eigenstate of these generators.

Recall that the Maurer-Cartan form is given by

$$\Theta = g^{-1} dg \ . \tag{A.18}$$

The Berry phase is

$$\theta(\gamma) = \oint_\gamma A \ , \quad A = i\,\langle\phi|\,\mathcal{D}(\Theta)\,|\phi\rangle \ . \tag{A.19}$$

We now use Eq. (A.12) to evaluate the pullback of the Maurer-Cartan form from $SL(2,\mathbb{R})$ to dS_2. Taking the expectation value of the generators in the state $|\phi\rangle$,

then applying the commutation relations, the eigenvalue condition Eq. (A.17) and using $\zeta \in \mathbb{R}$, we see that only t_2 has a nonvanishing expectation value in $|\phi\rangle$. Thus, only this part contributes to the Berry phase. We find

$$A = i \langle \phi | \mathcal{D}(\Theta) | \phi \rangle = i\zeta \csc t \cos\left(\frac{t+\theta}{2}\right) \sec\left(\frac{t-\theta}{2}\right)(dt - d\theta) \ . \tag{A.20}$$

From this we can define the Berry curvature

$$F = dA = \frac{i\zeta}{\sin^2 t} dt \wedge d\theta \ . \tag{A.21}$$

Using Stokes' theorem one can write the integral of the Berry connection in Eq. (A.20) as

$$\theta(\gamma) = i\zeta \int_B \frac{1}{\sin^2 t} dt \wedge d\theta \ , \tag{A.22}$$

where B is any two-dimensional region with boundary $\partial B = \gamma$.

For a CFT_2 restricted to a time-slice, kinematic space consists of the space of intervals on this time-slice. Given a causal ordering based on containment of intervals, this is just a dS_2 spacetime, Eq. (A.9), with a time coordinate set by the interval radius, $(\theta_R - \theta_L)/2$ [94]. The curvature, Eq. (A.21), is a volume form on kinematic space. Recalling the relation between time and interval size, it matches the kinematic space curvature, Eq. (3.2.25), derived from the operator-based method in Section 3.2.2 (note that an exact matching of the normalization is unimportant, as the overall normalization for the modular Berry phase will be at any rate affected by the choice of normalization for the modular Hamiltonian). The Berry phase, Eq. (A.22), computes the volume of region B within this dS_2 spacetime. It also precisely reproduces the Berry phase for kinematic space derived by other means in [28, 32].

B General formulation

We will derive a general formula for the curvature assuming that there is a unique way of separating out the zero mode. As we discuss in the next appendix, this is not generally true when the state-changing transformations are elements of the Virasoro algebra, however it holds for the transformations that we consider in the main text. The results of Section 3.3 utilize the formula for the curvature presented in this appendix.

Consider a Lie algebra $\mathfrak{g}$ and a trajectory of elements $X(\lambda) \in \mathfrak{g}$ specified by some parameter λ. We write Ad_X for the adjoint action of X on $\mathfrak{g}$, $\mathrm{Ad}_X(Y) = [X, Y]$. We make the assumption that the kernel of Ad_X and the image of Ad_X do not intersect anywhere along the path, which is guaranteed if $[X, Y] \neq 0$ implies $[X, [X, Y]] \neq 0$. Moreover, we will be interested in smooth trajectories $X(\lambda)$ along which the kernel and image of Ad_X vary smoothly. In particular, we will assume their dimensions do not jump.

Crucially, we will make the further assumption[1] that any Y can be uniquely decomposed as $Y = K + I$ with K in the kernel and I in the image of Ad_X. We will call the corresponding projection operators P_K and P_I, with the property that

$$P_I + P_K = 1 \ . \tag{B.1}$$

Notice that we are not using an inner product, which means that the projectors are not orthogonal in any sense.

Besides the projectors P_K and P_I, we will denote Ad_X simply by A, and its inverse by A^{-1}. Note that A has a kernel so it does not have an inverse, but since by assumption A defines a non-degenerate map from the image of the image of Ad_X to itself, it does have a well-defined inverse on these subspaces. The map A^{-1}

[1] For finite-dimensional Lie algebras the dimensions of the kernel and the image add up to the total dimension of the Lie algebra. Since they do not intersect, this then implies that the kernel and image of Ad_X together span the full Lie algebra. For infinite-dimensional Lie algebras the situation is more complicated, as we explain in Appendix C.

is defined to be the inverse on these subspaces and zero everywhere else. These operators then obey the following set of identities:

$$AP_K = P_K A = 0 \,, \tag{B.2}$$
$$A^{-1}P_K = P_K A^{-1} = 0 \,, \tag{B.3}$$
$$AA^{-1} = A^{-1}A = P_I \,. \tag{B.4}$$

We now vary X to $X+\delta X$ by some small change $\delta\lambda$ along the path. In particular, we can use the above identities to express the variations of P_K, P_I and A^{-1} in terms of the variation of A. After some algebra we find that

$$\delta P_K = -\delta P_I = -P_K \delta A A^{-1} P_I - P_I A^{-1} \delta A P_K \,, \tag{B.5}$$
$$\delta A^{-1} = -A^{-1}\delta A A^{-1} + P_I A^{-2} \delta A P_K + P_K \delta A A^{-2} P_I \,. \tag{B.6}$$

In particular, we used

$$P_K \delta P_I = P_K \delta A^{-1} A P_I \,, \quad P_I \delta P_I = P_I A^{-1} \delta A P_K \,, \tag{B.7}$$

for deriving Eq. (B.5) and

$$P_K \delta A^{-1} = \delta P_I A^{-1} \,, \quad P_I \delta A^{-1} = A^{-1}\delta P_I - A^{-1}\delta A A^{-1} \,, \tag{B.8}$$

for Eq. (B.6). We also used that $P_I A^{-1} = A^{-1} P_I = A^{-1}$ and $P_I A = A P_I = A$.

Given a variation δX, we want to express it as

$$\delta X = [S, X] + P_K \delta X \,, \tag{B.9}$$

where $P_K \delta X$ is in the kernel of Ad_X. Moreover, we want to remove the modular zero mode from S, so that S is uniquely defined. We do this by requiring that $P_K S = S P_K = 0$, and with the above equations it is then easy to see that

$$S = -A^{-1}(\delta X) \,. \tag{B.10}$$

We are now going to compute the parallel transport along a small square, by first doing the variation $\delta_1 X$ and then $\delta_2 X$, and then subtracting the reverse order. For the difference, we get

$$F = (1 - (A^{-1} + \delta_1 A^{-1})(\delta_2 X))(1 - A^{-1}(\delta_1 X)) - (1 \leftrightarrow 2) \,. \tag{B.11}$$

The first order terms vanish, thus it is necessary to expand to second order. One term we get at second order is

$$F_1 = -[A^{-1}(\delta_1 X), A^{-1}(\delta_2 X)] \,. \tag{B.12}$$

There is also another term coming from the variations of A^{-1}, which evaluates to

$$F_2 = (A^{-1}\delta_1 A A^{-1} - P_I A^{-2}\delta_1 A P_K - P_K \delta_1 A A^{-2} P_I)(\delta_2 X) - (1 \leftrightarrow 2) \ . \quad \text{(B.13)}$$

In order to simplify Eq. (B.13) further, we need several other identities. For example, multiplying

$$A([Y,Z]) = [AY,Z] + [Y,AZ] \quad \text{(B.14)}$$

by A^{-1} we get the identity

$$A^{-1}([AY,Z] + [Y,AZ]) = P_I([Y,Z]) \ . \quad \text{(B.15)}$$

From this it follows that

$$A^{-1}[Y,P_K Z] = A^{-1}[P_I Y, P_K Z] = P_I([A^{-1}Y, P_K Z]) \ , \quad \text{(B.16)}$$

where we used Eqs. (B.1), (B.3) and (B.4).

Next we consider the first term in F_2 minus the same term with 1 and 2 interchanged. It is given by

$$F_2^1 = A^{-1}\delta_1 A A^{-1}(\delta_2 X) - (1 \leftrightarrow 2) \ . \quad \text{(B.17)}$$

We use $\delta_1 AY = [\delta_1 X, Y]$ to rewrite it as

$$\begin{aligned} F_2^1 &= A^{-1}([\delta_1 X, A^{-1}(\delta_2 X)] + [A^{-1}(\delta_1 X), \delta_2 X]) \\ &= A^{-1}([(AA^{-1} + P_K)\delta_1 X, A^{-1}(\delta_2 X)] + [A^{-1}(\delta_1 X), (AA^{-1} + P_K)\delta_2 X]) \\ &= P_I([A^{-1}(\delta_1 X), A^{-1}(\delta_2 X)]) + A^{-1}([P_K\delta_1 X, A^{-1}(\delta_2 X)] + [A^{-1}(\delta_1 X), P_K \delta_2 X]) \ . \end{aligned} \quad \text{(B.18)}$$

In the last equality we make use of Eq. (B.15). Applying Eq. (B.16) to the last two terms gives

$$F_2^1 = P_I([A^{-1}(\delta_1 X), A^{-1}(\delta_2 X)] + [A^{-2}(\delta_1 X), P_K \delta_2 X] - [A^{-2}(\delta_2 X), P_K \delta_1 X]) \ . \quad \text{(B.19)}$$

The second term in F_2 reads

$$\begin{aligned} F_2^2 &= -P_I A^{-2}\delta_1 A P_K(\delta_2 X) + P_I A^{-2}\delta_2 A P_K(\delta_1 X) \\ &= -A^{-2}([\delta_1 X, P_K \delta_2 X] - [\delta_2 X, P_K \delta_1 X]) \ . \end{aligned} \quad \text{(B.20)}$$

Using the identity Eq. (B.16) twice it follows that

$$F_2^2 = -P_I([A^{-2}(\delta_1 X), P_K \delta_2 X] - [A^{-2}(\delta_2 X), P_K \delta_1 X]) \ . \quad \text{(B.21)}$$

The last term to consider is

$$\begin{aligned} F_2^3 &= P_K \delta_2 A A^{-2} P_I(\delta_1 X) - P_K \delta_1 A A^{-2} P_I(\delta_2 X) \\ &= P_K([\delta_2 X, A^{-2}(\delta_1 X)] - [\delta_1 X, A^{-2}(\delta_2 X)]) \ . \end{aligned} \quad \text{(B.22)}$$

This expression does not admit an obvious simplification. Combining all terms we see that the first term in F_2^1 cancels part of F_1, the second and third terms in F_2^1 cancel against F_2^2, so that we are left with a simple and compact expression for the full curvature:

$$F = -P_K([A^{-1}(\delta_1 X), A^{-1}(\delta_2 X)] + [\delta_1 X, A^{-2}(\delta_2 X)] - [\delta_2 X, A^{-2}(\delta_1 X)]) \ . \quad \text{(B.23)}$$

One can easily check that the curvature commutes with X.

Notice that only the P_I components of δX contribute to the curvature due to the observation that

$$P_K([P_I Y, P_K Z]) = P_K([AA^{-1}Y, P_K Z]) = P_K A([A^{-1}Y, P_K Z]) = 0 \ , \quad \text{(B.24)}$$

where we used Eq. (B.14). Moreover, we find that

$$\begin{aligned} W &= A^2([A^{-2}(\delta_1 X), A^{-2}(\delta_2 X)]) \\ &= 2[A^{-1}(\delta_1 X), A^{-1}(\delta_2 X)] + [P_I \delta_1 X, A^{-2}(\delta_2 X)] + [A^{-2}(\delta_1 X), P_I \delta_2 X] \end{aligned} \quad \text{(B.25)}$$

is almost the same as Eq. (B.23), except for the factor of two, and the appearance of the projector P_I. It is obvious that $P_K W = 0$ and if we add $P_K W$ to F we can drop the P_I in the resulting expression, as follows from Eq. (B.24). Therefore, the final expression for the curvature reads

$$F = P_K([A^{-1}(\delta_1 X), A^{-1}(\delta_2 X)]) \ . \quad \text{(B.26)}$$

The simple form of this result suggests that there is a shorter derivation and it would be interesting to further investigate this possibility.

C Non-diagonalization for Virasoro

There are subtleties in expressing a Virasoro generator X as $X = X_0 + [H_{\text{mod}}, Y]$ with X_0 a zero mode of the modular Hamiltonian H_{mod} in the Virasoro algebra. We will give here a summary of why the assumed decomposition, Eq. (B.9), used to derive the curvature cannot be applied to the full Virasoro algebra, and hence why we have chosen to restrict to a different set of transformations.

We will first be more precise about the notion of 'generator.' A generator of $\text{Diff}(S^1)$ can be expressed as

$$X = \sum_n c_n L_n \ , \tag{C.1}$$

where the modes L_n satisfy the Virasoro algebra, Eq. (3.3.11). We can equivalently represent X as a function on S^1, $f(\theta) = \sum c_n e^{in\theta}$, or as a vector field, $\xi = \sum c_n z^{n+1}\partial_z$ in radial quantization. For the arguments we are interested in the central charge can be considered separately, see Section 3.3.3.

One can ask what values of c_n are allowed in Eq. (C.1). This leads to different 'definitions' of the Virasoro algebra. Some choices that are preserved under commutation are:

- algebraic: require only a finite number of the c_n to be non-zero ,
- semi-algebraic: require that $c_n = 0$ for n sufficiently negative (alternatively, one could require $c_n = 0$ for n sufficiently positive) ,
- analytic: require the function f or vector field ξ to be smooth .

In the case where the generators are self-adjoint, then semi-algebraic reduces to algebraic.

For each of these choices of infinite-dimensional Lie algebras, we can ask to what extent the statement that any generator X can be written as $X = X_0 + [H_{\text{mod}}, Y]$ with X_0 a zero mode of the modular Hamiltonian H_{mod} holds.

Algebraic and semi-algebraic case

In the algebraic case, one can prove that the only algebra element that commutes with $H_{\rm mod}$ is $H_{\rm mod}$ itself. First, recall that

$$H_{\rm mod} = \pi(L_1 + L_{-1}) \ . \tag{C.2}$$

Now consider elements with only a finite number of non-zero c_n, running from $n = -L, ..., K$, with K and L positive. Then, the commutator

$$[H_{\rm mod}, \sum_{n=-L}^{K} c_n L_n] = \sum_{n=-L-1}^{K+1} c'_n L_n \tag{C.3}$$

maps a vector space of dimension $K+L+1$ into a vector space of dimension $K+L+3$. Its kernel is dimension one so its cokernel must be dimension three. Therefore, the number of generators which can be written as $[H_{\rm mod}, X]$ is codimension three. In fact, one can write every generator as

$$X = aH_{\rm mod} + bL_2 + cL_{-2} + [H_{\rm mod}, Y] \ , \tag{C.4}$$

for some a, b, c, which can be seen iteratively by taking a suitable Y with $L = K = 1$ and combining $H_{\rm mod}, L_2, L_{-2}$ to isolate L_0, then taking a suitable Y with $L = 1, K = 2$ combined with all the previous generators to isolate L_3, and so on and so forth. Crucially, this decomposition is not unique. For instance, we could have equally well written a similar decomposition with L_3, L_{-3} instead of L_2, L_{-2}.

To solve

$$L_{-2} = [H_{\rm mod}, Y] \ , \tag{C.5}$$

it is necessary to express Y as an infinite series $Y = \sum_{k=-3}^{-\infty} c_k L_k$ which is not part of the algebra:

$$Y = \frac{1}{4} L_{-3} - \frac{2}{4 \cdot 6} L_{-5} + \frac{2}{6 \cdot 8} L_{-7} - \frac{2}{8 \cdot 10} L_{-9} + \dots \tag{C.6}$$

If we denote by Y_k the sum of the first k terms which truncates at L_{-2k-1}, then we have

$$\frac{1}{\pi}[H_{\rm mod}, Y_k] = L_{-2} + \frac{(-1)^{k+1}}{k+1} L_{-2k-2} \ , \tag{C.7}$$

so that for large k this becomes 'close' to L_{-2}. We can introduce a metric so that this notion of closeness becomes more precise, e.g.,

$$|| \sum_n c_n L_n ||^2 \equiv \sum_n |c_n|^2 \tag{C.8}$$

defines a metric on the Lie algebra. But the Lie algebra is not complete with respect to this metric, i.e., limits of Lie algebra elements which converge in this norm will not in general converge to an element of the Lie algebra.

Even ignoring the fact that the algebra is not complete with respect to Eq. (C.8), there is the additional issue that this way of interpreting L_{-2} as the commutator of an element of the algebra with Y is too strong. Indeed, we can also find an infinite series Y obeying

$$[H_{\text{mod}}, Y] = H_{\text{mod}} \ , \tag{C.9}$$

which looks like

$$Y = \ldots + c_6 L_6 + c_4 L_4 + c_2 L_2 + c_{-2} L_{-2} + c_{_4} L_{-4} + c_{-6} L_{-6} + \ldots \tag{C.10}$$

This also has the property that if one truncates Y, the Y_k obeys $[H_{\text{mod}}, Y_k] = H_{\text{mod}} + Z_k$, with Z_k small defined with respect to the above norm. This would not allow for a decomposition separating out the zero mode part from the image of the adjoint action without intersection.

Notice that considering the semi-algebraic rather than algebraic case also does not fix the issue. A semi-infinite series in one direction can either remove L_2 or L_{-2} from the expression Eq. (C.4), but not both.

Analytic case

In the analytic case, the equation $[H_{\text{mod}}, X] = Y$ is the differential equation

$$(1+z^2)X'(z) - 2zX(z) = -\frac{1}{\pi} Y(z) \ , \tag{C.11}$$

where we replaced everything by the corresponding smooth function. This differential equation is equivalent to

$$\frac{d}{dz}\left(\frac{X(z)}{1+z^2}\right) = -\frac{1}{\pi}\frac{Y(z)}{(1+z^2)^2} \ . \tag{C.12}$$

Therefore,

$$X(z) = -\frac{c_0}{2}(1+z^2) - \frac{1}{\pi}(1+z^2)\int^z \frac{Y(z')}{(1+z'^2)^2}\, dz' \ , \tag{C.13}$$

where c_0 is an integration constant, and the integration is over the circle. The differential equation does not have an analytic solution for all $Y(z)$. In fact, we will argue that in order to find an analytic solution we require three conditions on Y, so that once again the space of smooth vector fields which can be written as $[H_{\text{mod}}, X]$ is codimension three.

The first two conditions come from exploring the behavior of the integrand near $z = \pm i$, where we find that there will be logarithmic branch cut singularities unless the residues at $z = \pm i$ vanish. Thus, the first two conditions on $Y(z)$ for Eq. (C.13) to be analytic are

$$\text{Res}_{z=\pm i} \frac{Y(z)}{(1+z^2)^2} = 0 \ . \tag{C.14}$$

Note that it is admissible for $Y(z)/(1+z^2)^2$ to have double pole at $z = \pm i$, as these integrate to a single pole, which is then canceled by the $(1+z^2)$ prefactor in Eq. (C.13). Therefore, the double poles do not give rise to singularities.

There is also another condition, namely that the contour integral of $X'(z)$ around the unit circle vanishes so that we get a periodic function $X(z)$ after integration. Since polynomials in z are automatically periodic, it suffices to consider the behavior of the integrand, $Y(z)/(1+z^2)^2$. Assuming that $Y(z)$ is analytic except possibly at $z = 0$, this amounts to the condition

$$\mathrm{Res}_{z=0} \frac{Y(z)}{(1+z^2)^2} = 0 \ . \tag{C.15}$$

Note that poles near $z = \pm i$ do not affect the periodicity so we can subtract them before applying this condition if necessary, and we also assume the residues vanish as above, so that we have a well-defined integral.

To see how this works in practice, it is useful to evaluate this for a trial function Y inspired by the algebraic case:

$$Y_0 = a(1+z^2) + bz^{-1} + cz^3 \ , \tag{C.16}$$

which contains L_2, L_{-2} and H_{mod}. We notice that

$$\frac{Y_0}{(1+z^2)^2} = \frac{i(b+c)}{4(z-i)^2} + \frac{-b-ia+c}{2(z-i)} + \dots \ , \tag{C.17}$$

$$\frac{Y_0}{(1+z^2)^2} = \frac{-i(b+c)}{4(z+i)^2} + \frac{-b+ia+c}{2(z+i)} + \dots \tag{C.18}$$

near $z = \pm i$ respectively. The residue of $Y_0/(1+z^2)^2$ at $z = i$ equals $-(iY_0(i) + Y_0'(i))/4$ and the residue at $z = -i$ equals $(iY_0(-i) - Y_0'(-i))/4$, and these are required to vanish by Eq. (C.14). This translates to $b = c$ and $a = 0$. Recall that the differential equation, Eq. (C.11), extracts the non-zero mode part, i.e., the vector fields that can be written as $[H_{\mathrm{mod}}, X]$. We could also ask how to extract the zero mode part. In this case it seems the most natural choice to extract a, which is given by the difference of the two residues, as the coefficient of the zero mode.

Even in the case $b = c$ and $a = 0$ with vanishing residues, we see that X will now involve a term $(1+z^2)\log z$ since $Y = z^{-1} + z^3 = (z^2+1)^2 z^{-1} - 2z$. This still has a branch cut singularity, and therefore will not be single-valued. This is where a version of the third condition, Eq. (C.15), is necessary. To be more precise about this requirement, take a finite polynomial in z, z^{-1} for Y. We first subtract the harmless double poles and the harmful single poles (which we require to vanish

independently) so that we get an expression of the type

$$Z(z) \equiv \frac{Y(z) - A - Bz - Cz^2 - Dz^3}{(1+z^2)^2} \ , \tag{C.19}$$

where the coefficients A, B, C, D are chosen so as to cancel the single and double poles. To accomplish this, it is necessary for an overall factor $(1+z^2)^2$ to factor out of the numerator. The choice of coefficients can then be determined by the requirement that the numerator of Z and its derivative both vanish at $z = \pm i$. Explicitly, they are given by

$$A = \frac{1}{4}(2Y(-i) + 2Y(i) + iY'(-i) - iY'(i)) \ , \tag{C.20}$$

$$B = \frac{1}{4}(3iY(-i) - 3iY(i) - Y'(-i) - Y'(i)) \ , \tag{C.21}$$

$$C = \frac{i}{4}(Y'(-i) - Y'(i)) \ , \tag{C.22}$$

$$D = \frac{1}{4}(iY(-i) - iY(i) - Y'(-i) - Y'(i)) \ . \tag{C.23}$$

With this choice of coefficients the expression, Eq. (C.19), is now well-behaved everywhere, i.e., the numerator has a factor $(1+z^2)^2$, and the quotient is also a finite polynomial in z and z^{-1}. The only problematic contribution to the integral is coming from the z^{-1} term which does not become a periodic function when integrated. So the remaining number is the coefficient in front of z^{-1} in the polynomial $Z(z)$ in Eq. (C.19).

We denote by Y_- the terms in Y with a negative power of z. The non-negative powers in Y only give rise to non-negative powers in Z and are never problematic. So we can equivalently consider

$$Z_-(z) \equiv \frac{Y_-(z) - A - Bz - Cz^2 - Dz^3}{(1+z^2)^2} \ , \tag{C.24}$$

and we are interested in the coefficient in front of z^{-1} in $Z_-(z)$. We can extract this using a small contour integral. But we might as well extract it using a large contour integral as Z_- is analytic everywhere except at 0 and ∞. Then the integral is dominated by D, so it is necessary that $D = 0$ for the integral to be single-valued. In fact, D is equal to the sum of the residues at $z = i$ and $z = -i$, as can be seen from Eq. (C.23), so this version of the third condition with the double poles subtracted out reduces to

$$\mathrm{Res}_{z=i} \frac{Y_-}{(1+z^2)^2} + \mathrm{Res}_{z=-i} \frac{Y_-}{(1+z^2)^2} = 0 \ . \tag{C.25}$$

Since the residues of the complete $Y/(1+z^2)^2$ have to vanish separately, we could equivalently require the same condition for Y_+.

For more general non-polynomial Y, we can apply the same argument, except that now Y_- is analytic outside the unit disk and Y_+ is analytic inside the unit disk. By the version of the Riemann-Hilbert problem that applies to simple closed curves, a decomposition of analytic functions on the circle of the type $Y_- + Y_+$ exists.

Issues from non-diagonalization

In this subsection, we will show that the ambiguities in the diagonalization of the Virasoro algebra with respect to the adjoint action translate to ambiguities in the projection operator. This leads to different answers for the Berry curvature that are physically inequivalent. As a result, there is no sensible bulk interpretation. It is because parallel transport acting by elements of the usual Virasoro algebra is plagued with ambiguities that we are forced to extend to a non-standard algebra constructed from vector fields on the half-circle as in Section 3.3, where the construction is unique.

For the ordinary Virasoro case, we want to construct a zero-mode projector P_0 so that it evaluates to zero for the integrand of Eq. (3.3.15), while it gives a non-zero value for Eq. (3.3.9). In other words we can devise a contour integral prescription in such a way as to satisfy the properties:

- The functional is non-zero on the modular Hamiltonian, i.e., $P_0\left(H_{\text{mod}}\right) = 1$,
- It projects out the commutator of the modular Hamiltonian with anything else, i.e., $P_0\left([H_{\text{mod}}, X_\xi]\right) = 0$, for any vector field $\xi(z)$.

We emphasize that this is a different projection operator than the one considered in Section 3.3, in particular it is finite rather than a delta function.

There are several different choices that obey both of these properties:

$$P_0^{(1)}(X_\xi) \equiv -\frac{1}{\pi^2}\int_{|z+i\epsilon|=1} \frac{\xi(z)}{(1+z^2)^2}\, dz \ , \tag{C.26}$$

$$P_0^{(2)}(X_\xi) \equiv \frac{1}{\pi^2}\int_{|z-i\epsilon|=1} \frac{\xi(z)}{(1+z^2)^2}\, dz \ , \tag{C.27}$$

$$P_0^{(3)}(X_\xi) \equiv \frac{1}{2}\left(P_0^{(1)}(X_\xi) + P_0^{(2)}(X_\xi)\right) \ . \tag{C.28}$$

By explicitly computing the residues, one can express these in terms of the diffeomorphism ξ and its derivative evaluated at the endpoints of the interval as

$$P_0^{(1)}(X_\xi) = \frac{1}{2\pi}\left[\xi(-i) + i\xi'(-i)\right] \ , \tag{C.29}$$

$$P_0^{(2)}(X_\xi) = \frac{1}{2\pi}\left[\xi(i) - i\xi'(i)\right] \ , \tag{C.30}$$

$$P_0^{(3)}(X_\xi) = \frac{1}{4\pi}\left[i\,\xi'(-i) - i\,\xi'(i) + \xi(-i) + \xi(i)\right] \ . \tag{C.31}$$

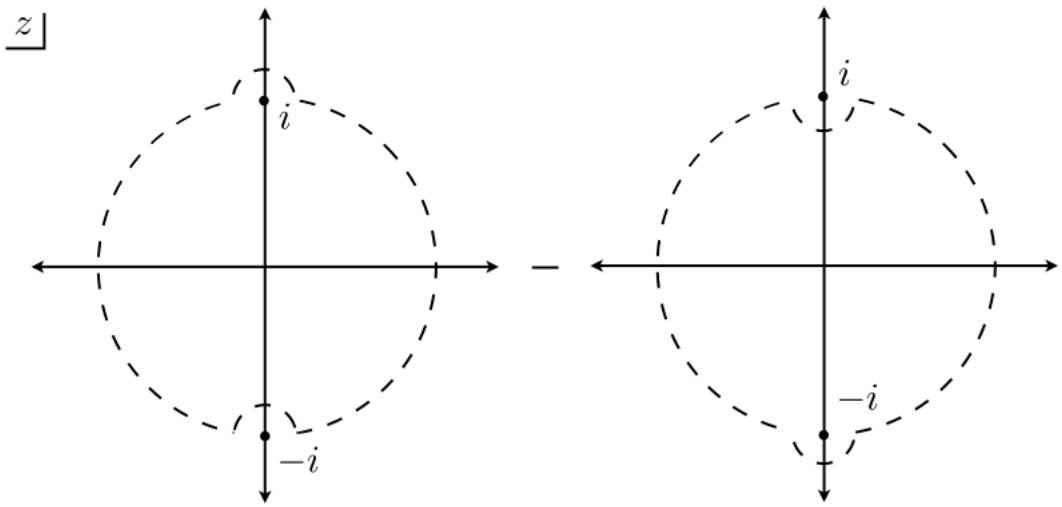

Figure C.1: One simple choice of linear functional, constructed from the difference of $|z - i\epsilon| = 1$ and $|z + i\epsilon| = 1$ contours. When considering a non-restricted set of generators, there is an ambiguity in the choice of projection. For instance, it is also possible to choose either of these contours separately (but not their sum) and still satisfy the required properties for the linear functional. This ambiguity is tied to the fact that the adjoint action is not diagonalizable over the Virasoro algebra.

Note that the sum of contours $P_0^{(2)} - P_0^{(1)}$ does not satisfy the required properties, as it vanishes on the modular Hamiltonian. The difference of contours, Eqs. (C.28) and (C.31), is perhaps the most symmetrical choice. It can be seen to result from the decomposition, Eq. (C.4), by additionally imposing that the linear functional evaluated on the extra terms L_2, L_{-2} in the decomposition give zero. However, recall that this decomposition was not unique. A different choice would have resulted in a different linear functional, and therefore a different P_0.

Moreover, we have considered the possibility of defining a zero mode projector P_0 using very early or very late time modular flow. However, we found that this prescription is also ambiguous and depends on whether one considers very early or very late times.

It is also easy to see that this has a direct physical implication by leading to different results for the curvature. For instance, consider an infinitesimal diffeomorphism of the form

$$\theta \to \theta + 2\epsilon \sin(m\theta) \,, \tag{C.32}$$

where $m \in \mathbb{Z}$. The parameter ϵ is assumed to be small and dimensionless.

One can consider a parallel transport process consisting of a series of such infinitesimal transformations, where m can vary from step to step. It is described by a function $m(\lambda)$, where λ denotes the point along the path evaluated in the continuum limit.

Mapping from the cylinder to the plane using Eq. (C.32) and expanding to first order in ϵ, this sinusoidal perturbation becomes

$$\xi(z) = z + \epsilon(z^{m+1} - z^{-m+1}) + \mathcal{O}(\epsilon^2) \ . \tag{C.33}$$

Up to terms that are higher order in ϵ, Eq. (C.33) can be inverted to $z = \xi - \epsilon(\xi^{m+1} - \xi^{-m+1}) + \mathcal{O}(\epsilon^2)$. Inserting this in Eq. (3.3.9) for H_{mod}, we find the correction to the modular Hamiltonian:

$$H^{(1)} = \pi\left[(m+1)(L_{-m+1} + L_{m-1}) + (m-1)(L_{-m-1} + L_{m+1})\right] \ . \tag{C.34}$$

Recall that expanding both the parallel transport equation $H_{\text{mod}} = [S, H_{\text{mod}}]$ order by order in ϵ gave Eq. (3.3.41). Solving for the correction to the parallel transport operator gives

$$S^{(1)} = L_m - L_{-m} \ , S^{(0)} = 0 \ . \tag{C.35}$$

Take two transformations of the form Eq. (C.33) with different values for the integer m, say m_1 and m_2. This gives two different parallel transport operators, S_1 and S_2. To compute the curvature, Eq. (3.3.3), we are interested in computing the commutator

$$[S_1^{(1)} - \kappa_1 H^{(0)}, S_2^{(1)} - \kappa_2 H^{(0)}] \ , \tag{C.36}$$

where $\kappa_i = P_0(S_i)$, is the zero mode coefficient of the parallel transport operator S_i. We can split Eq. (C.36) into terms that we can treat separately. Notice that the term proportional to $[H^{(0)}, H^{(0)}]$ is zero and can be neglected. By definition, the projection operator vanishes on $[S_i^{(1)}, H^{(0)}]$, so this contribution to the curvature is zero. An explicit computation shows that

$$[S_1^{(1)}, S_2^{(1)}] = (m_1 - m_2)(L_{m_1+m_2} - L_{-m_1-m_2}) + (m_1 + m_2)(L_{-m_1+m_2} - L_{m_1-m_2}) \ . \tag{C.37}$$

We will now project onto the zero modes of each of the terms. This is where the ambiguity enters since the result depends on the choice of linear functional. We find

$$F^{(1)} = P_0^{(1)}([S_1^{(1)}, S_2^{(1)}]) = \frac{2i}{\pi}(m_2^2 - m_1^2)\sin\left(\frac{m_1\pi}{2}\right)\sin\left(\frac{m_2\pi}{2}\right) \ , \tag{C.38}$$

$$F^{(2)} = P_0^{(2)}([S_1^{(1)}, S_2^{(1)}]) = -F^{(1)} \ , \tag{C.39}$$

$$F^{(3)} = P_0^{(3)}([S_1^{(1)}, S_2^{(1)}]) = 0 \ . \tag{C.40}$$

Notice that in the case where the m_1, m_2 are even, all curvatures agree and in fact identically vanish. Indeed, it is possible to argue that the curvature defined in this way always vanishes for diffeomorphisms that vanish on the interval endpoint. However, in general they do not agree and the result is ambiguous.

4 Islands in FRW Cosmologies

4.1 Introduction

One of the long-standing puzzles in modern physics is the black hole information paradox. Its essence can be captured by examining the entropy of the sub-systems of an evaporating black hole. In Hawking's seminal calculation [5, 33], the fine-grained entropy of the radiation seemingly exceeds the Bekenstein-Hawking entropy of the black hole. This signifies information loss. In a unitary process, a pure state evolves into a pure state. Page showed [35] that initially the fine-grained entropy grows, following the Hawking curve, but approximately halfway through the evaporation process, it starts decreasing and eventually vanishes, which is consistent with unitary evolution. In a series of breakthrough papers [21–23,36,152,153], it was shown that the Page curve can be recovered within semiclassical gravity. The key to this advance was realizing that the fine-grained entropy of the radiation receives contributions from a disconnected region that lies in the gravitating system, namely, the island. The exact entropy of the radiation is given by the island formula

$$S(\mathbf{R}) = \min_I \Big\{ \operatorname*{ext}_I \Big[\frac{A(\partial I)}{4G_N} + S_{\rm mat}(R \cup I) \Big] \Big\} , \tag{4.1.1}$$

where $A(\partial I)$ is the area of the boundary of the island I, and $S_{\rm mat}(R \cup I)$ is the renormalized entropy of the quantum fields on the union of the regions R and I. The formula instructs us to extremize and minimize over all possible islands. Before the evaporation begins, there are not any non-trivial islands and no Hawking pairs have been emitted. So, initially, the exact entropy of the radiation is

$$S(\mathbf{R}) \approx S_{\rm mat}(R) \, . \tag{4.1.2}$$

When the process starts, more and more Hawking partners escape from the black hole and (4.1.2) steadily grows. As the evaporation proceeds, a non-trivial island appears in the interior of the black hole. Its boundary is very close to the black hole horizon. Since it extends almost through the whole black hole interior, it

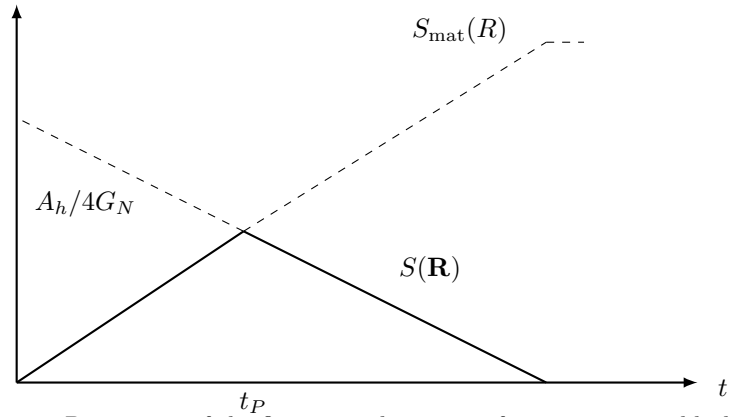

Figure 4.1: Page curve of the fine-grained entropy of an evaporating black hole.

contains most of the partners of the Hawking radiation that have escaped from the black hole. The partners contained in the island region purify the ones of the black hole, so the term $S_{\rm mat}(R \cup I)$ in (4.1.1) vanishes and the exact entropy of the radiation becomes

$$S(\mathbf{R}) \approx \frac{A(\partial I)}{4G_N}\,. \tag{4.1.3}$$

As the black hole horizon shrinks, (4.1.3) decreases and finally vanishes. Thus, the Page curve is followed and the black hole evaporation process is unitary (see Figure 4.1). Remarkably, the island formula (4.1.1) has been derived using the Euclidean path integral by applying the gravitational replica trick [15] (See [153] for a review). It was shown that after the Page time replica wormholes become dominant [23,36]. The island formula (4.1.1) is a generalization of Ryu-Takayanagi formula [13, 14, 16–18, 133] which has been extensively studied in the literature [154–168].

It is worth emphasizing once more that in [23,36] the Page curve was recovered in the context of semiclassical gravity. This leads one to ask whether islands exist in cosmological spacetimes, where we do not have AdS/CFT duality [169] to assist us. Moreover, since our universe has positive cosmological constant, it is natural to wonder whether or not we might be living in an island.

The first cosmological islands were found in [37]. The authors considered a setup where a radiation-dominated, flat Friedmann-Robertson-Walker (FRW) spacetime is entangled with a non-gravitating auxiliary system. They examined the cases with zero, positive and negative cosmological constant and concluded that islands appear only in the last case. The way they achieved this was by introducing three conditions that aid the search for islands. The beauty of these conditions is that they are independent of the radiation region R. Once a non-trivial island region is

found, it is natural to wonder where the information of the degrees of freedom in I is encoded. One possible way to answer this question is by introducing an auxiliary system that purifies the state of the system in I, for example preparing the whole state in a thermofield double like state. This process is however non-unique.

In this paper, we build upon the work of [37]. We extend their analysis to FRW universes with non-zero spatial curvature. We consider a state that is approximately thermal with inverse temperature β. We use the island conditions proposed in [37] along with an extra set of conditions that ensure our candidate islands are in the semiclassical regime. In regions of spacetime where all of the above are satisfied we conclude that islands can exist. Our main results are summarized below.

Summary of results: As was mentioned before, we study FRW cosmologies that are supported by radiation in a thermal state, cosmological constant and non-zero spatial curvature. In closed universes, with any type of cosmological constant, there is always an island that is the whole Cauchy slice. Additionally, when $\Lambda < 0$, for any spatial curvature, we find that there is a different type of candidate island region. These universes are recollapsing and have a time-symmetric slice. For $k > 0$ and $\Lambda < 0$, we find that there is a candidate island region in the middle of the Penrose diagram around the time-symmetric slice. This region is shown in Figure 4.9. For $k < 0$ and $\Lambda < 0$, we have a similar situation, i.e. a candidate island region around the time-symmetric slice, only this time it starts at a finite value of the radial coordinate and extends to infinity, as shown in Figure 4.12. This island is similar to the one found in [37] for $k = 0$ and $\Lambda < 0$. We conclude that the main element that allows for the existence of candidate island regions is a negative cosmological constant.

For the purpose of this study, we use both analytical and numerical methods. In order to have analytic control of the solution to the Friedmann equation, in all the universes that it is possible, we focus on the time-symmetric slice, where $a'(\eta)|_{\eta=\eta_0} = 0$. We study the solution, $a(\eta)|_{\eta=\eta_0} = a_0$, at the low and high temperature limits and find that for $\Lambda < 0$ islands appear only in the latter case, as the former is always in the non-semiclassical regime. In the high temperature limit, we see that a_0 does not have contributions from the curvature, i.e., to leading order it coincides with the solution of the flat radiation-dominated FRW universe evaluated at its time-symmetric slice. Hence, we conclude that at the turnaround time, in the high temperature limit, the spatial curvature is negligible. In order to support and complement our analytic calculations, we also "scan" the whole spacetime for candidate island regions numerically and provide multiple figures that show where the existence of islands is possible.

Outline: This chapter is organized as follows. We begin in Section 4.2 by intro-

ducing the setup and general framework. In Section 4.3 we review the analysis of the radiation-dominated, flat FRW universes done in [37]. In Sections 4.4 and 4.5, we explore the possibility of islands in radiation-dominated FRW cosmologies with positive and negative curvature respectively. Finally, in Section 4.6 we briefly summarize our results and discuss future directions.

Note added: While finishing this work, the paper [170] appeared on the arXiv which has some overlap with our results.

4.2 General framework

We are interested in finding candidate island regions in four dimensional FRW cosmologies. The metric in conformal coordinates is given by

$$ds^2 = a^2(\eta)\left(-d\eta^2 + d\chi^2 + S_k^2(\chi)d\Omega_2^2\right) \ , \quad S_k(\chi) := \begin{cases} R_0 \sinh(\chi/R_0) \ , & k=-1 \\ \chi \ , & k=0 \ , \\ R_0 \sin(\chi/R_0) \ , & k=1 \end{cases} \tag{4.2.1}$$

for open, flat, and closed universes, respectively. Here, R_0 is a fixed length scale and $a(\eta)$ is the scale factor. We assume that the state of the system is approximately thermal

$$\rho \approx \frac{1}{Z} e^{-\beta H} \ , \tag{4.2.2}$$

where $\beta = \beta_0 a(\eta)$ is the inverse temperature at conformal time η, and β_0 refers to the temperature in Minkowski spacetime. Given a subregion I on a particular Cauchy slice at time $\eta = \eta_0$, the matter entropy of the bulk fields enclosed in it is given by the thermal entropy

$$S_{\rm mat}(I) = s_{\rm th}\widetilde{V}(I) \ , \tag{4.2.3}$$

where $s_{\rm th}$ is the thermal entropy density, and $\widetilde{V}(I)$ is the comoving volume enclosed by I. For the metric (4.2.1), the comoving volume is

$$\widetilde{V}(I) = 4\pi \int_0^{\chi_I} d\chi \ S_k^2(\chi) \ . \tag{4.2.4}$$

We define the region G as the complement of region I in the gravitating system such that they share the same boundary, $\partial I = \partial G$. The entropy of matter fields enclosed by G is also extensive and is simply

$$S_{\rm mat}(G) = s_{\rm th}\left(\widetilde{V}_{\rm total} - \widetilde{V}(I)\right) \ , \tag{4.2.5}$$

where $\widetilde{V}_{\text{total}}$ is the total volume enclosing both regions G and I. We consider FRW cosmologies supported by radiation, spatial curvature, and cosmological constant. The radiation and entropy densities have the form

$$\rho_{\text{rad}} = \frac{c_{\text{th}} T_0^4}{a(\eta)^4} \quad \text{and} \quad s_{\text{th}} = \frac{3}{4} c_{\text{th}} T_0^3 \ , \tag{4.2.6}$$

respectively. Here, c_{th} is proportional to the number of degrees of freedom and T_0 is the temperature in Minkowski spacetime. The scale factor $a(\eta)$ is the solution to the Friedmann equation[1]

$$\frac{1}{a(\eta)^2}\left(\frac{a'(\eta)}{a(\eta)}\right)^2 = \frac{8\pi G_N}{3}\frac{c_{\text{th}} T_0^4}{a(\eta)^4} - \frac{k}{a(\eta)^2 R_0^2} + \frac{\Lambda}{3} \, . \tag{4.2.7}$$

We will apply the necessary island conditions for the existence of islands [37]. The explicit form of these three conditions in spacetimes arising from (4.2.1) are as follows

- The Bekenstein bound is violated:

$$\widehat{S}_{\text{mat}}(I) \gtrsim \frac{A(\partial I)}{4G_N} \ , \tag{4.2.8}$$

  where $\widehat{S}_{\text{mat}}$ is the finite part of the matter entropy and the wiggly inequality means that the subleading terms compared to right hand side are ignored. The derivation of this condition needs a careful treatment of UV divergences of the matter entropy [37]. In our case, the thermal entropy (4.2.3) represents the extensive part of $\widehat{S}_{\text{mat}}(I)$ and is finite.

- I is a quantum normal region:

$$(\pm\partial_\eta + \partial_\chi)\, S_{\text{gen}}(I) \geq 0 \ . \tag{4.2.9}$$

- G is a quantum normal region:

$$(\pm\partial_\eta - \partial_\chi)\, S_{\text{gen}}(G) \geq 0 \ . \tag{4.2.10}$$

Notice that in both conditions, we are using the null directions to deform the surfaces ∂I and ∂G with respect to the region I. For a closed universe, for example, the entire Cauchy slice always satisfies these three conditions.

Once an overlapping region is found in a FRW cosmology, we still need to be sure that they live in the semiclassical regime. In order to do so, we use the following semiclassical conditions:

[1]For the case of a negative cosmological constant, we will define a positive $\Lambda_0 > 0$ such that $\Lambda = -\Lambda_0$.

- The proper time to the singularity requires

$$\Delta\tau = \int_0^\eta d\eta\, a(\eta) \gg l_P \ . \tag{4.2.11}$$

- The thermal length scale should satisfy

$$\beta \gg l_P \ , \quad i.e., \quad \frac{a(\eta)}{T_0} \gg l_P \ . \tag{4.2.12}$$

- The energy density should satisfy

$$\rho_{\rm rad} = \frac{c_{\rm th} T_0^4}{a(\eta)^4} \ll M_P^4 \ . \tag{4.2.13}$$

- The size of the S^2 obeys

$$a(\eta) S_k(\chi) \gg l_P \ . \tag{4.2.14}$$

- The curvature radius requires

$$a(\eta) R_0 \gg l_P \ . \tag{4.2.15}$$

Let us emphasize that the island conditions together with the semiclassical conditions give a strong indication that an island exists in a given spacetime without making any reference to the radiation region R.

Consider the case when we find a candidate island region I, *i.e.,* , a region in spacetime that fulfills the above criteria. A natural question to ask is in which auxiliary system, R, is this region encoded? Following [37], one possible way to answer this question is by purifying the original thermal state with a second copy of Minkowski space and preparing the whole system in the thermofield double state (TFD) using the Euclidean path integral

$$|\beta_0\rangle = \frac{1}{\sqrt{Z}} \sum_n e^{-\beta_0 E_n} |n\rangle_1^* |n\rangle_2 \ . \tag{4.2.16}$$

This is of course a non-unique procedure. In this paper, we are agnostic about the radiation region R and focus more on the question of whether islands can exist in FRW cosmologies.

4.3 Flat slicing

In this section, we review the results of [37] for FRW cosmologies with flat slicing.

4.3.1 Zero cosmological constant

We first consider the case where the vacuum energy density is zero. The solution of the Friedmann equation (4.2.7) has the simple form. It is given by

$$a(\eta) = \sqrt{\frac{8\pi G_N c_{\text{th}} T_0^4}{3}}\eta \ . \tag{4.3.1}$$

Island conditions

For a spherical region I located at χ_I at time η_I, the Bekenstein bound is violated for

$$\frac{\chi_I}{\eta_I} \gtrsim \frac{3\pi}{2} T_0 \eta_I \ . \tag{4.3.2}$$

In order for region I to be quantum normal, the ingoing condition is true for values

$$\frac{\chi_I}{\eta_I} \geq \begin{cases} \frac{\pi T_0 \eta_I}{\pi T_0 \eta_I - 1} \ , & \pi T_0 \eta > 1 \\ 0 \ , & \pi T_0 \eta < 1 \ , \end{cases} \tag{4.3.3}$$

while the outgoing condition is always satisfied. The third condition implies that the outward part is true for

$$\frac{\chi_I}{\eta_I} \geq \frac{\pi T_0 \eta_I}{\pi T_0 \eta_I + 1} \ , \tag{4.3.4}$$

whereas the ingoing, for $\pi T_0 \eta < 1$, is satisfied when

$$\frac{\chi_I}{\eta_I} \geq \frac{\pi T_0 \eta_I}{1 - \pi T_0 \eta_I} \ . \tag{4.3.5}$$

There is an overlapping region where the three conditions are fulfilled for values of conformal time such that

$$T_0 \eta_I < \frac{1}{\pi} \ . \tag{4.3.6}$$

Semiclassical regime

Using the proper time condition (4.2.11), we find that we are in the semiclassical regime when

$$T_0 \eta_I \gg \frac{1}{c_{\text{th}}^{1/4}} \ , \tag{4.3.7}$$

which is in conflict with (4.3.6).

Conclusion

There is an overlapping region where all three island conditions are simultaneously satisfied and it is shown in teal in Figure 4.2. However, this region is outside of the semiclassical regime of validity. We conclude that we do not have islands in this universe.

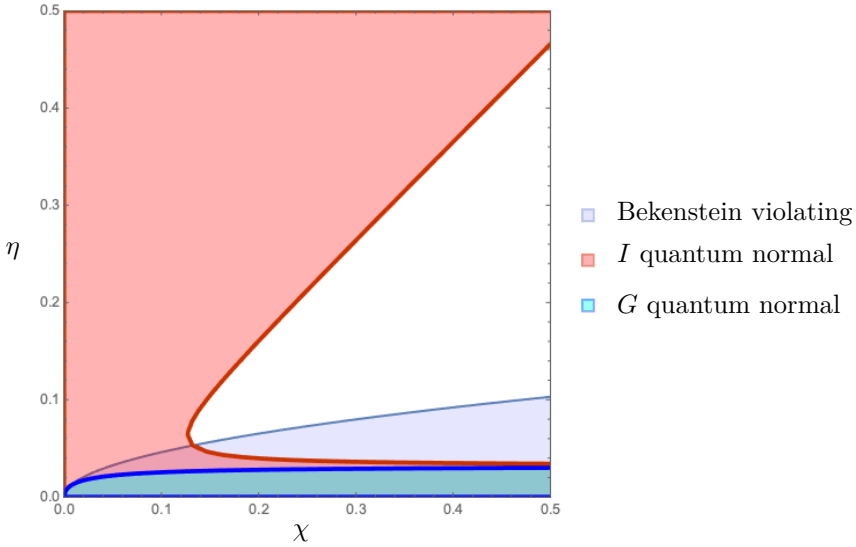

Figure 4.2: Regions where the three island conditions are satisfied. We chose the numeric values $k = 0$, $\Lambda = 0$, $c_{th} = 1$, $T_0 = 10$, and $G_N = 0.01$. There is an overlapping region close to $\eta \approx 0$. However, this region is outside of the semiclassical regime as it violates the proper time condition (4.2.11).

4.3.2 Positive cosmological constant

We proceed by turning on the cosmological constant and checking the three conditions. The Bekenstein bound is violated when

$$\chi_I \gtrsim \frac{3a(\eta)^2}{4Gs_{\text{th}}} \ . \tag{4.3.8}$$

The region I should be quantum normal. The outgoing condition is always satisfied while the ingoing condition requires

$$\chi_I \leq a(\eta)/a'(\eta). \tag{4.3.9}$$

The G quantum normal condition implies

$$a(\eta)(\pm a'(\eta)\chi_I - a(\eta)) + 2G_N s_{\text{th}}\chi_I \geq 0 \ . \tag{4.3.10}$$

Similarly as before, the overlap occurs outside of the semiclassical region. This part of the geometry is depicted in teal in Figure 4.3.

4.3.3 Negative cosmological constant

Finally, we consider the case with negative cosmological constant. There is a recollapsing FRW universe as a solution to the Friedmann equation (4.2.7). Importantly, a new ingredient of this cosmology is the existence of a time-symmetric

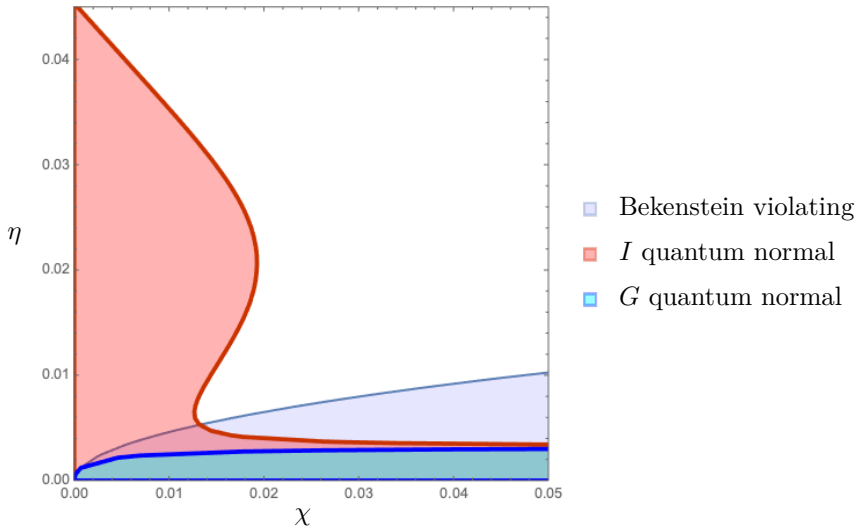

Figure 4.3: Regions where the three island conditions are satisfied. We chose the numeric values $k = 0$, $c_{th} = 1$, $T_0 = 100$, and $\Lambda_0 G_N = 0.01$. There is an overlapping region close to $\eta \approx 0$ where the proper time condition (4.2.11) is not satisfied.

slice. By solving (4.2.7) at the time $\eta = \eta_0$ such that $a'(\eta_0) = 0$, we get

$$a_0 = \left(\frac{8\pi G_N c_{\text{th}} T_0^4}{\Lambda_0} \right)^{\frac{1}{4}} . \tag{4.3.11}$$

Island conditions

At this particular time the Bekenstein bound is violated for values

$$\chi_I \gtrsim \frac{9}{4T_0} \left(\frac{\pi}{2c_{\text{th}} \Lambda_0 G_N} \right)^{1/2} . \tag{4.3.12}$$

The ingoing and outgoing quantum normal conditions for region I are reduced to one condition

$$\partial_\chi S_{\text{gen}}(I) \geq 0 \, , \tag{4.3.13}$$

which is always satisfied in this case. Similarly, the G quantum normal condition becomes

$$-\partial_\chi S_{\text{gen}}(G) \geq 0 \implies \chi_I \geq \frac{3}{2T_0} \left(\frac{\pi}{2c_{\text{th}} \Lambda_0 G_N} \right)^{1/2} , \tag{4.3.14}$$

which is approximately the same result as the one we get from the first condition. Hence, there is triple overlap when (4.3.12) is fulfilled.

Semiclassical regime

We still have to check that these regions, along the time-symmetric slice, are in the semiclassical regime. The thermal length (4.2.12) and energy density (4.2.13) conditions imply $\Lambda_0 G_N \ll 1$. From (4.2.14), the size of the region has to be

$$T_0 \chi_I \gg \left(\frac{\Lambda_0 G_N}{c_{\rm th}}\right)^{1/4} , \tag{4.3.15}$$

which is a less restrictive condition than (4.3.12). The curvature radius condition (4.2.15) gives

$$T_0 R_0 \gg \left(\frac{\Lambda_0 G_N}{c_{\rm th}}\right)^{1/4} . \tag{4.3.16}$$

All of the semiclassical conditions are satisfied and compatible with the island conditions in the overlapping region (4.3.12).

Conclusion

We conclude that there is an island region in the semiclassical regime for values that satisfy (4.3.12). This region is shown in green in Figure 4.4 together with the island conditions in the whole spacetime.

4.4 Positive curvature

4.4.1 Zero cosmological constant

We first consider the case where the vacuum energy density is vanishing and the FRW cosmology is supported by radiation and positive curvature. Without loss of generality, we can fix $k = 1$. In these coordinates, $\chi \in [0, \pi R_0]$ is one of the angles that parametrize the $\mathcal{S}^3$. Solving (4.2.7), gives a scaling factor of the form

$$a(\eta) = \left(\frac{8\pi G_N R_0^2 c_{\rm th} T_0^4}{3}\right)^{1/2} \sin\left(\frac{\eta}{R_0}\right) . \tag{4.4.1}$$

Island conditions

In order to look for island regions in this cosmology, we impose the three conditions to the region I located at $\chi = \chi_I$ and $\eta = \eta_I$. The Bekenstein bound has the form

$$2\chi_I - R_0 \sin\left(\frac{2\chi_I}{R_0}\right) \gtrsim \frac{a(\eta_I)^2}{s_{\rm th} G_N} \sin^2\left(\frac{\chi_I}{R_0}\right) . \tag{4.4.2}$$

In this equation we are basically comparing the comoving volume of the $\mathcal{S}^3$, with the area term $A(\partial I)/4G_N$. A natural place to look for island regions is the point

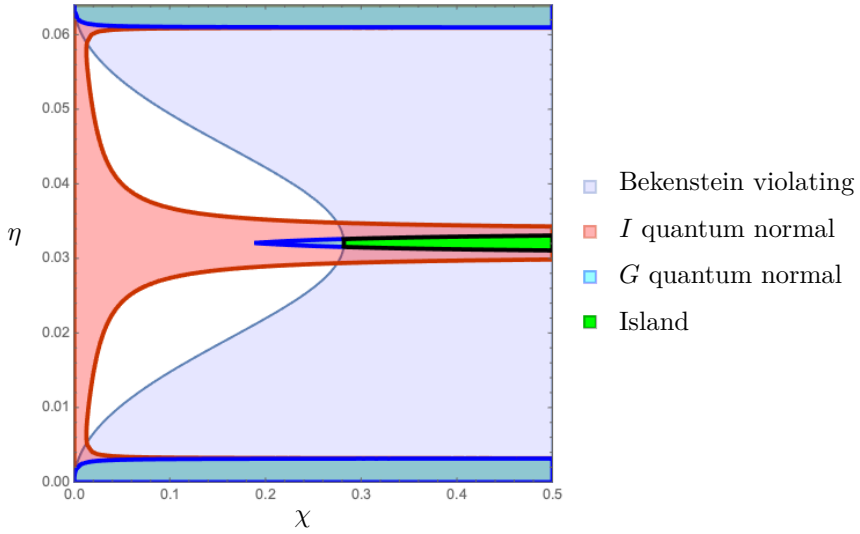

Figure 4.4: Regions where the three island conditions are satisfied. We chose the numeric values, $k = 0$, $c_{\rm th} = 1$, $T_0 = 10$, and $\Lambda G_N = -0.01$. We see that all conditions are simultaneously satisfied starting from the value $\chi_I = 3a_0^2/4G_N s_{\rm th}$. The island region is depicted in green. There are also overlapping regions at times where the solution $a(\eta)$ recollapses. However, they lie outside the semiclassical regime of validity given by the proper time condition (4.2.11).

where the volume is maximum and the area is very small. In fact, the $\mathcal{S}^3$ acquires its maximum size at $\chi_I = \pi R_0$. Close to this particular value (4.4.2) becomes

$$\delta^2 \lesssim \frac{R_0}{T_0} \frac{1}{\sin\left(\frac{\eta_I}{R_0}\right)^2} \ , \quad \delta := \pi R_0 - \chi_I \ . \tag{4.4.3}$$

Going to small times, $\eta_I/R_0 \ll 1$, so that the area term shrinks, we get

$$\left(\frac{\delta}{R_0}\right)^2 \lesssim \frac{R_0}{T_0 \eta_I^2} \ . \tag{4.4.4}$$

Imposing that I and G should be quantum normal results in

$$T_0 \eta_I \leq \frac{1}{\pi} \ . \tag{4.4.5}$$

This region, however, is non-semiclassical. We can see this by computing the proper time to the singularity and the thermal length. Both (4.2.11) and (4.2.12) are valid when

$$T_0 \eta_I \gg 1 \ , \tag{4.4.6}$$

which is clearly in conflict with (4.4.5).

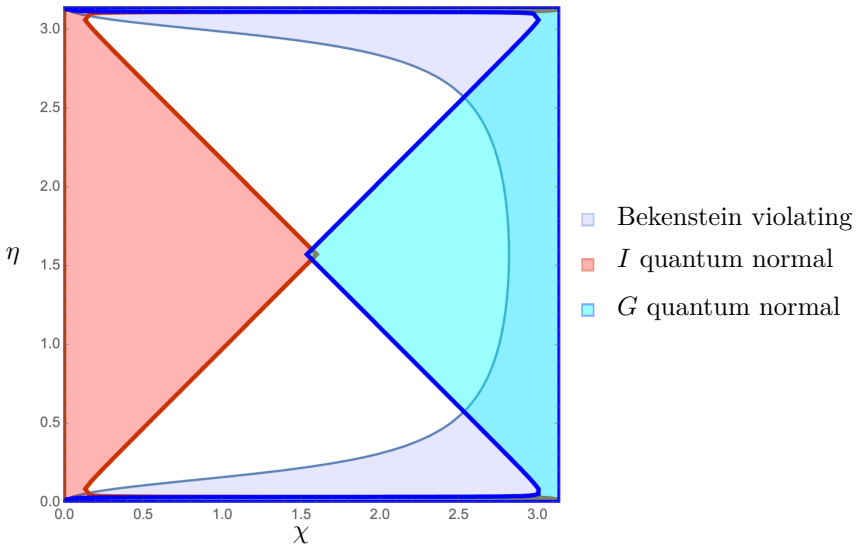

Figure 4.5: Regions where the three conditions are satisfied. We chose the numeric values $k = 1$, $\Lambda = 0$, $c_{th} = 1$ and $R_0 T_0 = 10$ and $G_N = 0.01$. There are overlapping regions close to the singularities, which are outside the semiclassical regime given by the proper time condition (4.2.11).

Therefore, there are no island regions close to the singularities located at $\eta_I \approx 0$ and $\eta_I \approx \pi$, and the place where the area term shrinks $\chi_I \approx \pi R_0$. We now proceed to analyze the time-symmetric slice. At $\eta_I = \pi R_0/2$, the scale factor is

$$a_0 = \sqrt{\frac{8\pi c_{\rm th} G_N}{3}} R_0 T_0^2 \ . \tag{4.4.7}$$

Let us examine again the region close to $\chi_I = \pi R_0$. Expanding (4.4.2), we obtain

$$\left(\frac{\delta}{R_0}\right)^2 \lesssim \frac{1}{R_0 T_0} \ . \tag{4.4.8}$$

For I to be quantum normal, we have

$$\frac{\delta}{R_0} \geq \pi R_0 T_0 \ , \tag{4.4.9}$$

while the condition for region G is always satisfied. We see that the three conditions are simultaneously true in the regime where $R_0 T_0 < 1$.

Semiclassical regime

The semiclassical conditions for the thermal length (4.2.12) and the energy density (4.2.13) are satisfied for large values of the temperature

$$R_0 T_0 \gg 1 \ . \tag{4.4.10}$$

In this limit, the island conditions do not overlap and therefore there is no finite-size island at the time-symmetric slice. In Figure 4.5, we show the regions where the three conditions are valid in the semiclassical regime. As the temperature decreases into non-semiclassical values, the Bekenstein violating region progressively covers half of the spacetime, creating a triple overlap in the middle of the Penrose diagram. Moreover, there are overlapping regions close to the singularities outside the scope of the semiclassical analysis.

Conclusion

The only possible island is the the entire Cauchy slice.

4.4.2 Positive cosmological constant

As a warm-up example, we first neglect the density of radiation. This cosmology then corresponds to the thermal state in de Sitter space. Here, it is convenient to translate everything to the de Sitter radius $\ell_{\rm dS}$. In four dimensions, we have

$$\ell_{\rm dS} = \sqrt{\frac{3}{\Lambda_0}} \ . \tag{4.4.11}$$

The Friedmann equation (4.2.7) reads

$$\frac{1}{a(\eta)^2}\left(\frac{a'(\eta)}{a(\eta)}\right)^2 + \frac{1}{a(\eta)^2\ell_{\rm dS}^2} - \frac{\Lambda_0}{3} = 0 \ , \tag{4.4.12}$$

and the solution is found to be

$$a(\eta) = \frac{1}{\cos\left(\frac{\eta}{\ell_{\rm dS}}\right)} \ . \tag{4.4.13}$$

Island conditions

We now check the three necessary conditions. We restrict to the time-symmetric slice, where $a_0 = 1$. Here, the entropy density has the form $s_{\rm th} = 1/\ell_{\rm dS}^3$. The Bekenstein bound then is

$$\frac{\pi}{G_N}\sin^2\left(\frac{\chi_I}{\ell_{\rm dS}}\right) \lesssim \frac{1}{\ell_{\rm dS}^3}\left(2\chi_I - \ell_{\rm dS}\sin\left(\frac{2\chi_I}{\ell_{\rm dS}}\right)\right) \ . \tag{4.4.14}$$

We notice that the first condition is satisfied at $\chi_I = \pi R_0$. If we expand close to that point, (4.4.14) gives

$$\delta^2 \lesssim G_N \ , \quad \delta := \pi R_0 - \chi_I \ . \tag{4.4.15}$$

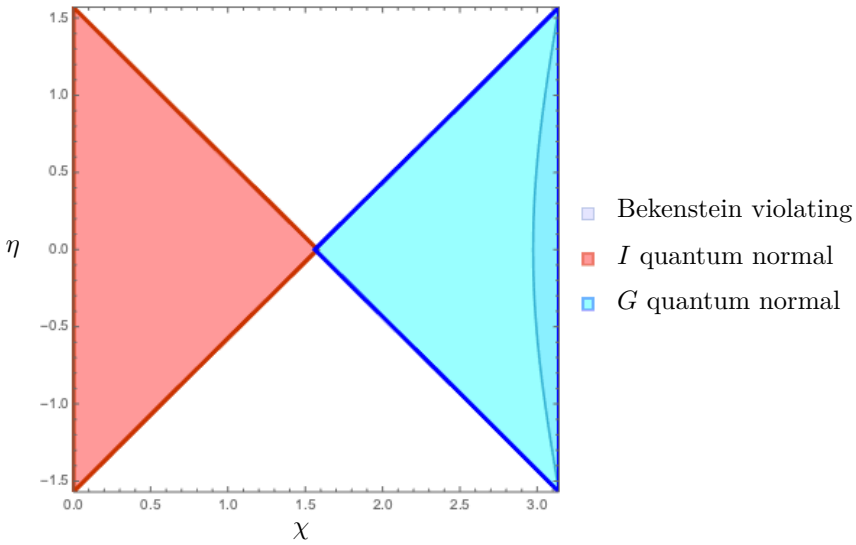

Figure 4.6: Regions where the three conditions are satisfied. The numeric values are chosen to be $k = 1$, $c_{th} = 1$, $\Lambda_0 G_N = 0.01$. There are no non-trivial island regions in thermal dS_4.

This means that in order to satisfy the first island condition we have to go to the distance that is smaller than l_P away from $\chi_I = \pi R_0$. Therefore, there are no islands smaller than the full Cauchy slice in the thermal dS_4. However, for completeness we continue the analysis. We consider the second condition which leads to

$$\delta \geq \frac{\ell_{dS}^3}{G_N} \ . \tag{4.4.16}$$

The third condition is always satisfied. In Figure 4.6, we show the three islands conditions in the semiclassical regime. We see that there are no overlapping regions.

Conclusion

The only possible island is the entire Cauchy slice.

Adding radiation

We now add radiation. We focus on the time-symmetric slice where (4.2.7) takes the form

$$-\frac{8\pi G_N c_{\rm th} T_0^4}{3a(\eta_0)^4} + \frac{1}{a(\eta_0)^2 R_0^2} - \frac{\Lambda_0}{3} = 0 \ . \tag{4.4.17}$$

By solving (4.4.17) we obtain

$$a_0 = \sqrt{\frac{3 \pm \sqrt{9 - 32\pi c_{\rm th}\Lambda_0 G_N R_0^4 T_0^4}}{2R_0^2\Lambda_0}} \ . \tag{4.4.18}$$

In order for this cosmology to have a time-symmetric solution, the following bound must be satisfied

$$c_{\rm th}\Lambda_0 G_N (R_0 T_0)^4 \leq \frac{9}{32\pi} \ . \tag{4.4.19}$$

It is obvious that it is not possible to go to the high temperature limit since that would lead to a negative argument under the root in (4.4.18). So, we focus on the low temperature limit.

Low temperatures

In the low temperature limit,

$$R_0 T_0 \ll \frac{1}{(\Lambda_0 G_N)^{1/4}} \ , \tag{4.4.20}$$

there are two possible values for the scale factor, *i.e.,* , $a_0 \approx 1/R_0\sqrt{\Lambda_0}$ and $a_0 \approx c_{\rm th} G_N^{1/2} R_0 T_0^2$. The latter is Planckian, so we do not explore this case further. The former represents the limit where the radiation becomes almost negligible and we check the island conditions below.

Island conditions

For scale factor equal to $a_0 \approx 1/R_0\sqrt{\Lambda_0}$, we look for island regions other than the full Cauchy slice close to $\chi = \pi R_0$. As we explained before, in a closed universe, this is the region where the probability of violating the Bekenstein bound is the highest, since that is where the volume has its maximum value and the area its minimum. The Bekenstein bound close to $\chi_I = \pi R_0$ leads to

$$\left(\frac{\delta}{R_0}\right)^2 \lesssim \frac{8\pi}{9} c_{\rm th} (R_0 T_0)^3 \Lambda_0 G_N \ . \tag{4.4.21}$$

Next, we consider the quantum normal condition for region I, which gives

$$\frac{\delta}{R_0} \geq \frac{1}{c_{\rm th}(R_0 T_0)^3 \Lambda_0 G_N} \ . \tag{4.4.22}$$

The third condition is always satisfied. Consequently, there is triple overlap when

$$R_0 T_0 \gtrsim \frac{1}{(c_{\rm th}\Lambda_0 G_N)^{1/3}} \ . \tag{4.4.23}$$

However, (4.4.23) together with (4.4.20) imply $\Lambda_0 G_N \gg 1$. The overlapping region is therefore outside the semiclassical regime.

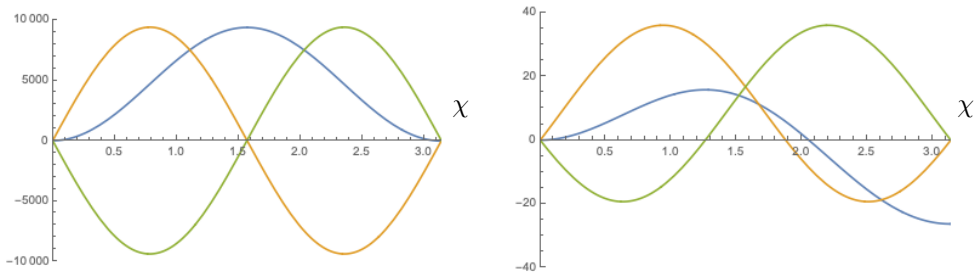

Figure 4.7: Three island conditions in the semiclassical regime for the two physical roots in (4.4.18). The Bekenstein condition, $A(\partial I)/4G_N - s_{\rm th}\widetilde{V}(I)$, is shown in blue, I quantum normal condition in yellow and G quantum normal condition in green. We chose the numeric values $k = 1$, $c_{\rm th} = 1$, $R_0T_0 = 1$, and $\Lambda_0 G_N = 0.001$. (Left) The Bekenstein bound is never satisfied, as $A(\partial I)/4G_N - s_{\rm th}\widetilde{V}(I)$ is always positive. (Right) Bekenstein and G conditions are both satisfied close to $\chi \approx \pi R$. In all cases, the I and G quantum normal conditions are mutually exclusive. The three islands conditions are never satisfied.

Semiclassical regime

For semiclassical spacetimes, we know that $\Lambda_0 G_N \ll 1$, as can be easily seen from (4.2.15). In Figure 4.7, we show three island conditions in the semiclassical limit. We see that for the two physical roots in (4.4.18) the island conditions are never simultaneously satisfied.

Conclusion

The only possible island is the entire Cauchy slice.

4.4.3 Negative cosmological constant

We now turn to the case where $\Lambda = -\Lambda_0$, with $\Lambda_0 > 0$. At the time-symmetric slice (4.2.7) reduces to

$$-\frac{8\pi G_N c_{\rm th} T_0^4}{3a(\eta_0)^4} + \frac{1}{a(\eta_0)^2 R_0^2} + \frac{\Lambda_0}{3} = 0\ . \tag{4.4.24}$$

At this time, the scale factor acquires the value

$$a_0 = \frac{1}{R_0\sqrt{2\Lambda_0}}\sqrt{-3 + \sqrt{9 + 32\pi c_{\rm th} G_N R_0^4 T_0^4 \Lambda_0}}\ . \tag{4.4.25}$$

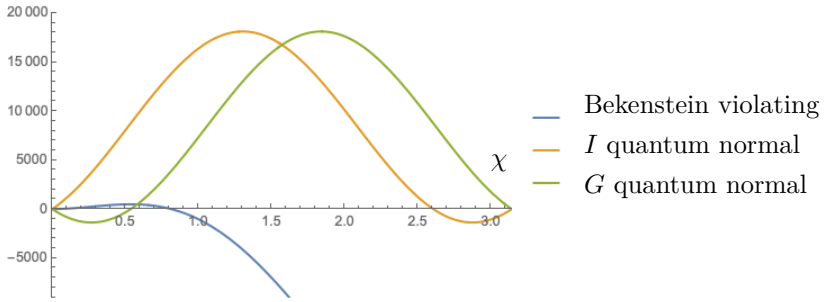

Figure 4.8: Three island conditions in the semiclassical regime along the time-symmetric slice. We use the scale factor (4.4.28). The Bekenstein condition shown is $A(\partial I)/4G_N - s_{th}\widetilde{V}(I)$, which is satisfied when this quantity is negative. We chose the numeric values $k = 1$, $c_{\rm th} = 1$, $R_0T_0 = 10$, and $\Lambda_0 G_N = 0.1$. The three islands conditions are satisfied in the overlapping region 2δ around the value $\chi_I = \pi R_0/2$.

In the small temperature limit, $R_0T_0 \ll 1/(\Lambda_0 G_N)^{1/4}$, (4.4.25) takes the form

$$a_0 \approx \sqrt{\frac{8\pi c_{th} G_N}{3}} R_0 T_0^2 \ . \tag{4.4.26}$$

This is effectively the limit where the vacuum energy density is negligible and coincides with the analysis in Section 4.4.1 where there are no island regions.

High temperatures

We now analyze the high temperature limit

$$R_0T_0 \gg 1/(\Lambda_0 G_N)^{1/4} \ . \tag{4.4.27}$$

Here, (4.4.25) becomes

$$a_0 \approx \left(\frac{8\pi c_{\rm th} G_N T_0^4}{\Lambda_0}\right)^{1/4} \ . \tag{4.4.28}$$

Importantly, in this limit the curvature contribution is negligible since the scale factor coincides with (4.3.11). Naively, one might think that the best place to look for islands is where the volume is maximal as in the spatially flat case. However, for a closed universe, regions close to $\chi_I = \pi R_0/2$ are in fact anti-normal.

Island conditions

It turns out that the best place to look for islands is at the middle of the $\mathcal{S}^3$ in the direction of χ, *i.e.*, , $\chi_I = \pi R_0/2$. Let us first take values of χ_I such that $0 < \pi/2 - \chi_I/R_0 \ll 1$. For high temperatures, the Bekenstein bound reduces to the condition

$$\frac{\delta}{R_0} \lesssim \frac{\pi}{4} - \frac{3}{8}\frac{1}{\sqrt{\pi c_{\rm th}\Lambda_0 G_N}}\frac{1}{R_0T_0} \ , \quad \delta := \frac{\pi R_0}{2} - \chi_I \ . \tag{4.4.29}$$

The G quantum normal condition to first order implies

$$\frac{\delta}{R_0} \leq \frac{2}{3}\sqrt{\frac{2c_{\rm th}\Lambda_0 G_N}{\pi}} R_0 T_0 \ , \tag{4.4.30}$$

while the condition for I quantum normal is always satisfied. We see that both (4.4.29) and (4.4.30) are satisfied when

$$R_0 T_0 > \frac{1}{\sqrt{c_{\rm th}\Lambda_0 G_N}} \ . \tag{4.4.31}$$

This regime of parameters, where the three island conditions are satisfied, is consistent with the high temperature limit (4.4.27).

Semiclassical regime

We proceed to determine if the overlapping region is in the semiclassical regime. The condition for the proper time (4.2.11) is valid for times $T_0\eta_I \gg (G_N\Lambda_0)^{1/4}$. The conditions (4.2.12) and (4.2.13) are satisfied when $\Lambda_0 G_N \ll 1$. The curvature condition (4.2.15) implies $R_0 T_0 \gg (G_N\Lambda_0)^{1/4}$. Finally, the sphere size condition (4.2.14), to leading order in the separation δ, has the following form

$$R_0 T_0 \gg \left(\frac{\Lambda_0 G_N}{8\pi c_{\rm th}}\right)^{1/4} + \frac{1}{2}\left(\frac{\Lambda_0 G_N}{8\pi c_{\rm th}}\right)^{1/4}\left(\frac{\delta}{R_0}\right)^2 + \dots \ . \tag{4.4.32}$$

We see that all these conditions are compatible with (4.4.31) in the high temperature limit (4.4.27). We present the three island conditions in Figure 4.8 for the time-symmetric slice.

Conclusion

There is a semi-classical region at the time-symmetric slice and around the half-sphere point, $\chi_I = \pi R_0/2$, where the three island conditions are satisfied. Therefore, an island region appears when (4.4.31) is satisfied together with $R_0 T_0 \gg 1$ and $\Lambda_0 G_N \ll 1$. A similar analysis follows for the values $\pi/2 - \chi_I/R_0 < 0$. In fact, there is a symmetric island region with respect to the half-sphere location. These regions are depicted in Figure 4.9.

4.5 Negative curvature

4.5.1 Zero or positive cosmological constant

These types of universes do not admit recollapsing solutions where $a'(\eta)|_{\eta=\eta_0} = 0$. Both of them expand forever.

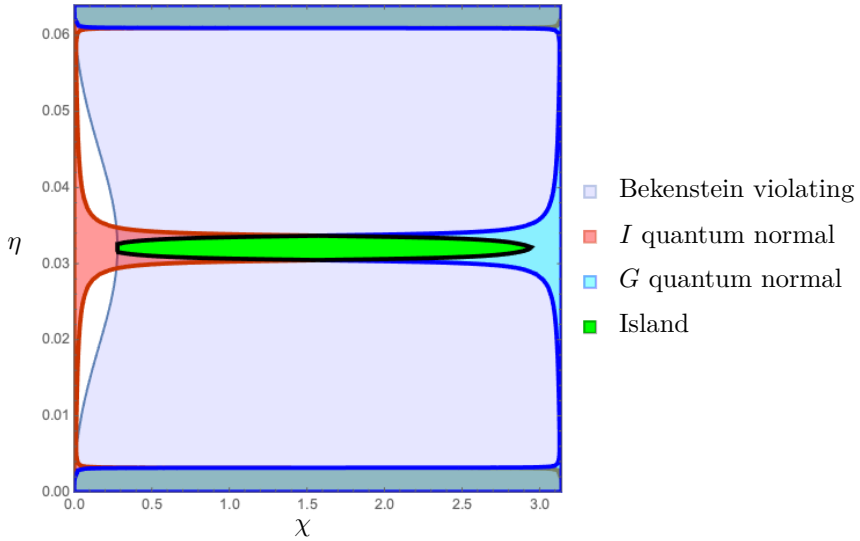

Figure 4.9: Regions where the three island conditions are satisfied in the semiclassical regime for a closed FRW cosmology. We chose the numeric values $k = 1$, $c_{\text{th}} = 1$ and $R_0 T_0 = 100$ and $\Lambda_0 G_N = 0.01$. There is an island region along the time-symmetric slice and around $\chi_I = \pi R_0/2$. There are also overlapping regions at times where the solution $a(\eta)$ recollapses. However, they lie outside the semiclassical regime.

4.5.2 Negative cosmological constant

We take the values $k = -1$ and $\Lambda = -\Lambda_0$. When we focus on the time-symmetric slice, (4.2.7) simplifies to

$$-\frac{8\pi G_N \epsilon_0}{3a(\eta_0)^4} - \frac{1}{a(\eta_0)^2 R_0^2} + \frac{\Lambda_0}{3} = 0 \ . \tag{4.5.1}$$

Then the scale factor is

$$a_0 = \frac{1}{R_0\sqrt{2\Lambda_0}}\sqrt{3 + \sqrt{9 + 32\pi c_{\text{th}} \Lambda_0 G_N R^4 T_0^4}} \ . \tag{4.5.2}$$

Low temperatures

First, in the low temperature limit $R_0 T_0 \ll 1/\left(c_{\text{th}} G_N \Lambda_0\right)^{1/4}$, (4.5.2) becomes

$$a_0 \approx \frac{1}{R_0}\sqrt{\frac{3}{\Lambda_0}} \ . \tag{4.5.3}$$

We do not expect to find islands in this case, as this limit corresponds to having almost no radiation. In fact, when we analytically check the first condition, we

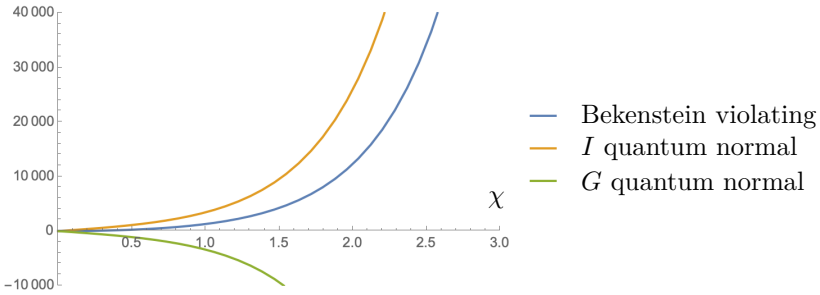

Figure 4.10: Three island conditions in the semiclassical regime along the time-symmetric slice in the low temperature limit. We use the scale factor in (4.5.3). The Bekenstein condition shown is given by $A(\partial I)/4G_N - s_{\rm th}\widetilde{V}(I)$, which is satisfied when this quantity is negative. We chose the numeric values $k = -1$, $c_{th} = 1$, $R_0T_0 = 1$, and $\Lambda_0 G_N = 0.01$. The I quantum normal condition is always valid. The G condition is never satisfed. The Bekenstein bound is never violated.

end up in contradictions. Using (4.5.3) for large values of $\chi/R_0 \gg 1$, we find that in order to violate the Bekenstein bound, we need

$$R_0T_0 \gtrsim \frac{1}{(c_{\rm th}G_N\Lambda_0)^{1/3}} \ , \tag{4.5.4}$$

which is very large in the semiclassical regime. However, our initial assumption was that the temperature is very low. Similarly, for small values of $\chi_I/R \ll 1$, we find that the same condition (4.2.8) requires

$$\frac{\chi_I}{R_0} \gtrsim \frac{1}{(R_0T_0)^3 G\Lambda_0} \ , \tag{4.5.5}$$

which together with the small temperature limit imply that $\chi_I/R_0 \gg 1/(c_{\rm th}G_N\Lambda_0)^{1/4}$ outside of the regime of validity. Hence, the first condition is never satisfied and consequently it is not possible to have islands. In Figure 4.10, we show the three conditions in the small temperature limit.

High temperatures

We now look at the high temperature limit $R_0T_0 \gg 1/\left(c_{\rm th}G_N\Lambda_0\right)^{1/4}$. Here, (4.5.2) takes the form

$$a_0 = \left(\frac{8\pi G_N c_{th} T_0^4}{\Lambda_0}\right)^{1/4} \ , \tag{4.5.6}$$

which corresponds to having negligible curvature at the turnaround time.

Island conditions

For small $\chi_I/R_0 \ll 1$, we find for the Bekenstein bound

$$\frac{\chi_I}{R_0} \gtrsim \frac{9}{4R_0T_0}\left(\frac{\pi}{2c_{\rm th}\Lambda_0 G_N}\right)^{1/2} . \tag{4.5.7}$$

For large $\chi_I/R_0 \gg 1$, we get

$$R_0T_0 \gtrsim \frac{3}{2}\left(\frac{\pi}{2c_{\rm th}G_N\Lambda_0}\right)^{1/2} . \tag{4.5.8}$$

The second condition that requires I to be quantum normal is always satisfied at the time-symmetric slice, and the third results to the same inequalities up to small order one numbers as the first condition. Therefore, there is an overlapping region when (4.5.7) is valid.

Semiclassical regime

We also check that the semiclassical conditions at the time-symmetric slice are satisfied. The conditions for the thermal length (4.2.12) and energy density (4.2.13) are obeyed for $G_N\Lambda_0 \ll 1$, which are true for reasonable spacetimes. Moreover, we require that the size of the $\mathcal{S}^2$ sphere is bigger than the Planck length. For large $\chi/R_0 \gg 1$ the condition is automatically satisfied. For small $\chi/R_0 \ll 1$, we have

$$\frac{\chi}{R_0} \gg \frac{1}{R_0T_0}\left(\frac{G_N\Lambda_0}{c_{\rm th}}\right)^{1/4} , \tag{4.5.9}$$

which is compatible with (4.5.7). Finally, we check the radius of curvature condition (4.2.15)

$$R_0T_0 \gg \left(\frac{G_N\Lambda_0}{c_{\rm th}}\right)^{1/4} , \tag{4.5.10}$$

which is again compatible with (4.5.8). Therefore, when we combine all the conditions, we get an elongated teardrop region, (4.5.7). In Figure 4.11, we show three island conditions in the semiclassical limit.

Conclusion

There is a semiclassical region at the time-symmetric slice where the three island conditions are satisfied. Therefore, the existence of islands is possible for the values in (4.5.8) together with $R_0T_0 \gg 1$, and $\Lambda_0 G_N \ll 1$. This region is shown in green in Figure 4.12.

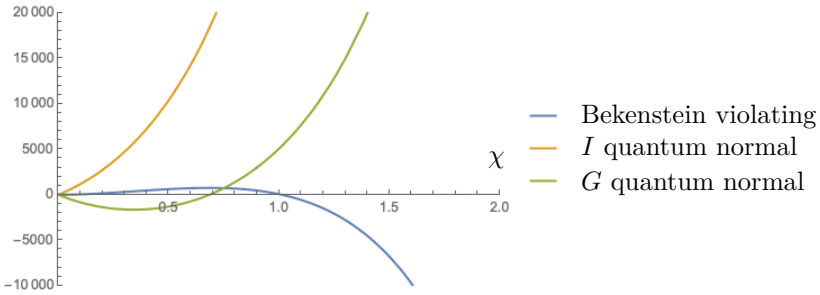

Figure 4.11: Three island conditions in the semiclassical regime along the time-symmetric slice in the high temperature limit. We use the scale factor in (4.5.6). The Bekenstein condition shown is given by $A(\partial I)/4G_N - s_{\rm th}\widetilde{V}(I)$, which is satisfied when this quantity is negative. We chose the numeric values $k = -1$, $c_{\rm th} = 1$, $R_0T_0 = 10$, and $\Lambda_0 G_N = 0.1$. The I quantum normal condition is always valid. The three island conditions are satisfied for values in (4.5.7).

4.6 Discussion

In this paper, we studied the possible existence of islands in FRW cosmologies supported by radiation, curvature, and cosmological constant. To this end, we applied the three necessary conditions to subregions of the spacetime I and G, together with the semiclassical conditions introduced in Section 4.2. We found that the key element for the existence of non-trivial islands is a negative cosmological constant. In the case of a closed universe, there is an island region around the half-sphere point located at $\chi_I = \pi R_0/2$. This island is finite in size and is qualitatively different from the island found in [37]. For open universes, an island region shows up for large enough radius and extends all the way to infinity. By studying the spacetime at the time-symmetric slice, we provided analytic evidence for the existence of these islands in the high temperature limit where the spatial curvature is negligible. We also performed a numerical analysis in the entire spacetime.

It turns out that having an FRW cosmology with a time-symmetric slice is not sufficient for the existence of islands smaller than the whole Cauchy slice. For example, closed de Sitter and a recollapsing universe with $\Lambda = 0$ and closed slicing have time-symmetric slices, but the only possible island is the full Cauchy slice.

The analysis carried out in this paper is valid for more general class of cosmologies. We expect to find islands in cosmologies with $\Lambda < 0$ for which the effective potential $V_{\rm eff}(a)$ vanishes at the turning point $a'(\eta) = 0$. For example, we expect that adding ordinary matter would not change the conclusions of this paper.

There are a few exciting avenues of research related to our work that are worth

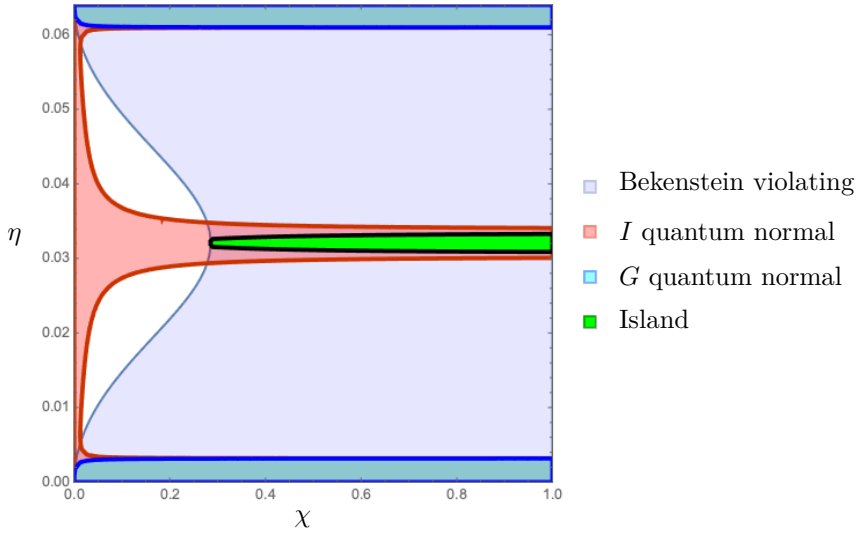

Figure 4.12: Regions where the three island conditions are satisfied in the semiclassical regime for an open FRW cosmology. We chose the numeric values $k = -1$, $c_{\text{th}} = 1$, $R_0 T_0 = 100$, and $\Lambda_0 G_N = 0.01$. There is an island region along the time-symmetric slice that extends to infinity. There are also overlapping regions at times where the solution $a(\eta)$ recollapses. However, they lie outside the semiclassical regime.

exploring. Since currently our universe is undergoing another period of inflation, it would be interesting to study if islands are relevant in the context of inflation. This can be modeled by bubbles of false vacuum where an inflating region forms behind the horizon [171–173]. It is worth understanding whether inflating regions are encoded in non-gravitating systems and if their formation is allowed in our universe. Additionally, it would also be interesting to understand the implications of our work in the case of eternally inflating multiverse studied in [174] where islands have been shown to appear in collapsing AdS bubbles. Furthermore, islands in Jackiw–Teitelboim de Sitter multiverse have been studied in [175] where they appeared in the crunching regions. Another direction of inquiry would be to explore the existence of islands in more general cosmologies in the spirit of [175].

A Islands conditions

In this appendix, we review the necessary criteria for having an island introduced in [37].

First condition: Violation of the Bekenstein bound

Adding the contribution of a non-empty island region I should decrease the original entropy of radiation then

$$S_{\text{gen}}(I \cup R) \leq S_{\text{mat}}(R) \ . \tag{A.1}$$

Rearranging the terms we get

$$I_{\text{mat}}(I, R) \geq S_{\text{gen}}(I) \ , \tag{A.2}$$

where $I_{\text{mat}}(I, R)$ is the mutual information between I and R. Let a region R' that contains R. Strong subadditivity for any region R' implies

$$I_{\text{mat}}(I, R') \geq I_{\text{mat}}(I, R) \ . \tag{A.3}$$

We then pick the region $R' = (I \cup C)^c$ where C is a thin region enclosing I, and such that state in the full region, $R' \cup (I \cup C)$, is pure. Combining (A.2) and (A.3) gives the following condition

$$I_{\text{mat}}(I, (I \cup C)^c) \geq S_{\text{gen}}(I) \ , \tag{A.4}$$

which can be written in terms of renormalized entropies[1] as

$$\widehat{S}_{\text{mat}}(I \cup C) \geq \frac{A(\partial I)}{4G_N} + \widehat{S}_{\text{mat}}(C) \ . \tag{A.6}$$

[1]The finite part of the matter entropy is defined to be

$$\widehat{S}_{\text{mat}}(I \cup R) := S_{\text{mat}}(I \cup R) - S_{\text{ct}}(\partial I) \ , \tag{A.5}$$

where S_{ct} is the UV divergent part of the entropy.

Since C is a very small region, we can approximate the matter entropies

$$\widehat{S}_{\text{mat}}(I \cup C) \approx \widehat{S}(I) \text{ and } \widehat{S}_{\text{mat}}(C) \approx 0. \tag{A.7}$$

Finally, the first condition becomes

$$\widehat{S}_{\text{mat}}(I) \gtrsim \frac{A(\partial I)}{4G_N} \ , \tag{A.8}$$

where the wiggly inequality means that the subleading terms compared to right hand side are ignored[2]. This indicates that the Bekenstein bound must be violated for the island region.

Second condition: I is quantum normal

Let us start with the extremality condition

$$\frac{d}{d\lambda} S_{\text{gen}}(R \cup I) = 0 \ , \tag{A.9}$$

where the derivative is defined by deforming ∂I in a null direction while keeping region R fixed. Adding the term $S_{\text{mat}}(R)$, which is constant under the deformation, and adding and subtracting $S_{\text{mat}}(I)$ to (A.9) we can rewrite this condition in terms of the mutual information

$$\frac{d}{d\lambda} S_{\text{gen}}(I) = \frac{d}{d\lambda} I_{\text{mat}}(I, R) \ . \tag{A.10}$$

Let us focus first on deforming in the outward direction denoted by λ_+. Using strong subadditivity, we note that

$$I_{\text{mat}}(I', R) - I_{\text{mat}}(I, R) \geq 0 \ . \tag{A.11}$$

Therefore, we conclude that

$$\frac{d}{d\lambda_+} I_{\text{mat}}(I, R) \geq 0 \ . \tag{A.12}$$

In other words, moving ∂I outward, by monotonicity of the mutual information, $I_{\text{mat}}(I, R)$ should grow or stay the same. Likewise, $I_{\text{mat}}(I, R)$ should decrease or stay the same when moving in the inward direction denoted by λ_-. Therefore, we find the second necessary condition for having an island to be

$$\pm \frac{d}{d\lambda_\pm} S_{\text{gen}}(I) \geq 0 \ . \tag{A.13}$$

This means that I is a *quantum normal* region.

[2]For a careful treatment of the UV divergences see .

Third condition: G is quantum normal

Consider a region G spacelike separated from R that surrounds the island I and shares a boundary with it. We first start with the extremality condition

$$\frac{d}{d\lambda_\pm} S_{\text{gen}}(I \cup R) = 0 \ . \tag{A.14}$$

Adding $S_{\text{mat}}(I)$ to both sides and rearranging the terms leads to

$$\frac{d}{d\lambda_\pm} \left[S_{\text{mat}}(I) - S_{\text{gen}}(I) \right] = \frac{d}{d\lambda_\pm} S_{\text{mat}}(I \cup R) \ . \tag{A.15}$$

Let us take a region $R \subset R'$. Using the strong subadditivity of the matter entropy leads to the following

$$\pm \frac{d}{d\lambda_\pm} S_{\text{mat}}(I \cup R') \leq \pm \frac{d}{d\lambda_\pm} S_{\text{mat}}(I \cup R) \ . \tag{A.16}$$

Combining (A.15) and (A.16) gives

$$\pm \frac{d}{d\lambda_\pm} S_{\text{gen}}(I) \leq \pm \frac{d}{d\lambda_\pm} \left[S_{\text{mat}}(I) - S_{\text{mat}}(I \cup R') \right] . \tag{A.17}$$

Then replacing $I \cup R'$ by its complement, the third condition is found to be

$$\pm \frac{d}{d\lambda_\pm} S_{\text{gen}}(I) \leq \pm \frac{d}{d\lambda_\pm} \left[S_{\text{mat}}(I) - S_{\text{mat}}(G) \right] \ . \tag{A.18}$$

Adding $S_{\text{mat}}(G)$ to both sides of (A.18) and using the fact that $\partial I = \partial G$, we arrive at

$$\pm \frac{d}{d\lambda_\pm} S_{\text{gen}}(G) \leq 0 \ . \tag{A.19}$$

Notice that since regions I and G share the same boundary, outward (inward) deformations of ∂I are inward (outward) deformations of ∂G. Referring equation (A.19) to the null directions of region I, the third condition becomes

$$\pm \frac{d}{d\lambda_\pm} S_{\text{gen}}(G) \geq 0 \ . \tag{A.20}$$

Then, the region G is also quantum normal.

It is important to emphasize that these criteria are independent of the region R and only depend on the properties of the candidate island region I. Furthermore, an island region, *i.e.,* one that extremizes (1.4.2), would also obey these three conditions. In the other direction, these three conditions are strong enough that can hint the existence of islands despite being agnostic about the region R.

5 Future directions

In Chapters 2, 3 and 4, we have studied three topics: traversable wormholes, modular Berry phases and entanglement islands. These three concepts are intimately related to entanglement. Wormholes can render traversable due to the extra amount of entanglement present in the GJW protocol. On the other hand, the modular Berry connection is an explicit realization of the idea that entanglement 'builds' spacetime. Finally, islands emerge when the pattern of entanglement between the island I and the ancillary region R is comparable with the area term in Planck units.

In this final Chapter, we make some concluding remarks and discuss possible future directions as well as open questions.

5.1 Traversable wormholes

In Chapter 2, we constructed an eternal traversable wormhole in a four-dimensional asymptotically AdS background. This solution has the following two crucial ingredients. First, we added a chemical potential that makes the decoupled system closer to being traversable, as in the near horizon limit they develop an $\mathrm{AdS}_{\times}\mathcal{S}^2$ throat where the transverse sphere has constant size. Second, charged fermions are moving in the magnetically charged background enhancing the negative energy due to quantum effects. Basically a single four-dimensional fermion is described as q (the degeneracy of the Landau level) massless two-dimensional fermions. A large number of fields would increase the negative energy needed to support the traversable wormhole.

We showed that the traversable wormhole is dual to the ground state of a simple Hamiltonian

$$H = H_L + H_R - \frac{ih}{\ell}\int d\Omega_2 \left(\bar{\mathbf{\Psi}}^R_- \mathbf{\Psi}^L_+ + \bar{\mathbf{\Psi}}^L_+ \mathbf{\Psi}^R_-\right) + \mu(Q_L - Q_R) \ , \tag{5.1}$$

where H_L and H_R are the Hamiltonians of the two decoupled systems. Finding the

quantum state of the dual CFT's in boundary variables is also a very interesting line of research. Naturally, we may expect that the dual state is a thermofield double type state, but notice that our wormhole is a semiclassical solution at zero temperature. Therefore, it cannot be exactly the TFD state. Techniques similar to the ones implemented in [176] might be useful to fully characterize this dual state.

In a different line of research, it would be interesting to find asymptotically AdS_4 *multi-mouth* wormholes similar to those studied in [177]. In particular, our four-dimensional solution might shed some light towards understanding explicitly the role of multipartite entanglement in the wormhole traversability. Moreover, it would be interesting to investigate the amount of information that can be sent through this type of wormhole as in [63].

5.2 Modular Berry phase

In Chapter 3, we studied the modular Berry transport generated by a change in the global state while keeping an interval fixed. This state-changing parallel transport is related to a certain family of bulk solutions. In fact, a precise definition of a bulk symplectic form associated with an entanglement wedge is absent in the literature. We filled in this gap with a proposal [2]: *the modular Berry curvature associated to state-changing parallel transport process computes the entanglement wedge symplectic form of a family of Euclidean cosmic brane solutions.*

The Lorentzian phase space interpretation of our configuration is an interesting avenue to explore in the future. It might be possible to use the relation with the hyperbolic black hole [106] to give a precise definition of the Lorentzian symplectic form. This connection would need to understand first the allowed boundary conditions at the associated entanglement wedge.

The connection between complexity, modular Berry phases, and modular chaos [104] represents also an interesting line to study in the future. For example, the computation of the Krylov complexity performed in [151] used a similar basis of vector fields to the one we used for Berry phases. We hope to make this connection more precise in future work.

The relation between Berry curvature for state-changing parallel transport and the entanglement wedge symplectic form of a cosmic brane geometry is similar in spirit to the results of [130, 131], but in the case of mixed states. This novel symplectic form might be used to derive linearized Einstein's equations from the first law of complexity following a similar approach as [178, 179]. Further developing the detailed connection between bit threads, complexity, and modular Berry transport

is very appealing.

A more general transport problem would involve both shape-changing and state-changing deformations in the CFT. Of course, not all deformations would involve a semiclassical gravity dual, since the bulk geometry must satisfy Einstein's equations. It would be interesting to geometrize the action of these asymptotic transformations together in the bulk, and understand the geometry that captures both types of modular transport.

5.3 Islands in FRW Cosmologies

We expect that the emergence of islands is a broader physical phenomenon. In higher dimensions, it is hard to compute the entanglement entropy of the bulk quantum fields, so extremizing the island formula (1.4.2) becomes a complicated problem. Instead, a criterion based on three necessary conditions was introduced in [37]. Importantly, these conditions depend only on the candidate island region I' while being agnostic about the auxiliary system R. Chapter 3 was devoted to exploring the existence of islands in cosmological spacetimes. We applied the three necessary conditions for having islands to the case of FRW universes supported with thermal radiation, cosmological constant, and non-zero spatial curvature. We found that the key ingredient that allows for the existence of islands is a negative cosmological constant.

The island formula suggests that the degrees of freedom in I are encoded in the radiation region R. This can be derived using the technology of quantum error correction [36, 180]. Having found candidate island regions I', *i.e.,* those regions that satisfy the three necessary conditions, it is natural to wonder: where are encoded the degrees of freedom of an island living in a cosmological spacetime? The degrees of freedom in the gravitating region I' would be encoded in some ancillary region R where gravity is unimportant. There are many ways in which region R can be assigned to I', one for each purification of the system R together with the gravitating system. Understanding further how this connection works in cosmology is also very interesting. Are there only crunching regions encoded in the region R or this connection can work for more general cosmologies?

Finally, investigating the implications of the quantum singularity theorem [181] for 'hyperentangled' regions B, *i.e.,* spacetimes regions with a purification R such that the entropy $S_{\text{gen}}(B \cup R) < S_{\text{gen}}(R)$, is very appealing, as the backward time evolution of ∂B might point out to a new class of singularities in spacetime. In fact, it was recently introduced a notion of *quantum singularity* for hyperentangled regions [182, 183]. What are the implications of these singularities in cosmological spacetimes?

5.4 Final thoughts

We conclude this thesis with a final discussion of open problems in a broader context.

- **Black hole interior**
  The island formula provides a precise recipe to compute the fine-grained entropy of a region R. It would be very interesting to think on the island formula in the 'opposite' direction. In order words, using the quantum state in R to learn about the dynamical bulk geometry. Maybe we can gain inspiration from the modular Berry program. In its early developments [31], it provided a way of reconstructing bulk geometry using the pattern of entanglement at the boundary. Similarly, maybe we can use the freedom in choosing R to obtain information about the geometry near ∂I. Being a bit more ambitious, maybe there is a way to obtain Einstein's equations using the entanglement between R and I. In the case of an evaporating black hole, the answer to these questions might provide a way to probe the geometry behind the event horizon and perhaps get closer to the singularity.

- **Cosmological horizon**
  The emergence of islands provides evidence supporting the central dogma of black hole physics [153]: *black holes, seen from the outside, can be replaced with a quantum mechanical system with $A/4G_N$ degrees of freedom.* Cosmological horizons also have an associated Gibbons-Hawking radiation [184]. Then, it is natural to explore whether a similar central dogma for cosmology is physically reasonable given the similarities between the cosmological horizon and the black hole horizon. In particular, the study of cosmological islands can shed some light on the quantum aspects of the cosmological horizon [185].

- **Information encoded in the Island**
  As we mentioned above, the island in the gravitating region is encoded in the ancillary region R by some sort of holographic duality. In principle, it is possible to extract information of the degrees of freedom in the island if we have access to the ancillary region R. The Petz map gives an explicit example of this encoding, as it maps operators acting in R to operators acting in I [36]. In general, this map is non-local and complicated to realize in the bulk. Nevertheless, there is an alternative procedure coming from traversable wormholes. The GJW protocol can be used to extract information of the island in some simple setups [186]. It would be interesting to probe the interior of a black hole with a similar simple protocol and understand how the information of the island is encoded in the ancillary system. More broadly,

understand to what extent I encoded in R works as a holographic duality?

- **Where is the hologram in dS?**
  As a consequence of entanglement wedge reconstruction, the degrees of freedom in the island are encoded in the ancillary system R. This is similar to a holographic duality in the sense that the state of a gravitational system is encoded in a dual theory where gravity is unimportant. Finding islands in de Sitter spacetime would give a strong hint to understanding where the hologram is in de Sitter [185]. Perhaps, allowing us in the future to state a 'dS/CFT' correspondence from first principles.

- **Other cosmological observables?**
  The holographic encoding of the island degrees of freedom in R, *i.e.,* operators in the region I can be rewritten as operators acting on R, works very well in the context of fine-grained entanglement entropy computations. But what about other observables? It would be very interesting to understand, for example, how the information of cosmological correlators or the wave function of the universe is encoded in the state of region R. What is the set of allowed boundary conditions in region R?

- **Bit threads for islands**
  An alternative way to compute entanglement entropy was proposed recently [187]. This procedure does not rely on bulk surfaces, but instead, it is phrased in terms of a specific flow maximization problem: finding a bulk vector field with maximum flux through the corresponding boundary region. This formulation has conceptual advantages in the bulk interpretation of various aspects of entanglement. More recently, a bit thread proposal that incorporates quantum corrections due to bulk entanglement entropy was presented in [188, 189]. It might be interesting to construct quantum corrected thread configurations in Lorentzian setups such as evaporating black holes to understand the relation between bit threads and entanglement islands. A similar picture of bit threads in cosmology has been proposed in [185]. How are they related to cosmological islands?

Summary

The microscopic world can be described with very good precision with the principles of quantum mechanics. The basic ingredient is the concept of the wave function, which specifies fully the state of a particle. Macroscopic concepts such as positions, angular momentum, etc. are probabilistic in nature. This is very different from the macroscopic world where uncertainty is only due to our ignorance or limited computational control. At much bigger length scales, the theory that describes the dynamics of galaxies and planets with great accuracy is general relativity. Very complicated dynamics such as gravitational collapse, gravitational waves, etc. are captured by Einstein's equations. Modern theoretical physics finds its pillars in these two theories: Quantum Mechanics and the General Theory of Relativity.

The combination quantum mechanics and special relativity lead to a new phenomenon: creation and annihilation of particles. There is no mechanism in standard non-relativistic quantum mechanics that deals with this new phenomenon and naive attempts to write a relativistic version of the one-particle Schrödinger equation results in sick theories (negative probabilities, energies, etc). It is clear that the new theory should account for a change in the number of particles and the correct formalism to treat it turns out to be quantum field theory.

In quantum field theory, the basic ingredients are quantum fields. These are dynamical objects that can fluctuate like jellies that fill in the spacetime. Particles and their interactions can be modeled as fluctuations of the fields. Together with a few basic principles, the framework of quantum field theory allows us to model different theories with interactions and matter content. The most successful theory of this approach is known as the Standard Model, and describes three of the four fundamental forces of nature with incredible precision.

Despite its great success in particle colliders, there are various open questions outside the scope of the Standard Model. Perhaps, the most challenging is to include gravitational effects at the quantum level, since radical new concepts are

needed. Imagine, for example, a region of spacetime with area A, at very high energies a black hole would form and its entropy would be proportional to its area $A/4$ in Planck units rather than the volume. This very counterintuitive result cannot be reproduced using local quantum field theory. Therefore, at very high energies a new theory is needed if we want to include the physics of black holes.

Black holes are fascinating objects. These are massive objects that perturb the spacetime around them so drastically that light cannot escape from their interior. Black holes take physics to its limits and they are the perfect lab to study quantum gravity. For example, studying quantum effects in the context of black hole evaporation led Hawking to conclude that black holes are not so black, but they have a thermal spectrum. This has profound implications. Black holes can radiate and evaporate! But what happens with the information that falls into the black hole once it completely evaporates? This puzzle is known as the 'information paradox'. It is a paradox because a basic principle of quantum mechanics states that information cannot be lost in a unitary evolution. A black hole must not be the exception.

When a black hole forms the number of degrees of freedom seems to reduce drastically since the entropy of a black hole is proportional to its area. This property together with unitarity led 't Hooft and Susskind to propose a *holographic principle*, which states that the number of fundamental degrees of freedom in a region cannot exceed the area of the region in Planck units. The most explicit realization of the holographic principle is given by the AdS/CFT or holographic correspondence. This novel duality states the equivalence between a theory of quantum fields in d dimensions and a theory of quantum gravity in at least one dimension more. Similar to a hologram, the information of the higher dimensional theory (called the 'bulk') is encoded in the degrees of freedom of lower-dimensional theory (called the 'boundary') that does not include gravity. The AdS/CFT correspondence works like a dictionary that takes boundary physics and translates it into a different language, the language of gravity in the bulk. The holographic dictionary is still under construction and a very active area of research.

Entanglement is the most counterintuitive feature of quantum mechanics. This implies, for example, for a two-qubit state that knowing that the first qubit is in a particular state determines the state of the second qubit. This is true even if we take the two qubits far apart. This "spooky action at a distance," as Einstein colorfully called it, is the property of entanglement. A measure of entanglement is the entanglement entropy associated with a subsystem. It turns out that it is also part of the holographic dictionary, and can be related to areas of bulk surfaces through the Ryu-Takayanagi (RT) formula. This relation shows a very deep connection between entanglement and the connectivity of spacetime.

In recent years, a more refined version of the RT prescription known as the 'Island formula' has shed light on the resolution of some aspects of the black hole information paradox. It has helped to understand what happens to the information during the evaporation and where is the interior of the black hole encoded after the end of evaporation. It turns out that during the evaporation a disconnected region of spacetime emerges in the interior of the black hole, *i.e.,* an island appears, and accounts for the entanglement of the partners that fall into the black hole.

In this doctoral thesis, we study three different aspects of entanglement entropy in holography: traversable wormholes, modular Berry phases and entanglement islands. In Chapter 1, we introduce all these concepts and explain how they are intimately related with entanglement entropy.

We review the non-local protocol that allows for traversable wormholes using ordinary matter. In Chapter 2, we implement this non-local coupling to construct an eternal traversable wormhole in asymptotically anti-de Sitter space in four dimensions. We show that this geometry is dual to the ground state of a simple Hamiltonian.

We then review the elements of the modular Berry transport problem. In the context of three-dimensional gravity, in Chapter 3, we study the parallel transport of modular Hamiltonians governed by a change of global state. Using this state-changing parallel transport, we find that the Berry curvature for a fixed interval and changing state computes the symplectic form for an Euclidean conical singularity geometry obtained from the backreaction of a cosmic brane.

Finally, after a review of the island formula and its use in the resolution of some aspects of the black hole information paradox, we discuss its possible application in cosmology. We study the possible existence of islands in FRW cosmologies supported by thermal radiation, cosmological constant, and non-zero spatial curvature in Chapter 4. We apply the three necessary conditions dependent only on the island region to find candidate island regions.

Samenvatting

De microscopische wereld kan met zeer goede precisie worden beschreven met de principes van de kwantummechanica. Het basisingrediënt is het concept van de golffunctie, die de toestand van een deeltje volledig specificeert. Macroscopische concepten zoals posities, impulsmoment, enz. zijn probabilistisch van aard. Dit werkt heel anders dan in de macroscopische wereld waar onzekerheid enkel te wijten is aan onze onwetendheid of beperkte computationele controle. Op veel grotere lengteschalen is de theorie die de dynamica van sterrenstelsels en planeten met grote nauwkeurigheid beschrijft de algemene relativiteitstheorie. Zeer gecompliceerde dynamica zoals de vorming van een zwart gat, zwaartekrachtgolven, enz. worden bepaald door de Einsteinvergelijkingen. De moderne theoretische fysica is gebaseerd op deze twee theorieën: de kwantummechanica en de algemene relativiteitstheorie.

De combinatie van kwantummechanica en speciale relativiteitstheorie leidt tot een nieuw fenomeen: de creatie en annihilatie van deeltjes. Er is geen mechanisme in de niet-relativistische kwantummechanica dat zich bezighoudt met dit fenomeen, en naïeve pogingen om een relativistische versie van de Schrödinger-vergelijking voor één deeltje op te schrijven resulteren in 'zieke' theorieën (met negatieve kansen, energieën, enz.) Het is daarom duidelijk dat de nieuwe theorie rekening moet houden met een verandering in het aantal deeltjes, en het juiste formalisme om dit te beschrijven blijkt kwantumveldentheorie te zijn.

In kwantumveldentheorie zijn de basisingrediënten kwantumvelden. Dit zijn dynamische objecten die kunnen fluctueren in de ruimtetijd. Deeltjes en hun interacties kunnen worden gemodelleerd als fluctuaties van deze velden. Samen met enkele basisprincipes stelt het raamwerk van de kwantumveldentheorie ons in staat om theorieën te modelleren met verschillende interacties en materie-inhoud. De meest succesvolle theorie met deze benadering staat bekend als het standaardmodel en beschrijft drie van de vier fundamentele natuurkrachten met ongelooflijke precisie.

Ondanks het grote succes, zijn er verschillende open vragen die buiten het bereik

van het standaardmodel liggen. De grootste uitdaging is misschien wel om zwaartekrachteffecten op kwantumniveau mee te nemen, aangezien daarvoor radicaal nieuwe concepten nodig zijn. Stel je bijvoorbeeld een gebied van ruimtetijd voor met oppervlakte A, bij zeer hoge energieën zou zich een zwart gat vormen en de entropie zou dan evenredig zijn met het oppervlak $A/4$ in Planck-eenheden, in plaats van het volume. Dit zeer tegenintuïtieve resultaat kan niet worden gereproduceerd met behulp van lokale kwantumveldentheorie. Daarom is bij zeer hoge energieën een nieuwe theorie nodig als we de fysica van zwarte gaten willen begrijpen.

Zwarte gaten zijn fascinerende objecten. Ze zijn massieve objecten die de ruimtetijd om hen heen zo drastisch verstoren dat licht niet uit hun inwendige kan ontsnappen. Zwarte gaten drijven de natuurkunde tot het uiterste en zijn het perfecte laboratorium om kwantumzwaartekracht te bestuderen. Door bijvoorbeeld kwantumeffecten te bestuderen in de context van de verdamping van zwarte gaten, concludeerde Hawking dat zwarte gaten niet volledig zwart zijn, maar een thermisch spectrum hebben. Dit heeft ingrijpende gevolgen. Zwarte gaten kunnen stralen en verdampen! Maar wat gebeurt er met de informatie die in het zwarte gat valt als het volledig verdampt is? Deze puzzel staat bekend als de 'informatieparadox'. Het is een paradox omdat een basisprincipe van de kwantummechanica stelt dat informatie niet verloren kan gaan bij een unitaire evolutie. Een zwart gat mag daarop geen uitzondering zijn.

Wanneer een zwart gat wordt gevormd, lijkt het aantal vrijheidsgraden drastisch te verminderen, aangezien de entropie van een zwart gat evenredig is met zijn oppervlakte. Deze eigenschap, samen met unitariteit, bracht 't Hooft en Susskind ertoe om een *holografisch principe* voor te stellen, dat stelt dat het aantal fundamentele vrijheidsgraden in een regio niet groter mag zijn dan de oppervlakte van de regio in Planck-eenheden. De meest expliciete realisatie van het holografische principe wordt gegeven door de AdS/CFT of holografische correspondentie. Deze nieuwe dualiteit stelt de gelijkwaardigheid vast tussen een theorie van kwantumvelden in d dimensies en een theorie van kwantumzwaartekracht in minstens één dimensie meer. Net als bij een hologram, wordt de informatie van de hogerdimensionale theorie (het 'inwendige' genoemd) gecodeerd in de vrijheidsgraden van de lagerdimensionale theorie (de 'rand' genoemd) die de zwaartekracht niet omvat. De AdS/CFT-correspondentie werkt als een woordenboek dat fysica op rand gebruikt en vertaalt in een andere taal, de taal van de zwaartekracht in het inwendige. Het holografische woordenboek is nog niet af en een zeer actief onderzoeksgebied.

Verstrengeling is het meest tegenintuïtieve kenmerk van de kwantummechanica. Dit houdt bijvoorbeeld in dat voor een toestand van twee qubits, de wetenschap dat de eerste qubit zich in een bepaalde toestand bevindt, de toestand van de tweede qubit bepaalt. Dit geldt zelfs als we de twee qubits ver uit elkaar bren-

gen. Deze 'spookachtige actie op afstand', zoals Einstein het kleurrijk noemde, wordt veroorzaakt door de verstrengeling. Een maat voor deze verstrengeling is de verstrengelingsentropie die is gekoppeld aan een subsysteem. Het blijkt dat dit ook deel uitmaakt van het holografische woordenboek, en kan worden gerelateerd aan de oppervlakte van gebieden in het inwendige via de Ryu-Takayanagi (RT)-formule. Deze relatie toont een zeer diep verband aan tussen verstrengeling in de randtheorie en het feit dat de ruimtetijd samenhangend is.

In de afgelopen jaren heeft een meer verfijnde versie van het RT-voorschrift, bekend als de 'eilandformule', bijgedragen aan een resolutie van sommige aspecten van de informatieparadox. Zo heeft het geholpen in het begrijpen van wat er met de informatie gebeurt tijdens de verdamping, en waar het binnenste van het zwarte gat wordt gecodeerd nadat de verdamping is geeindigd. Het blijkt dat tijdens de verdamping een niet-samenhangend gebied van ruimtetijd ontstaat in het binnenste van het zwarte gat, dat wil zeggen dat er een eiland verschijnt, dat de verstrengeling verklaart van de qubitpartners die in het zwarte gat vallen.

In dit proefschrift bestuderen we drie verschillende aspecten van verstrengelingsentropie in holografie: doorkruisbare wormgaten, modulaire Berry-fasen en verstrengelingseilanden. In hoofdstuk 1 introduceren we al deze concepten en leggen we uit hoe ze nauw verbonden zijn met verstrengelingsentropie.

We bekijken het niet-lokale protocol dat doorkruisbare wormgaten mogelijk maakt met behulp van gewone materie. In Hoofdstuk 2 implementeren we deze niet-lokale koppeling om een eeuwig doorkruisbaar wormgat te construeren in asymptotische anti-de Sitterruimte in vier dimensies. We laten zien dat deze meetkunde duaal is aan de grondtoestand van een eenvoudige Hamiltoniaan.

Vervolgens bekijken we het modulaire Berrytransportprobleem. In de context van driedimensionale zwaartekracht bestuderen we in Hoofdstuk 3 het parallelle transport van modulaire Hamiltonianen die worden bestuurd door een verandering van de toestand. Met behulp van dit toestandsveranderende parallelle transport, vinden we dat de Berrykromming voor een vast interval en veranderende toestand de symplectische vorm berekent voor een Euclidische conische singulariteitsgeometrie verkregen door het invoegen van een kosmische braan.

Tot slot, na een bespreking van de eilandformule en het gebruik ervan bij het oplossen van sommige aspecten van de informatieparadox van het zwarte gat, bespreken we de mogelijke toepassing ervan in de kosmologie. We bestuderen het mogelijke bestaan van eilanden in FRW-kosmologieën ondersteund door thermische straling, kosmologische constante en niet-nul ruimtelijke kromming in hoofdstuk 4. We passen de drie noodzakelijke voorwaarden alleen toe afhankelijk van de eilandregio om kandidaat-eilandregio's te vinden.

Acknowledgements

I am very grateful to my advisors Jan de Boer and Ben Freivogel for all your support, guidance, and amazing discussions. Thanks a lot for sharing your ideas with me and encouraging me to find my path in physics.

I am deeply grateful to my advisors in Mexico Antonio García and Alberto Güijosa for introducing me to this fantastic field of research. Thanks for all the invaluable time and continuous support.

I would like to thank my collaborators and colleagues, whose unique approach to physics has taught me many lessons over the years. Thanks for the work and many fruitful discussions: Elena Cáceres, Juan Pedraza, Cesar Agón, Marika Taylor, Kostas Skenderis, Leo Pando Zayas, Freddy Cachazo, Andrew Rolph, Ignacio Reyes, Andrew Svesko, Mariano Chernicoff, Yaithd Olivas, Jay Armas, Tarek Anous, Suzanne Bintanja, Erik Verlinde, Dora Nikolakopoulou, Jeremy van der Heijden, Bahman Najian, Dimitrios Patramanis, Claire Zukowski, Natalia Pinzani-Fokeeva, Damián Galante, Jackson R. Fliss, Ana-Maria Raclariu, Shira Chapman, Bartek Czech, Alejandra Castro, Diego Hofman, Viktor Jahnke, Luis Apolo, Facundo Rost, Ramesh Ammanamanchi, Grégoire Mathys, Gui Pimentel, Carlos Duaso Pueyo, Saúl Ramos, Edward Morvan, Victor Godet, José Edelstein, Leonardo Patiño, Gustavo Arciniega, Daniel Ávila, Alex Belin, Antonio Rotundo, Dario Nuñez, Alberto Landetta, Evita Verheijden, Diego Liška, and Stathis Vitouladitis.

I am also grateful to all the members of the Amsterdam String Theory group. It has been a pleasure to be part of such a vibrant community.

Finally, I would like to thank my family for their unconditional love and support.

Bibliography

[1] S. Bintanja, R. Espíndola, B. Freivogel and D. Nikolakopoulou, *How to make traversable wormholes: eternal AdS_4 wormholes from coupled CFT's*, *JHEP* **10** (2021) 173 [2102.06628].

[2] J. de Boer, R. Espíndola, B. Najian, D. Patramanis, J. van der Heijden and C. Zukowski, *Virasoro entanglement Berry phases*, *JHEP* **03** (2022) 179 [2111.05345].

[3] R. Espíndola, B. Najian and D. Nikolakopoulou, *Islands in FRW Cosmologies*, 2203.04433.

[4] D.N. Page, *Hawking radiation and black hole thermodynamics*, *New J. Phys.* **7** (2005) 203 [hep-th/0409024].

[5] S.W. Hawking, *Particle Creation by Black Holes*, *Commun. Math. Phys.* **43** (1975) 199.

[6] J.D. Bekenstein, *Black holes and the second law*, *Lett. Nuovo Cim.* **4** (1972) 737.

[7] G. 't Hooft, *Dimensional reduction in quantum gravity*, *Conf. Proc. C* **930308** (1993) 284 [gr-qc/9310026].

[8] L. Susskind, *The World as a hologram*, *J. Math. Phys.* **36** (1995) 6377 [hep-th/9409089].

[9] R. Bousso, *The Holographic principle*, *Rev. Mod. Phys.* **74** (2002) 825 [hep-th/0203101].

[10] A. Güijosa, *QCD, with strings attached*, *Int. J. Mod. Phys. E* **25** (2016) 1630006 [1611.07472].

[11] A.V. Ramallo, *Introduction to the AdS/CFT correspondence*, *Springer Proc. Phys.* **161** (2015) 411 [1310.4319].

[12] J. Polchinski, *Introduction to Gauge/Gravity Duality*, in *Theoretical Advanced Study Institute in Elementary Particle Physics: String theory and its Applications: From meV to the Planck Scale*, pp. 3–46, 10, 2010, DOI [1010.6134].

[13] S. Ryu and T. Takayanagi, *Holographic derivation of entanglement entropy from AdS/CFT*, *Phys. Rev. Lett.* **96** (2006) 181602 [hep-th/0603001].

[14] V.E. Hubeny, M. Rangamani and T. Takayanagi, *A Covariant holographic entanglement entropy proposal*, *JHEP* **07** (2007) 062 [0705.0016].

[15] A. Lewkowycz and J. Maldacena, *Generalized gravitational entropy*, *JHEP* **08** (2013) 090 [1304.4926].

[16] X. Dong, A. Lewkowycz and M. Rangamani, *Deriving covariant holographic entanglement*, *JHEP* **11** (2016) 028 [1607.07506].

[17] T. Faulkner, A. Lewkowycz and J. Maldacena, *Quantum corrections to holographic entanglement entropy*, *JHEP* **11** (2013) 074 [1307.2892].

[18] N. Engelhardt and A.C. Wall, *Quantum Extremal Surfaces: Holographic Entanglement Entropy beyond the Classical Regime*, *JHEP* **01** (2015) 073 [1408.3203].

[19] R. Bousso, Z. Fisher, S. Leichenauer and A.C. Wall, *Quantum focusing conjecture*, *Phys. Rev. D* **93** (2016) 064044 [1506.02669].

[20] A.C. Wall, *Maximin Surfaces, and the Strong Subadditivity of the Covariant Holographic Entanglement Entropy*, *Class. Quant. Grav.* **31** (2014) 225007 [1211.3494].

[21] A. Almheiri, N. Engelhardt, D. Marolf and H. Maxfield, *The entropy of bulk quantum fields and the entanglement wedge of an evaporating black hole*, *JHEP* **12** (2019) 063 [1905.08762].

[22] G. Penington, *Entanglement Wedge Reconstruction and the Information Paradox*, *JHEP* **09** (2020) 002 [1905.08255].

[23] A. Almheiri, T. Hartman, J. Maldacena, E. Shaghoulian and A. Tajdini, *Replica Wormholes and the Entropy of Hawking Radiation*, *JHEP* **05** (2020) 013 [1911.12333].

[24] J.M. Maldacena, *Eternal black holes in anti-de Sitter*, *JHEP* **04** (2003) 021 [hep-th/0106112].

[25] M. Van Raamsdonk, *Building up spacetime with quantum entanglement*, *Gen. Rel. Grav.* **42** (2010) 2323 [1005.3035].

[26] P. Gao, D.L. Jafferis and A.C. Wall, *Traversable Wormholes via a Double Trace Deformation*, *JHEP* **12** (2017) 151 [1608.05687].

[27] M.V. Berry, *Quantal phase factors accompanying adiabatic changes*, *Proc. Roy. Soc. Lond. A* **392** (1984) 45.

[28] B. Czech, L. Lamprou, S. Mccandlish and J. Sully, *Modular Berry Connection for Entangled Subregions in AdS/CFT*, *Phys. Rev. Lett.* **120** (2018) 091601 [1712.07123].

[29] B. Czech, L. Lamprou and L. Susskind, *Entanglement Holonomies*, 1807.04276.

[30] B. Chen, B. Czech and Z.-z. Wang, *Quantum information in holographic duality*, *Rept. Prog. Phys.* **85** (2022) 046001 [2108.09188].

[31] V. Balasubramanian, B.D. Chowdhury, B. Czech, J. de Boer and M.P. Heller, *Bulk curves from boundary data in holography*, *Phys. Rev. D* **89** (2014) 086004 [1310.4204].

[32] B. Czech, J. De Boer, D. Ge and L. Lamprou, *A modular sewing kit for entanglement wedges*, *JHEP* **11** (2019) 094 [1903.04493].

[33] S.W. Hawking, *Breakdown of Predictability in Gravitational Collapse*, *Phys. Rev. D* **14** (1976) 2460.

[34] J. Polchinski, *The Black Hole Information Problem*, in *Theoretical Advanced Study Institute in Elementary Particle Physics: New Frontiers in Fields and Strings*, pp. 353–397, 2017, DOI [1609.04036].

[35] D.N. Page, *Information in black hole radiation*, *Phys. Rev. Lett.* **71** (1993) 3743 [hep-th/9306083].

[36] G. Penington, S.H. Shenker, D. Stanford and Z. Yang, *Replica wormholes and the black hole interior*, 1911.11977.

[37] T. Hartman, Y. Jiang and E. Shaghoulian, *Islands in cosmology*, *JHEP* **11** (2020) 111 [2008.01022].

[38] J. Maldacena, D. Stanford and Z. Yang, *Diving into traversable wormholes*, *Fortsch. Phys.* **65** (2017) 1700034 [1704.05333].

[39] J. Maldacena and L. Susskind, *Cool horizons for entangled black holes*, *Fortsch. Phys.* **61** (2013) 781 [1306.0533].

[40] M.S. Morris and K.S. Thorne, *Wormholes in space-time and their use for interstellar travel: A tool for teaching general relativity*, *Am. J. Phys.* **56**

(1988) 395.

[41] M.S. Morris, K.S. Thorne and U. Yurtsever, *Wormholes, Time Machines, and the Weak Energy Condition*, *Phys. Rev. Lett.* **61** (1988) 1446.

[42] M. Visser, *Traversable wormholes: Some simple examples*, *Physical Review D* **39** (1989) 3182 [0809.0907].

[43] M. Visser, *Traversable wormholes from surgically modified Schwarzschild space-times*, *Nucl. Phys.* **B328** (1989) 203 [0809.0927].

[44] E. Poisson and M. Visser, *Thin shell wormholes: Linearization stability*, *Phys. Rev.* **D52** (1995) 7318 [gr-qc/9506083].

[45] C. Barcelo and M. Visser, *Traversable wormholes from massless conformally coupled scalar fields*, *Phys. Lett.* **B466** (1999) 127 [gr-qc/9908029].

[46] M. Visser, S. Kar and N. Dadhich, *Traversable wormholes with arbitrarily small energy condition violations*, *Phys. Rev. Lett.* **90** (2003) 201102 [gr-qc/0301003].

[47] B. Bhawal and S. Kar, *Lorentzian wormholes in Einstein-Gauss-Bonnet theory*, *Phys. Rev.* **D46** (1992) 2464.

[48] M. Thibeault, C. Simeone and E.F. Eiroa, *Thin-shell wormholes in Einstein-Maxwell theory with a Gauss-Bonnet term*, *Gen. Rel. Grav.* **38** (2006) 1593 [gr-qc/0512029].

[49] R.E. Arias, M. Botta Cantcheff and G.A. Silva, *Lorentzian AdS, Wormholes and Holography*, *Phys. Rev.* **D83** (2011) 066015 [1012.4478].

[50] M. Chernicoff, E. García, G. Giribet and E. Rubín de Celis, *Thin-shell wormholes in AdS_5 and string dioptrics*, 2006.07428.

[51] X.O. Camanho, J.D. Edelstein, J. Maldacena and A. Zhiboedov, *Causality constraints on corrections to the graviton three-point coupling*, *Journal of High Energy Physics* **2016** (2016) 20 [1407.5597].

[52] P. Gao, D.L. Jafferis and A.C. Wall, *Traversable Wormholes via a Double Trace Deformation*, *JHEP* **12** (2017) 151 [1608.05687].

[53] R. van Breukelen and K. Papadodimas, *Quantum teleportation through time-shifted AdS wormholes*, *JHEP* **08** (2018) 142 [1708.09370].

[54] J. de Boer, R. Van Breukelen, S.F. Lokhande, K. Papadodimas and E. Verlinde, *On the interior geometry of a typical black hole microstate*,

JHEP **05** (2019) 010 [1804.10580].

[55] A. Almheiri, A. Mousatov and M. Shyani, *Escaping the Interiors of Pure Boundary-State Black Holes*, 1803.04434.

[56] D. Bak, C. Kim and S.-H. Yi, *Bulk view of teleportation and traversable wormholes*, *JHEP* **08** (2018) 140 [1805.12349].

[57] Z. Fu, B. Grado-White and D. Marolf, *A perturbative perspective on self-supporting wormholes*, *Class. Quant. Grav.* **36** (2019) 045006 [1807.07917].

[58] E. Caceres, A.S. Misobuchi and M.-L. Xiao, *Rotating traversable wormholes in AdS*, *JHEP* **12** (2018) 005 [1807.07239].

[59] S. Hirano, Y. Lei and S. van Leuven, *Information Transfer and Black Hole Evaporation via Traversable BTZ Wormholes*, *JHEP* **09** (2019) 070 [1906.10715].

[60] J. De Boer, R. Van Breukelen, S.F. Lokhande, K. Papadodimas and E. Verlinde, *Probing typical black hole microstates*, *JHEP* **01** (2020) 062 [1901.08527].

[61] Z. Fu, B. Grado-White and D. Marolf, *Traversable Asymptotically Flat Wormholes with Short Transit Times*, *Class. Quant. Grav.* **36** (2019) 245018 [1908.03273].

[62] B. Freivogel, V. Godet, E. Morvan, J.F. Pedraza and A. Rotundo, *Lessons on Eternal Traversable Wormholes in AdS*, *JHEP* **07** (2019) 122 [1903.05732].

[63] B. Freivogel, D.A. Galante, D. Nikolakopoulou and A. Rotundo, *Traversable wormholes in AdS and bounds on information transfer*, *JHEP* **01** (2020) 050 [1907.13140].

[64] A. May and M. Van Raamsdonk, *Interpolating between multi-boundary wormholes and single-boundary geometries in holography*, 2011.14258.

[65] S. Fallows and S.F. Ross, *Making near-extremal wormholes traversable*, 2008.07946.

[66] R. Emparan, B. Grado-White, D. Marolf and M. Tomasevic, *Multi-mouth Traversable Wormholes*, 2012.07821.

[67] A.A. Balushi, Z. Wang and D. Marolf, *Traversability of Multi-Boundary Wormholes*, 2012.04635.

[68] J. Maldacena and X.-L. Qi, *Eternal traversable wormhole*, 1804.00491.

[69] J. Maldacena, A. Milekhin and F. Popov, *Traversable wormholes in four dimensions*, 1807.04726.

[70] J. Maldacena, *Comments on magnetic black holes*, 2004.06084.

[71] L. Susskind and Y. Zhao, *Teleportation through the wormhole*, *Phys. Rev. D* **98** (2018) 046016 [1707.04354].

[72] A.R. Brown, H. Gharibyan, S. Leichenauer, H.W. Lin, S. Nezami, G. Salton et al., *Quantum Gravity in the Lab: Teleportation by Size and Traversable Wormholes*, 1911.06314.

[73] S. Nezami, H.W. Lin, A.R. Brown, H. Gharibyan, S. Leichenauer, G. Salton et al., *Quantum Gravity in the Lab: Teleportation by Size and Traversable Wormholes, Part II*, 2102.01064.

[74] W. Cottrell, B. Freivogel, D.M. Hofman and S.F. Lokhande, *How to Build the Thermofield Double State*, *JHEP* **02** (2019) 058 [1811.11528].

[75] S. Banerjee and J. Kames-King, *Traversable wormholes in AdS and their CFT duals*, to appear.

[76] M. Van Raamsdonk, *Cosmology from confinement?*, 2102.05057.

[77] M. Henningson and K. Sfetsos, *Spinors and the AdS / CFT correspondence*, *Phys. Lett. B* **431** (1998) 63 [hep-th/9803251].

[78] M. Henneaux, *Boundary terms in the AdS / CFT correspondence for spinor fields*, in *International Meeting on Mathematical Methods in Modern Theoretical Physics (ISPM 98)*, pp. 161–170, 9, 1998 [hep-th/9902137].

[79] A.J. Amsel and D. Marolf, *Supersymmetric Multi-trace Boundary Conditions in AdS*, *Class. Quant. Grav.* **26** (2009) 025010 [0808.2184].

[80] J.M. Maldacena, J. Michelson and A. Strominger, *Anti-de Sitter fragmentation*, *JHEP* **02** (1999) 011 [hep-th/9812073].

[81] V. Balasubramanian and P. Kraus, *A Stress tensor for Anti-de Sitter gravity*, *Commun. Math. Phys.* **208** (1999) 413 [hep-th/9902121].

[82] S.A. Hartnoll, C.P. Herzog and G.T. Horowitz, *Holographic Superconductors*, *JHEP* **12** (2008) 015 [0810.1563].

[83] O.J. Dias, R. Masachs, O. Papadoulaki and P. Rodgers, *Hunting for fermionic instabilities in charged AdS black holes*, *JHEP* **04** (2020) 196

[1910.04181].

[84] L. Romans, *Supersymmetric, cold and lukewarm black holes in cosmological einstein-maxwell theory*, *Nuclear Physics B* **383** (1992) 395–415 [hep-th/9203018].

[85] H.K. Kunduri, J. Lucietti and H.S. Reall, *Supersymmetric multi-charge AdS_5 black holes*, *Journal of High Energy Physics* **2006** (2006) 036–036 [hep-th/0601156].

[86] J.B. Gutowski and H.S. Reall, *General supersymmetric AdS_5 black holes*, *Journal of High Energy Physics* **2004** (2004) 048–048 [hep-th/0401129].

[87] S. Bhattacharyya, S. Minwalla and K. Papadodimas, *Small hairy black holes in $AdS_5 \times S^5$*, *Journal of High Energy Physics* **2011** (2011) [1005.1287].

[88] Y. Chen, V. Gorbenko and J. Maldacena, *Bra-ket wormholes in gravitationally prepared states*, 2007.16091.

[89] T. Hartman, Y. Jiang and E. Shaghoulian, *Islands in cosmology*, *JHEP* **11** (2020) 111 [2008.01022].

[90] M. Van Raamsdonk, *Comments on wormholes, ensembles, and cosmology*, 2008.02259.

[91] B. Czech, L. Lamprou, S. McCandlish, B. Mosk and J. Sully, *A Stereoscopic Look into the Bulk*, *JHEP* **07** (2016) 129 [1604.03110].

[92] J. de Boer, F.M. Haehl, M.P. Heller and R.C. Myers, *Entanglement, holography and causal diamonds*, *JHEP* **08** (2016) 162 [1606.03307].

[93] J. de Boer, M.P. Heller, R.C. Myers and Y. Neiman, *Holographic de Sitter Geometry from Entanglement in Conformal Field Theory*, *Phys. Rev. Lett.* **116** (2016) 061602 [1509.00113].

[94] B. Czech, L. Lamprou, S. McCandlish and J. Sully, *Integral Geometry and Holography*, *JHEP* **10** (2015) 175 [1505.05515].

[95] C.T. Asplund, N. Callebaut and C. Zukowski, *Equivalence of Emergent de Sitter Spaces from Conformal Field Theory*, *JHEP* **09** (2016) 154 [1604.02687].

[96] B. Freivogel, R. Jefferson, L. Kabir, B. Mosk and I.-S. Yang, *Casting Shadows on Holographic Reconstruction*, *Phys. Rev. D* **91** (2015) 086013 [1412.5175].

[97] R. Espíndola, A. Guijosa and J.F. Pedraza, *Entanglement Wedge Reconstruction and Entanglement of Purification*, *Eur. Phys. J. C* **78** (2018) 646 [1804.05855].

[98] R.F. Penna and C. Zukowski, *Kinematic space and the orbit method*, *JHEP* **07** (2019) 045 [1812.02176].

[99] J. Maldacena, D. Simmons-Duffin and A. Zhiboedov, *Looking for a bulk point*, *JHEP* **01** (2017) 013 [1509.03612].

[100] N. Engelhardt and G.T. Horowitz, *Towards a Reconstruction of General Bulk Metrics*, *Class. Quant. Grav.* **34** (2017) 015004 [1605.01070].

[101] N. Engelhardt and G.T. Horowitz, *Recovering the spacetime metric from a holographic dual*, *Adv. Theor. Math. Phys.* **21** (2017) 1635 [1612.00391].

[102] N. Engelhardt and A.C. Wall, *Extremal Surface Barriers*, *JHEP* **03** (2014) 068 [1312.3699].

[103] N. Chagnet, S. Chapman, J. de Boer and C. Zukowski, *Complexity for Conformal Field Theories in General Dimensions*, 2103.06920.

[104] J. De Boer and L. Lamprou, *Holographic Order from Modular Chaos*, *JHEP* **06** (2020) 024 [1912.02810].

[105] J. Kirklin, *The Holographic Dual of the Entanglement Wedge Symplectic Form*, *JHEP* **01** (2020) 071 [1910.00457].

[106] H. Casini, M. Huerta and R.C. Myers, *Towards a derivation of holographic entanglement entropy*, *JHEP* **05** (2011) 036 [1102.0440].

[107] B. Oblak, *Berry Phases on Virasoro Orbits*, *JHEP* **10** (2017) 114 [1703.06142].

[108] A.M. Perelomov, *Generalized coherent states and their applications* (1986).

[109] L.G. Yaffe, *Large n Limits as Classical Mechanics*, *Rev. Mod. Phys.* **54** (1982) 407.

[110] P. Caputa and J.M. Magan, *Quantum Computation as Gravity*, *Phys. Rev. Lett.* **122** (2019) 231302 [1807.04422].

[111] P. Bueno, J.M. Magan and C.S. Shahbazi, *Complexity measures in QFT and constrained geometric actions*, 1908.03577.

[112] I. Akal, *Reflections on Virasoro circuit complexity and Berry phase*, 1908.08514.

[113] J. Erdmenger, M. Gerbershagen and A.-L. Weigel, *Complexity measures from geometric actions on Virasoro and Kac-Moody orbits*, *JHEP* **11** (2020) 003 [2004.03619].

[114] M. Flory and M.P. Heller, *Geometry of Complexity in Conformal Field Theory*, *Phys. Rev. Res.* **2** (2020) 043438 [2005.02415].

[115] M. Flory and M.P. Heller, *Conformal field theory complexity from Euler-Arnold equations*, *JHEP* **12** (2020) 091 [2007.11555].

[116] P. Caputa, J.M. Magan and D. Patramanis, *Geometry of Krylov Complexity*, 2109.03824.

[117] D. Patramanis, *Probing the entanglement of operator growth*, 2111.03424.

[118] J. Cardy and E. Tonni, *Entanglement hamiltonians in two-dimensional conformal field theory*, *J. Stat. Mech.* **1612** (2016) 123103 [1608.01283].

[119] D.D. Blanco, H. Casini, L.-Y. Hung and R.C. Myers, *Relative Entropy and Holography*, *JHEP* **08** (2013) 060 [1305.3182].

[120] S. Das, B. Ezhuthachan, S. Porey and B. Roy, *Virasoro algebras, kinematic space and the spectrum of modular Hamiltonians in CFT_2*, *JHEP* **21** (2020) 123 [2101.10211].

[121] N. Ishibashi and T. Tada, *Infinite circumference limit of conformal field theory*, *J. Phys. A* **48** (2015) 315402 [1504.00138].

[122] N. Ishibashi and T. Tada, *Dipolar quantization and the infinite circumference limit of two-dimensional conformal field theories*, *Int. J. Mod. Phys. A* **31** (2016) 1650170 [1602.01190].

[123] A. Gendiar, R. Krcmar and T. Nishino, *Spherical Deformation for One-Dimensional Quantum Systems*, *Prog. Theor. Phys.* **122** (2009) 953 [0810.0622].

[124] H. Katsura, *Sine-square deformation of solvable spin chains and conformal field theories*, *J. Phys. A* **45** (2012) 115003 [1110.2459].

[125] B. Doyon, M. Hoogeveen and D. Bernard, *Energy flow and fluctuations in non-equilibrium conformal field theory on star graphs*, *J. Stat. Mech.* **1403** (2014) P03002 [1306.3192].

[126] E. Witten, *Coadjoint Orbits of the Virasoro Group*, *Commun. Math. Phys.* **114** (1988) 1.

[127] A. Alekseev and S.L. Shatashvili, *Path Integral Quantization of the*

Coadjoint Orbits of the Virasoro Group and 2D Gravity, *Nucl. Phys. B* **323** (1989) 719.

[128] A. Kirillov, *Lectures on the Orbit Method*, vol. 64 of *Graduate Studies in Mathematics*, American Mathematical Society (July, 2004), http://dx.doi.org/10.1090/gsm/064.

[129] A. Alekseev and S.L. Shatashvili, *Coadjoint Orbits, Cocycles and Gravitational Wess–Zumino*, *Rev. Math. Phys.* **30** (2018) 1840001 [1801.07963].

[130] A. Belin, A. Lewkowycz and G. Sárosi, *The boundary dual of the bulk symplectic form*, *Phys. Lett. B* **789** (2019) 71 [1806.10144].

[131] A. Belin, A. Lewkowycz and G. Sárosi, *Complexity and the bulk volume, a new York time story*, *JHEP* **03** (2019) 044 [1811.03097].

[132] D. Marolf, O. Parrikar, C. Rabideau, A. Izadi Rad and M. Van Raamsdonk, *From Euclidean Sources to Lorentzian Spacetimes in Holographic Conformal Field Theories*, *JHEP* **06** (2018) 077 [1709.10101].

[133] X. Dong, *The Gravity Dual of Renyi Entropy*, *Nature Commun.* **7** (2016) 12472 [1601.06788].

[134] X. Dong, *Holographic Entanglement Entropy for General Higher Derivative Gravity*, *JHEP* **01** (2014) 044 [1310.5713].

[135] L.-Y. Hung, R.C. Myers, M. Smolkin and A. Yale, *Holographic Calculations of Renyi Entropy*, *JHEP* **12** (2011) 047 [1110.1084].

[136] K. Krasnov, *On holomorphic factorization in asymptotically AdS 3-D gravity*, *Class. Quant. Grav.* **20** (2003) 4015 [hep-th/0109198].

[137] P. Calabrese and J.L. Cardy, *Entanglement entropy and quantum field theory*, *J. Stat. Mech.* **0406** (2004) P06002 [hep-th/0405152].

[138] M. Banados, *Three-dimensional quantum geometry and black holes*, *AIP Conf. Proc.* **484** (1999) 147 [hep-th/9901148].

[139] E. Witten, *Quantization of Chern-Simons gauge theory with complex gauge group*, *Communications in Mathematical Physics* **137** (1991) 29 .

[140] J. Cotler and K. Jensen, *A theory of reparameterizations for AdS_3 gravity*, *JHEP* **02** (2019) 079 [1808.03263].

[141] G. Barnich, H.A. Gonzalez and P. Salgado-Rebolledo, *Geometric actions for three-dimensional gravity*, *Class. Quant. Grav.* **35** (2018) 014003

[1707.08887].

[142] O. Coussaert, M. Henneaux and P. van Driel, *The Asymptotic dynamics of three-dimensional Einstein gravity with a negative cosmological constant*, *Class. Quant. Grav.* **12** (1995) 2961 [gr-qc/9506019].

[143] P. Kraus, R. Monten and R.M. Myers, *3D Gravity in a Box*, 2103.13398.

[144] W. Donnelly and L. Freidel, *Local subsystems in gauge theory and gravity*, *JHEP* **09** (2016) 102 [1601.04744].

[145] A.J. Speranza, *Local phase space and edge modes for diffeomorphism-invariant theories*, *JHEP* **02** (2018) 021 [1706.05061].

[146] W. Donnelly, L. Freidel, S.F. Moosavian and A.J. Speranza, *Gravitational edge modes, coadjoint orbits, and hydrodynamics*, *JHEP* **09** (2021) 008 [2012.10367].

[147] T. Faulkner, R.G. Leigh and O. Parrikar, *Shape Dependence of Entanglement Entropy in Conformal Field Theories*, *JHEP* **04** (2016) 088 [1511.05179].

[148] T. Faulkner, R.G. Leigh, O. Parrikar and H. Wang, *Modular Hamiltonians for Deformed Half-Spaces and the Averaged Null Energy Condition*, *JHEP* **09** (2016) 038 [1605.08072].

[149] A. Lewkowycz and O. Parrikar, *The holographic shape of entanglement and Einstein's equations*, *JHEP* **05** (2018) 147 [1802.10103].

[150] S. Banerjee, *Wess-Zumino Consistency Condition for Entanglement Entropy*, *Phys. Rev. Lett.* **109** (2012) 010402 [1109.5672].

[151] P. Caputa and S. Datta, *Operator growth in 2d CFT*, 2110.10519.

[152] A. Almheiri, R. Mahajan, J. Maldacena and Y. Zhao, *The Page curve of Hawking radiation from semiclassical geometry*, *JHEP* **03** (2020) 149 [1908.10996].

[153] A. Almheiri, T. Hartman, J. Maldacena, E. Shaghoulian and A. Tajdini, *The entropy of Hawking radiation*, *Rev. Mod. Phys.* **93** (2021) 035002 [2006.06872].

[154] A. Almheiri, R. Mahajan and J. Maldacena, *Islands outside the horizon*, 1910.11077.

[155] A. Almheiri, R. Mahajan and J.E. Santos, *Entanglement islands in higher dimensions*, *SciPost Phys.* **9** (2020) 001 [1911.09666].

[156] H.Z. Chen, Z. Fisher, J. Hernandez, R.C. Myers and S.-M. Ruan, *Information Flow in Black Hole Evaporation*, *JHEP* **03** (2020) 152 [1911.03402].

[157] M. Rozali, J. Sully, M. Van Raamsdonk, C. Waddell and D. Wakeham, *Information radiation in BCFT models of black holes*, *JHEP* **05** (2020) 004 [1910.12836].

[158] H. Geng and A. Karch, *Massive islands*, *JHEP* **09** (2020) 121 [2006.02438].

[159] H. Geng, Y. Nomura and H.-Y. Sun, *Information paradox and its resolution in de Sitter holography*, *Phys. Rev. D* **103** (2021) 126004 [2103.07477].

[160] H.Z. Chen, R.C. Myers, D. Neuenfeld, I.A. Reyes and J. Sandor, *Quantum Extremal Islands Made Easy, Part I: Entanglement on the Brane*, *JHEP* **10** (2020) 166 [2006.04851].

[161] V. Balasubramanian, A. Kar and T. Ugajin, *Entanglement between two disjoint universes*, *JHEP* **02** (2021) 136 [2008.05274].

[162] V. Balasubramanian, A. Kar and T. Ugajin, *Islands in de Sitter space*, *JHEP* **02** (2021) 072 [2008.05275].

[163] D. Teresi, *Islands and the de Sitter entropy bound*, 2112.03922.

[164] S. Azarnia, R. Fareghbal, A. Naseh and H. Zolfi, *Islands in flat-space cosmology*, *Phys. Rev. D* **104** (2021) 126017 [2109.04795].

[165] R. Bousso and E. Wildenhain, *Gravity/ensemble duality*, *Phys. Rev. D* **102** (2020) 066005 [2006.16289].

[166] K. Goto, T. Hartman and A. Tajdini, *Replica wormholes for an evaporating 2D black hole*, *JHEP* **04** (2021) 289 [2011.09043].

[167] R. Bousso and A. Shahbazi-Moghaddam, *Island Finder and Entropy Bound*, *Phys. Rev. D* **103** (2021) 106005 [2101.11648].

[168] Y. Chen, V. Gorbenko and J. Maldacena, *Bra-ket wormholes in gravitationally prepared states*, *JHEP* **02** (2021) 009 [2007.16091].

[169] J.M. Maldacena, *The Large N limit of superconformal field theories and supergravity*, *Adv. Theor. Math. Phys.* **2** (1998) 231 [hep-th/9711200].

[170] R. Bousso and E. Wildenhain, *Islands in Closed and Open Universes*, 2202.05278.

[171] S.R. Coleman and F. De Luccia, *Gravitational Effects on and of Vacuum Decay*, *Phys. Rev. D* **21** (1980) 3305.

[172] E. Farhi and A.H. Guth, *An Obstacle to Creating a Universe in the Laboratory*, *Phys. Lett. B* **183** (1987) 149.

[173] B. Freivogel, V.E. Hubeny, A. Maloney, R.C. Myers, M. Rangamani and S. Shenker, *Inflation in AdS/CFT*, *JHEP* **03** (2006) 007 [hep-th/0510046].

[174] K. Langhoff, C. Murdia and Y. Nomura, *Multiverse in an inverted island*, *Phys. Rev. D* **104** (2021) 086007 [2106.05271].

[175] S.E. Aguilar-Gutierrez, A. Chatwin-Davies, T. Hertog, N. Pinzani-Fokeeva and B. Robinson, *Islands in Multiverse Models*, 2108.01278.

[176] W. Cottrell, B. Freivogel, D.M. Hofman and S.F. Lokhande, *How to Build the Thermofield Double State*, *JHEP* **02** (2019) 058 [1811.11528].

[177] R. Emparan, B. Grado-White, D. Marolf and M. Tomasevic, *Multi-mouth Traversable Wormholes*, *JHEP* **05** (2021) 032 [2012.07821].

[178] J.F. Pedraza, A. Russo, A. Svesko and Z. Weller-Davies, *Lorentzian Threads as Gatelines and Holographic Complexity*, *Phys. Rev. Lett.* **127** (2021) 271602 [2105.12735].

[179] J.F. Pedraza, A. Russo, A. Svesko and Z. Weller-Davies, *Sewing spacetime with Lorentzian threads: complexity and the emergence of time in quantum gravity*, *JHEP* **02** (2022) 093 [2106.12585].

[180] C. Akers, N. Engelhardt, D. Harlow, G. Penington and S. Vardhan, *The black hole interior from non-isometric codes and complexity*, 2207.06536.

[181] A.C. Wall, *The Generalized Second Law implies a Quantum Singularity Theorem*, *Class. Quant. Grav.* **30** (2013) 165003 [1010.5513].

[182] R. Bousso and A. Shahbazi-Moghaddam, *Singularities from Entropy*, *Phys. Rev. Lett.* **128** (2022) 231301 [2201.11132].

[183] R. Bousso and A. Shahbazi-Moghaddam, *Quantum Singularities*, 2206.07001.

[184] G.W. Gibbons and S.W. Hawking, *Cosmological Event Horizons, Thermodynamics, and Particle Creation*, *Phys. Rev. D* **15** (1977) 2738.

[185] E. Shaghoulian and L. Susskind, *Entanglement in De Sitter Space*, 2201.03603.

[186] R. Espíndola, B. Freivogel and D. Nikolakopoulou, *Work in progress*, .

[187] M. Freedman and M. Headrick, *Bit threads and holographic entanglement*, *Commun. Math. Phys.* **352** (2017) 407 [1604.00354].

[188] C.A. Agón and J.F. Pedraza, *Quantum bit threads and holographic entanglement*, *JHEP* **02** (2022) 180 [2105.08063].

[189] A. Rolph, *Quantum bit threads*, 2105.08072.